Tine Uberg Nærland

Characterization of light induced degradation in crystalline silicon

Thesis for the degree of Philosophiae Doctor

Trondheim, November 2013

Norwegian University of Science and Technology
Faculty of Natural Sciences and Technology
Department of Materials Science and Engineering

NTNU – Trondheim
Norwegian University of
Science and Technology

NTNU
Norwegian University of Science and Technology

Thesis for the degree of Philosophiae Doctor

Faculty of Natural Sciences and Technology
Department of Materials Science and Engineering

ISBN 978-82-471-4740-5 (printed ver.)
ISBN 978-82-471-4741-2 (electronic ver.)
ISSN 1503-8181

Doctoral theses at NTNU, 2013:303

Printed by NTNU-trykk

PREFACE

This thesis is submitted in partial fulfillment of the requirements for the degree of Doctor of Philosophy at the Norwegian University of Science and Technology (NTNU). The work has been carried out at the Institute for Energy Technology (IFE), Solar Energy Department from June 2009 - August 2013. The project has been funded by the Norwegian Research Council, REC Wafer, REC Solar, Elkem Solar and through the KMB project "Defect engineering for crystalline silicon solar cells".

Most of the experiments are performed at the Department for Solar Energy at IFE. Oxygen measurements by FTIR have been performed at Systems Engineering Inc. in Tokyo and the University of Oslo, MiNa lab. The summer (May - July) 2011 was spent at the Department of Photovoltaics at the University of Konstanz with focus on decay in open circuit voltage (V_{OC}) as a function of illumination time and decay in V_{OC} as a function of applied voltage over time in the dark.

The thesis consists of two sections. Section 1 is intended to be supplemental to section 2, which is the published papers from the work. Section one is thus meant to give an introduction to the topic of light induced degradation in solar cell materials, and to explain the applied methods and techniques in a more comprehensive way than what has been done in the papers. The results and conclusions reported in the papers will, however, not be repeated in this section.

The second section contains the main results from the experimental work that has been performed and consists of papers that have been published. The following papers are included:

PAPER I

T. U. Nærland, B. R. Olaisen, and L. Arnberg, "Studying light soaking of solar cells by the use of solar simulator," Solid State Phenomena, vol. 178-179, pp. 435-440, 2011.

PAPER II

T. U. Naerland, H. Angelskar, M. Kirkengen, R. Sondena, and E. S. Marstein, "The role of excess minority carriers in light induced degradation examined by photoluminescence imaging," Journal of Applied Physics, vol. 112, pp. 033703-8, 2012.

PAPER III

T. U. Naerland, H. Angelskar, and E. S. Marstein, "Direct monitoring of minority carrier density during light induced degradation in Czochralski silicon by photoluminescence imaging," Journal of Applied Physics, vol. 113, pp. 193707-7, 2013.

PAPER IV

Tine Uberg Nærland, Halvard Haug, Hallvard Angelskår, Rune Søndenå, Erik Stensrud Marstein and Lars Arnberg, "Studying light-induced degradation by lifetime decay analysis: Excellent fit to solution of simple second order rate equation", IEEE Journal of Photovoltaics, vol. 3, pp. 1265-1270, 2013.

Oslo, November 2013

Tine Uberg Nærland

ABSTRACT

Light induced degradation is an unfortunate characteristic of a very commonly used silicon material for solar cells: boron-doped Czochralski silicon. The degradation is attributed to a recombination center that is activated by excess charge carriers, i.e. electrons, and the energy conversion efficiency of the affected cells is severely reduced. The phenomenon has been known since the early 1970's but the fundamental mechanism is still a debated topic. The main focus of this thesis has been to study the role of the excess carrier concentration on the B-O related defect center generation and a new method has been developed to experimentally investigate the relation between the two. Local B-O related defect generation (Spot-LID), where the wafer is exposed to light in a confined area, causes the excess electrons to diffuse out into the wafer, allowing us to study the degradation of a continuously varying electron concentration. This concentration can be monitored by means of photoluminescence (PL) imaging. Through the direct monitoring of the diffused minority carrier density distribution (during light exposure) from an exposed into an unexposed wafer area, compared to the observed defect generation, we were able to monitor the generation of excess carrier induced defects over a range of carrier concentrations. It was verified that the generation of the B-O defect is directly related to the presence of excess minority carriers and that very low concentrations of minority excess carrier densities are sufficient to generate the B-O related defect. Carrier concentrations down to $1.7 \pm 0.2 \times 10^{9}$ cm^{-3} were observed to cause lifetime degradation. We experimentally demonstrated that there exists an excess carrier threshold value, Δn_{lim}, beyond which the generation rate becomes fully independent of the carrier concentration for the investigated silicon materials ($\Delta n_{lim} = 1.84 \pm 0.9 \times 10^{11}$ cm^{-3}). These results indicate that the role of the excess carriers during the *rapid decay* is to first change the charge state of the defects by shifting the electron quasi-Fermi level across the energy level of the defect center in its passive state ($E_{\text{lat}} = E_{\text{V}} + (635 \pm 18)$ meV) followed by another rate-determining step before the defect center becomes recombination active.

Another topic of this thesis has been to evaluate different ways of measuring the B-O related decay. In this work three different techniques have been employed; *Lifetime decay analysis by time-resolved QSSPC*, *B-O related degradation studied by time-resolved I-V measurements* and *current induced degradation of V_{OC} in the dark*. A part of this work is

concerned with the challenges of studying B-O related degradation using a high intensity light source with special attention on the potential increase of the temperature of the sample. For boron-doped Czochralski Cz-Si cells, where an initial decay is occurring during the first minutes, special attention must be given to the temperature rise in the beginning of the measurement in order to differentiate between the reduction in V_{OC} as a result of heating or as a result of B-O related degradation. In the last part of the work a range of silicon wafers were investigated by means of *Lifetime decay analysis by time-resolved QSSPC*. Curve fitting of the measured data to a single exponential (the solution of a first order rate equation) was attempted but a much better fit was achieved by a solution of a second order rate equation. This indicates that the defect generation process can be better described by second order reaction kinetics and the rate of the reaction is thus changing with the square of the latent defect concentration ${N'_t}^2$. The concentration of holes was identified to control the half-life of the degradation process and is either playing a role as a reactant in excess or as a catalyst.

ACKNOWLEDGEMENT

When I first started my PhD the summer 2009 one of the first things I did was to attend the GADEST conference. Since I did not know anyone, I had to make new friends and I particularly got to know a professor from The University of Oxford, Peter Wilshaw. One night Professor Wilshaw asked me how old I was and when I answered 27 his first response was: "If you are that old, you should go home and have babies!" – ten months later came Audun. My colleagues and supervisors were very happy for me but when I 10 months later announced that Sigurd was on his way they started worrying: Is she ever going to finish this Ph. D.? – I am about to do so and the person I owe the biggest gratitude is my husband, Jan-Erik Carlsen. Besides being a wonderful father to our boys he has cheered me up, believed in me and helped me whenever he could.

The next person I would like to express my sincere gratitude to is Hallvard Angelskår. The hours he spent with me in the lab, the simulations and the proof reading was all very tedious work. Nevertheless, Hallvard was always optimistic, constructive and supporting.

I would like to thank my supervisors; Lars Arnberg, Smagul Karazhanov and Rune Søndenå. Even though Lars, my main supervisor, has been located in another city I always received the help I needed and I am especially grateful for all the effort he put into reviewing my work. Smagul, my co-supervisor, has a broad competence on defects and his door was always open for all kinds of questions. Rune, also my co-supervisor, has skills and experience in the lab that has been invaluable in my work in addition to his expertise on LID-related questions.

I have been doing the majority of my work at the IFE and the time spent at here has been nothing else than four extraordinary years. This is because of the beautiful people that work there: Bent, Frode, Jo, Josefine, Marie, Trygve, Jostein, Chang, Nicoleta, Ellen, Merete, Ørnulf, Hallgeir and Werner. Thank you all for being so enjoyable and peculiar.

A special thanks goes to Halvard Haug for being of irreplaceable help in my work in addition to being the happiest person I have ever met. Also, thank you Birger Retterstøl Olaisen for patiently helping me with the I-V and QSSPC setup and thank you

Erik Stensrud Marstein for being an inspiration, a motivator and a priceless support during my years at IFE.

I also acknowledge the financial support by the Research Council of Norway and the industry partners in the project; REC Solar, REC wafer and Elkem Solar. I would like to thank the Solar group in Konstanz for making my stay in Germany so worthwhile. Also, I would like to thank Lars Arnbergs group in Trondheim for the nice trips we have been to together and for making me feel included in the group even though I did not meet with them on a daily basis.

At last I would like to thank my close family and extended family for always being there, believing in me, allowing me space to work and always taking so good care of me and my boys.

Thank you all!

ABBREVIATIONS AND PHYSICAL PARAMETERS

Physical parameters	Description	Unit
Δn_{lim}	Excess carrier threshold value where B-O defect generation rate starts being independent of Δn	cm^{-3}
B_{rad}	Radiative recombination coefficient of silicon at room temperature.	cm^3/s
D_n	Diffusivity of the electrons	cm^2/s
I_{PL}	Intensity of photoluminescence	counts
I_{SC}	Short circuit current	A
J_0	Dark current density	mA/cm^2
J_{mp}	Current corresponding to maximum power output	mA/cm^2
J_{SC}	Short circuit current	mA/cm^2
L_n	Diffusion length of the electrons	cm
n_0	Concentration of electrons in the equilibrium state	cm^{-3}
N_{a}	p-type doping concentration	cm^{-3}
N_t^*	Normalized defect concentration	μs^{-1}
$N_{t,sat}^*$	Saturated normalized defect concentration	μs^{-1}
N'_t	Normalized latent defect concentration	μs^{-1}
P_{in}	Irradiance value (power density from the sun)	W/cm^2
P_{max}	Maximum power density	W/cm^2
R_e	Reflectance of the sample	%
R_{rad}	Radiative band to band recombination rate	$cm^{-3}s^{-1}$
V_{mp}	Voltage corresponding to maximum power output	V
V_{OC}	Open circuit voltage	V
w_{slow}	Half life, time where the latent defect concentration for the slow defect has been reduced to its half	s
μ_n	Mobility of electrons	cm^2/Vs
μ_p	Mobility of holes	cm^2/Vs
σ_n	Electron capture cross section	cm^2
τ_{eff}	Effective lifetime	µs
$\tau_{n,eff}$	Effective lifetime of electrons	µs
τ_n	Electron lifetime	µs
υ_n	Mean thermal velocity of the electron	m/s
Φ_{ph}	Photon flux	$m^{-2}s^{-1}$

$\Delta\sigma_{ph}$	Photo conductance	S
Δn	Excess carrier concentration, injection level	cm^{-3}
C	Calibration constant to convert I_{PL} to Δn	
E_A	Activation energy	eV
E_C	Energy level of conduction band	eV
E_f	Activation energy for the fast defect	eV
E_{lat}	Energy level of the latent defect center in the band gap	eV
E_s	Activation energy for the slow defect	eV
E_V	Energy level of valence band	eV
f_{abs}	Fraction of photons absorbed	%
FF	Fill factor	%
G	Carrier generation rate	$cm^{-3}s^{-1}$
n	Concentration of electrons	cm^{-3}
p	Concentration of holes	cm^{-3}
p_0	Concentration of holes in the equilibrium state	cm^{-3}
R	Carrier recombination rate	$cm^{-3}s^{-1}$
t	Time	s
T	Temperature	K
W	Sample thickness	µm
η	Solar cell conversion efficiency	%
λ	Wave length	cm
τ_0	Initial carrier lifetime before light exposure	µs

Physical constants	Description	Value
k	The Boltzmann constant	1.38065 × 10-23 J/K
n_i	Intrinsic carrier density in silicon at 300 K	1.01×10^{10} cm^{-3}
q	Elementary charge	1.60218×10^{-19} C

Abbreviations	Description
AM1.5	Air Mass 1.5. Standard solar spectrum for solar cell efficiency measurement
B-O	Boron-oxygen
c-Si	Crystalline silicon
CDI	Carrier Density Imaging
CID	Current Induced degradation
CP5	Chemical Polish that gives isotropic etching of silicon (HF, HNO_3, and CH_3COOH with a 5:1 ratio between HNO_3 and HF)
Cz-Si	Czochralski silicon
DLTS	Deep-Level Transient Spectroscopy
FTIR	Fourier-Transform Infrared Spectroscopy
FZ-Si	Float Zone silicon
GW	Giga watt
I-V	Current-Voltage
IFE	Institute for Energy Technology
LID	Light Induced Degradation
PECVD	Plasma-Enhanced Chemical Vapor Deposition
PL	Photoluminescence
PV	Photovoltaic energy
QSSPC	Quasi-Steady State Photoconductance decay
RCA	Standard cleaning solution in silicon semiconductor industry (Radio Corporation of America)
Spot-LID	Localized light induced degradation technique to study the role of the excess carriers in B-O related defect generation
SRV	Surface Recombination Velocity
µW-PCD	Microwave Photoconductance Decay

CONTENTS

Section 1

CHAPTER 1

INTRODUCTION

Solar energy is free, unlimited, and available over the entire globe. The sun is expected to continue shining for the next five billion years, providing an abundant source of energy. Solar cells are simple semiconductor devices that convert sunlight directly into electricity with only minor impact on the environment. As the costs of production have been considerably reduced the solar cell electricity production has seen a remarkable growth over the past decade and is on its way to becoming a mature and mainstream source of energy. In 2012 the world's installed photovoltaic (PV) capacity surpassed 100 GW_p. This capacity is capable of producing as much annual electric energy as 16 1 GW coal power plants, and each year these PV installations save more than 53 million tons of CO_2 [1]. During the last 4 years the PV industry has, however, gone through a significant transformation. Since 2009 the PV global market capacity has evolved mainly in a context of production overcapacity. Although the demand for PV has grown rapidly, production capacity has grown even faster, resulting in a module production capacity in between 150-230% higher than the annual global installations [1].

Regardless of this difficult situation the prospects are looking promising for the coming years for PV. This has mainly to do with new emerging economies with rapidly growing PV markets in Brazil, China and India [2]. The overcapacity in the module production will continue for some years but there were already signs in 2012 of a more balanced PV market mainly driven by the Chinese market growth [1]. A continuous reduction in cost of PV energy is, however, necessary in order for PV to continue growing in both established and emerging markets. Currently crystalline silicon (c-Si) modules represent 85-90% of the global annual market and will most likely continue to be the dominant technology also in the years to come [2].

The real challenge in solar cell research is hence to improve efficiency while decreasing the overall cost of electricity production. High efficiency cells on crucible-grown single crystal Czochralski (Cz) silicon and cast multicrystalline (mc) silicon

both have the potential for reducing this cost, but Cz-Si (p-type) is unfortunately suffering from the formation of a metastable defect under carrier injection. This defect reduces the bulk lifetime and causes industrial screen-printed solar cells to lose 1 to 1.5% in absolute efficiency (or 7 to 10% relative efficiency). The phenomenon is often referred to as light induced degradation (LID) and is currently also becoming a problem for low cost materials like mc-Si and monolike-Si as the quality of these materials is continuously increasing.

Considerable research effort has been given to this topic over the last 40 years (see chapter 2.2.1). There has been focus both on the fundamental understanding of the defect and methods to eliminate or mitigate it. The attempt to mitigate the defect has only been partially successful and there are still several questions concerning the electrical and structural properties of the defect. Neither the chemical composition nor the energy level of the defect has been determined experimentally so far. The main objective of this thesis has been to contribute to new information on the fundamental understanding of light induced degradation. The thesis is organized into two major parts; part one is concerned with B-O related decay analysis, part two is concerned with the role of the excess carriers in the B-O related defect generation.

1.1 MOTIVATION OF THE THESIS

Until now, research on LID has been highly focused on finding correlations between the observed degradation and impurity/doping concentrations in the material. There is especially one publication that has been dominating this research [3] (Bothe *et al*.), and this work is also the first and only investigation to identify and quantify the *rapid degradation*. Light induced degradation is occurring in two steps; a *rapid degradation* taking place during the first minutes of light exposure, and a *slow degradation* proceeding for days. Assessing the level and rate of the rapid degradation requires dedicated gauging techniques and this is the topic of the first part of the present thesis where different techniques to quantify both the normalized defect concentration and the rate of the two degradation steps are tested, improved and reviewed. The analysis of the light induced defect concentration and generation rate performed with lifetime analysis within this thesis is the only large dataset available beside the work by Bothe and Schmidt *et al.* [3], [4]. Much theoretical work on the defect has, however, been done [5], [6], [7], [8], [9], [10], [11]. All of these are based on the experimental work by Bothe and Schmidt and our idea is that this experimental platform ought to be extended. The task was thus to try to replicate the measurements performed by Bothe *et al.*, and see if we could find the same correlations and draw the same conclusions as they did.

The other part of the thesis concerns a new approach for studying the B-O related defect generation, through the concentration of the excess minority carriers. It is widely known that the degradation of boron-doped silicon is caused by the presence of excess minority carriers, and that photons are not directly involved, but the determination of the excess minority carrier concentration responsible for the degradation has not yet been carried out experimentally. Several groups have

studied the influence of varying illumination intensity on the B-O defect generation rate. These studies[12],[13],[14] have shown that the generation rate of the defect saturates at a certain illumination intensity. The intensity of the illumination source and the excess carrier density are linked through the optical properties of the sample and the carrier lifetime. A certain illumination intensity threshold value therefore corresponds to a certain excess carrier threshold value, Δn_{lim}, but the same illumination intensity gives widely different excess minority carrier concentrations for different materials. The motivation for the second part of the thesis is thus to develop a technique to study the effect of the excess minority carrier concentration on the B-O related defect generation and experimentally determine the relation between the two.

1.2 THESIS OUTLINE

The thesis is divided into two sections. Section one serves as an introductory text to section two, which contains the manuscripts wherein the main findings of this work are presented. Section two is begun by describing my own and my co-authors' contributions to the manuscripts and the findings reported in the manuscripts will not be repeated in section one. Section one is meant to serve as an introduction to the field of light induced degradation, and provides additional theory and experimental details that are not presented in the papers.

Section one is divided into 6 chapters. In the present Chapter 1, the thesis is placed into a broader context and a brief status of the PV market is given. The motivation for the work is discussed and at the end of the chapter, a summary of the papers is given.

Chapter 2 is meant to provide the reader with some fundamental basics in order to understand the concepts that this thesis is built upon. At the end of the chapter a review of the research on the topic of LID is given.

In Chapter 3 I present the different techniques we have been employing to measure the B-O related decay in this work. The chapter is meant to give an overview and an introduction to these techniques, but also to address some strengths and weaknesses of these techniques. Further on, some additional experimental results that are not included in the papers are presented in this chapter. A summary of the chapter is given in the end.

Chapter 4 is concerned with the techniques developed for studying the role of the excess minority carriers in the generation of B-O related defects (Spot-LID). The chapter is starting with a discussion on the conventional PL imaging technique and then moves on to the two different techniques that we developed for this work. At the end of the chapter I go through some of the supplemental analysis required for the Spot-LID analysis before a summary of the chapter is given.

In chapter 5 some concluding remarks on the main results of the thesis as a whole is given.

In chapter 6 some suggestions for future investigations are presented.

1.3 SUMMARY OF PAPERS

This chapter presents an overview of the papers included in the thesis. The papers are appended at the end of the thesis.

PAPER I

T. U. Nærland, B. R. Olaisen, and L. Arnberg, "Studying light soaking of solar cells by the use of solar simulator," Solid State Phenomena, vol. 178-179, pp. 435-440, 2011.

In this work a review of light soaking of solar cells by the use of commercial I-V characterization instruments is presented. The paper addresses the challenges of studying light induced degradation using a high intensity light source. Depending on the light source, the illumination intensity can fluctuate substantially and must be adjusted for in both the J_{SC} and the V_{OC}. Furthermore, the limiting uncertainty in a voltage measurement is the ability to monitor and control the junction temperature accurately. A 100mW/cm^2 illumination source is introducing a substantial amount of heat to the cell and the setup in general. Consequently, the temperature rise of the cell must be carefully corrected for. For boron-doped Cz-Si cells, where an initial decay is occurring during the first minutes, special attention must be given to the temperature rise in the beginning of the measurement in order to differentiate between the heating and the bulk effect.

PAPER II

T. U. Naerland, H. Angelskar, M. Kirkengen, R. Sondena, and E. S. Marstein, "The role of excess minority carriers in light induced degradation examined by photoluminescence imaging," Journal of Applied Physics, vol. 112, pp. 033703-8, 2012.

In this work, we present a way to investigate the generation of the B-O related defect for a broad range of excess carrier concentrations (Δn) circumventing the operation at different illumination intensities. The Δn range studied is continuous and the B-O related defect generation dependence of Δn can be determined. The technique involves a mask which covers the major part of the sample but that enables exposure of the sample through a narrow slit. Through the examination of the Δn profile, diffused from the exposed area in the slit into the unexposed area of a wafer, and the observed defect generation by photoluminescence imaging, a lower limit of minority carrier concentration being responsible for lifetime degradation by B-O related defect generation is observed. For normal quality p-type Cz-Si material, degradation due to the B-O related defect center was detected down to a Δn value equal to 1.7×10^9 cm^{-3}.

PAPER III

T. U. Naerland, H. Angelskar, and E. S. Marstein, "Direct monitoring of minority carrier density during light induced degradation in Czochralski silicon by photoluminescence imaging," Journal of Applied Physics, vol. 113, pp. 193707-7, 2013.

Several groups have studied the influence of varying illumination intensity on the B-O related defect generation rate. These studies have shown that the generation rate of the defect saturates at a certain illumination intensity. For highly degradable material, the defect generation rate saturates at about 1mW/cm^2. The intensity of the illumination source and the excess carrier density are linked through the optical properties of the sample and the carrier lifetime. A certain illumination intensity threshold value therefore corresponds to a certain excess carrier threshold value, Δn_{lim}, but the same illumination intensity gives widely different excess carrier densities for different materials.

In this work we experimentally demonstrate that such an excess carrier threshold value, Δn_{lim}, exists and that above Δn_{lim} the generation rate is fully independent of Δn. These findings are uncovered by a new way of studying the B-O related degradation process, in which the excess carrier density is monitored directly during the light soaking. By applying simulations for the very low carrier concentrations, we are able to quantify Δn_{lim}. The procedure is performed on a series of samples and the results showed that there was no correlation between Δn_{lim} and the B-O defect concentration for the rapid decay (arithmetic averaged Δn_{lim} = 1.84 ± 0.9 × 10^{11} cm^{-3}). These results indicate that the role of the excess carriers during the rapid decay is to first change the charge state of the latent defects by shifting the electron quasi-Fermi level across the energy level of the defect center in its passive state ($E_{lat} = E_V +$ (635±18) meV) and that, subsequently, another rate-determining step proceeds before the defect center becomes recombination active.

PAPER IV

Tine Uberg Nærland, Halvard Haug, Hallvard Angelskår, Rune Søndenå, Erik Stensrud Marstein and Lars Arnberg, "Studying light-induced degradation by lifetime decay analysis: Excellent fit to solution of simple second order rate equation", IEEE Journal of Photovoltaics, vol. 3, pp. 1265-1270, 2013.

In this work a range of different boron-doped Czochralski silicon materials have been analyzed for B-O related lifetime decay. The carrier lifetime was measured and monitored by an automated quasi steady state photoconductance setup with an externally controlled bias lamp for in-situ illumination between measurements. Logarithmic plots of the time resolved lifetime decays clearly displayed the previously reported rapid and slow decays, but a satisfactory fit to a single exponential function could not be achieved. Fitting B-O related lifetime decay to exponentials has been the standard since 2001 [15]. In this work we found, however, that both decay curves, for all the investigated samples, can be fitted very well to the solution of a simple second order rate equation. This indicates that the defect generation process can be described by second order reaction kinetics and

that the rate equation describing our system shows that the rate of the reaction is changing with the square of the latent defect concentration $(N_t')^2$. The concentration of holes is identified to control the half-life of the degradation process and is either playing a role as a reactant in excess or as a catalyst.

REFERENCES

[1] European Photovoltaic Industry Association, "Global market outlook for photovoltaics 2013-2017," 2013.

[2] International Energy Agency, "Technology Roadmap, Solar photovoltaic energy," 2010.

[3] K. Bothe and J. Schmidt, "Electronically activated boron-oxygen-related recombination centers in crystalline silicon," *Journal of Applied Physics,* vol. 99, pp. 013701-11, 2006.

[4] J. Schmidt and K. Bothe, "Structure and transformation of the metastable boron- and oxygen-related defect center in crystalline silicon," *Physical Review B,* vol. 69, p. 024107, 2004.

[5] E. Napolitani, D. De Salvador, R. Storti, A. Carnera, S. Mirabella, and F. Priolo, "Room Temperature Migration of Boron in Crystalline Silicon," *Physical Review Letters,* vol. 93, p. 055901, 2004.

[6] J. Schmidt, K. Bothe, D. Macdonald, J. Adey, R. Jones, and D. W. Palmer, "Mechanisms of Light-Induced Degradation in Mono- and Multicrystalline silicon solar cells," in *20th European Photovoltaic Solar Energy Conference*, Barcelona, 2005.

[7] M. Sanati and S. K. Estreicher, "Boron-oxygen complexes in Si," *Physica B: Condensed Matter,* vol. 376-377, pp. 133-136, 2006.

[8] A. Carvalho, R. Jones, M. Sanati, S. K. Estreicher, J. Coutinho, and P. R. Briddon, "First-principles investigation of a bistable boron-oxygen interstitial pair in Si," *Physical Review B,* vol. 73, p. 245210, 2006.

[9] M.-H. Du, H. M. Branz, R. S. Crandall, and S. B. Zhang, "Bistability-Mediated Carrier Recombination at Light-Induced Boron-Oxygen Complexes in Silicon," *Physical Review Letters,* vol. 97, p. 256602, 2006.

[10] D. W. Palmer, K. Bothe, and J. Schmidt, "Kinetics of the electronically stimulated formation of a boron-oxygen complex in crystalline silicon," *Physical Review B (Condensed Matter and Materials Physics),* vol. 76, pp. 035210-6, 2007.

[11] V. V. Voronkov and R. Falster, "Latent complexes of interstitial boron and oxygen dimers as a reason for degradation of silicon-based solar cells," *Journal of Applied Physics,* vol. 107, pp. 053509-8, 2010.

[12] V. V. Voronkov, R. Falster, J. Schmidt, K. Bothe, and A. V. Batuninac, "Lifetime Degradation in Boron Doped Czochralski Silicon," *Electrochemical Society Transactions,* vol. 33, pp. 103-112, 2010.

[13] H. Hashigami, Y. Itakura, and T. Saitoh, "Effect of illumination conditions on Czochralski-grown silicon solar cell degradation," *Journal of Applied Physics,* vol. 93, pp. 4240-4245, 2003.

[14] J. Schmidt and K. Bothe, "Structure and transformation of the metastable boron- and oxygen-related defect center in crystalline silicon," *Physical Review B (Condensed Matter and Materials Physics),* vol. 69, pp. 024107-8, 2004.

[15] S. W. Glunz, S. Rein, J. Y. Lee, and W. Warta, "Minority carrier lifetime degradation in boron-doped Czochralski silicon," *Journal of Applied Physics,* vol. 90, pp. 2397-2404, 2001.

CHAPTER 2

BACKGROUND

2.1 BASIC CONCEPTS

2.1.1 PHOTOVOLTAIC EFFECT

Solar cells exploit the photovoltaic effect where sunlight is directly converted into electricity making use of the electronic properties of semiconductors. The explanation relies on ideas from quantum theory: Firstly, the semiconductor has two bands of energies, which the electrons are allowed to possess, namely the valence band (VB) and the conduction band (CB). These bands are separated by a band-gap, which is a range of energies that the electrons are not allowed to have. This characteristic is critical in order to make a solar cell. Secondly, light consists of small packets of energy, photons, whose energy depends only on the frequency, or color, of the light. Sunlight consists of photons with different energies together constituting the solar spectrum. A certain fraction of the light spectrum, the photons with an energy larger than the band-gap energy, may excite electrons in a semiconductor to the conduction band where they are free to move [16]. The mechanism is illustrated in Figure 2-1 where a photon hits the silicon lattice and kicks an electron up in the conduction band.

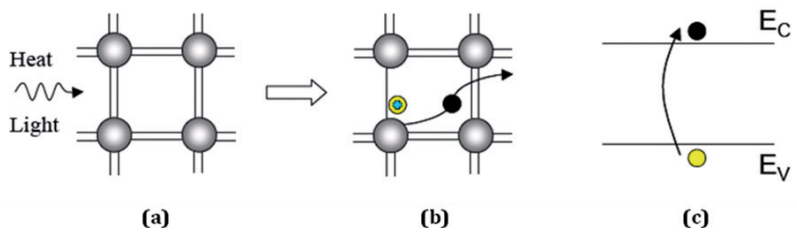

Figure 2-1 Radiation (light) strikes the atomic lattice of a semiconductor (a) with a frequency high enough to excite an electron (b) to the conduction band where it is free to move (c). The electron is leaving behind a hole in the valence band, which is also free to move. The gap in between the two bands contains no allowed states and is often denominated the forbidden band gap. E_C and E_V are the energies of the conduction band and the valence band, respectively. The figure is taken from [17].

The excitation process has created an excited electron in the conduction band and an excited hole in the valence band, but for the solar cell to be able to do electric work the excited electrons and holes must be separated and directed in opposite directions to produce a net current. This is accomplished by forming a p-n junction in the semiconductor, i.e. by joining two differently doped layers of semiconductor material as depicted in Figure 2-2. Doping is in brief a method to manipulate the conductivity of the material by adding small amounts of other elements. In silicon, which is a four-valent element, it is common to dope with boron, which is a three-valent element, in order to obtain mobile holes (p-doping). When negative doping (n-doping) is required it is common to dope with phosphorous, which is a five-valent element. In *p*-type silicon the number of electrons trapped in atom bonds is higher, thus effectively increasing the number of holes. In doped material, there is therefore an excess of one of the types of carriers (holes or electrons). The type of carrier with the higher concentration is called the "majority carriers", whereas the carriers with the lower concentration are called the "minority carriers."

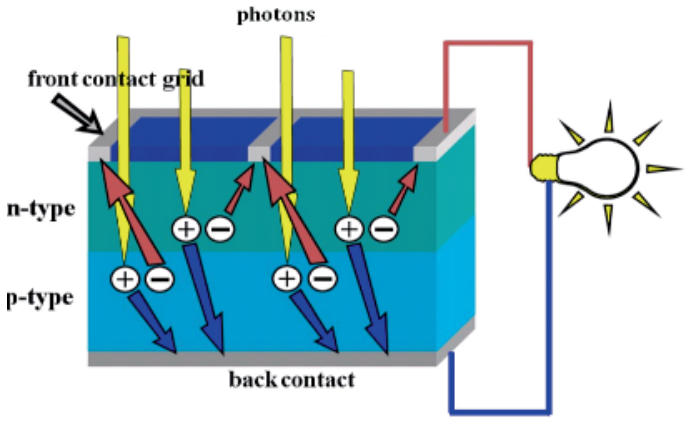

Figure 2-2 The concept of a solar cell illustrating how the two different charge carriers are separated by the electric field created by a p-n junction. The carriers are subsequently collected at the electrodes/contacts at the back and front of the cell. The figure is taken from [18].

Doping thus creates an excess of electrons in the n-type (negative) layer and an excess of holes in the p-type (positive) layer. When the two layers are in contact, electrons from the n-type layer diffuse over to the p-side, leaving behind a narrow layer, which is positively charged due to lack of electrons. Similarly, holes diffuse in the opposite direction, leaving behind a negatively charged layer depleted for holes. The resulting junction region then practically contains no mobile charge carriers and the fixed charges of the dopant atoms create a potential barrier acting against a further flow of electrons and holes. This is in practice a rectifying diode, pushing the electrons to one side and the holes to the other side of the junction. If contacts are made on each side of the junction and light is shone on the device power can now be harvested.

2.1.2 SOLAR CELL CHARACTERISTICS

An example of a current-voltage curve (I-V curve) for a solar cell is presented in Figure 2-3.

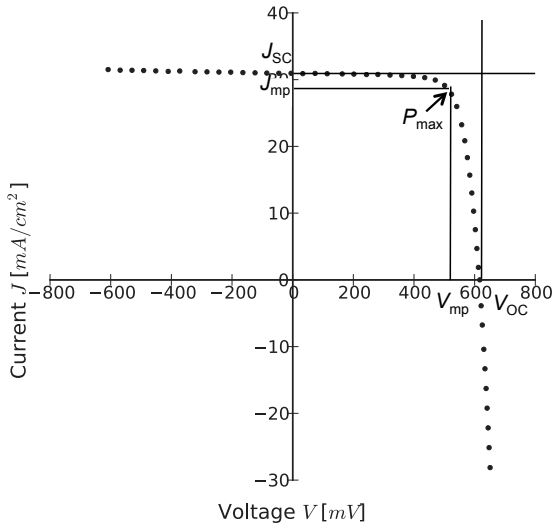

Figure 2-3 Current and voltage data for a solar cell produced at IFE. Several quantities are marked in the plot: P_{max} is the point at the I-V curve where the inner square has the biggest area. This is the working point at which the solar cell performs the best and has the highest energy conversion efficiency. V_{OC} and J_{SC} are the open circuit voltage and the short circuit current, respectively, and V_{mp} and J_{mp} are the voltage and the current corresponding to the maximum power point.

In Figure 2-3 some characteristic parameters are highlighted and a summary of most important features of the I-V curve of a given solar cell are given below:

1) The open circuit voltage V_{OC}, i.e. the voltage which builds up across the cell as long as its terminals are kept on a high impedance forcing the electrical current to $I = 0$. This quantity is related to the band-gap of the semiconductor, the temperature and the amount of recombination of carriers in the material. The open circuit voltage V_{OC} of an ideal solar cell can be expressed by the following equation [19]:

$$V_{OC} = \frac{kT}{q} ln\left(\frac{J_{SC}}{J_0}\right) \qquad 2.1$$

where: k is the Boltzmann constant and q is the electron charge, J_{SC} is the short circuit current, and J_0 is the dark current.

2) The short circuit current I_{sc}, i.e. the current which is generated by the solar cell if it is connected to a low impedance forcing the voltage across the device to $V = 0$. I_{sc} is the product of the photogeneration rate and the collection probability. The collection probability is the probability that an excited electron-hole pair reaches the contacts and is extracted as current. Recombination in the solar cell reduces the collection probability. The current is proportional to the surface area of the cell and is generally normalized by the cell area and expressed as current density denoted by J_{sc}.

3) The dark current J_0 is the current that flows in the opposite direction of the photogenerated current when an external load is connected to the cell. The explanation is that the recombination of the majority carriers due to the diffusion of the injected minority carriers into the bulk of the quasi-neutral regions results in a reduction of the concentration of the majority carriers compared to the concentration under equilibrium. The drop in the concentration of the majority carriers is balanced by the flow of the majority carriers from the electrodes into the bulk. This causes a dark current which depends on fundamental semiconductor parameters and which should be kept as low as possible.

4) Fill factor *FF* describes the "squareness" of the I-V curve, and should be as high as possible. *FF* is by definition the ratio between the maximum operating point and the ultimate operating point (I_{SC} and V_{OC}):

$$FF = \frac{J_{mp} \times V_{mp}}{J_{SC} \times V_{OC}} \qquad 2.2$$

5) Solar cell energy conversion efficiency η is calculated as the ratio between the generated maximum power (see Figure 2-3) and the incident power. The irradiance value, P_{in}, of 1000 W/m^2 of AM1.5 spectrum has become a standard for measuring the energy conversion efficiency of solar cells [20].

$$\eta = \frac{J_{mp} \times V_{mp}}{P_{in}} \qquad 2.3$$

2.1.3 THE CONCEPT OF CARRIER GENERATION, RECOMBINATION AND LIFETIME

When external generation of carriers (holes and electrons) in a semiconductor occurs, e.g. due to light exposure, the excess carrier concentration is at all times given by the balance between generation and recombination. Generation is the process where the electron-hole pairs are created and recombination the process where they are annihilated. Local defects such as impurities, dislocations and grain boundaries are typical sites where generated carriers will recombine. The topic for this thesis is a light induced defect complex that causes electron and hole recombination and by this lowers the power output from the solar cell. The concept of recombination will be discussed in the following but first the concept of lifetime will be introduced.

When a solar cell has a constant temperature and it is not subject to any light exposure the system is at thermal equilibrium and the density of electrons and holes

is constant at their equilibrium values, denoted n_0 and p_0, respectively. In p-type Si, electrons are the minority charge carriers and are thus responsible for the net current. The principle is the same independently of whether it is electrons or holes that are the minority carrier, so in the following only electrons (n) will be referred to. Under illumination the number of electrons increases and the total number is then given by:

$$n = n_0 + \Delta n \tag{2.4}$$

where Δn is the excess minority carrier concentration often referred to as the *injection level*. Excess minority carriers will eventually recombine, i.e. the electron will give up its energy and fall back to the valence band resulting in elimination of a hole. This recombination occurs at a given rate R. If we divide the excess minority carrier concentration by the rate of recombination R we obtain the *minority carrier recombination lifetime*, in this thesis referred to as simply the lifetime τ_n:

$$\tau_n = \frac{\Delta n}{R} = \frac{\Delta n}{\frac{\mathrm{d}\Delta n}{\mathrm{d}t}} \tag{2.5}$$

From this relation we can formulate an electron continuity expression where the rate of the carrier generation G minus the change in excess carriers due to recombination is given by:

$$G - \frac{\mathrm{d}\Delta n}{dt} = \frac{\Delta n}{\tau_n} \tag{2.6}$$

Rearranging this expression with respect to the lifetime we obtain

$$\tau_n = \frac{\Delta n}{G - \frac{\mathrm{d}\Delta n}{\mathrm{d}t}} \tag{2.7}$$

which is the basis for measuring effective lifetime described below. When the external generation is removed, the excess carriers will recombine and equilibrium will be restored again. The excess carrier density as a function of time is then given by solving the differential equation, so that

$$\Delta n(t) = \Delta n_0 exp\left(-\frac{t}{\tau_n}\right) \tag{2.8}$$

where $\Delta n_0 = G\tau_n$ is the excess carrier density prior to the removal of the external generation source.

Recombination occurs mainly by three physical mechanisms in silicon: Radiative recombination, Auger recombination and recombination through traps or Shockley Read Hall recombination [21]. The occurrence and relative strength of these mechanisms vary with the carrier injection level, but they will generally all coexist in the same material. To recognize this fact the measured lifetime is referred

to as the *effective lifetime*, τ_{eff}. The inverse effective lifetime is given as the inverse sum of the individual lifetime contributions:

$$\frac{1}{\tau_{eff}} = \frac{1}{\tau_{Auger}} + \frac{1}{\tau_{SRH}} + \frac{1}{\tau_{rad}} + \cdots \qquad 2.9$$

In silicon, radiative recombination is weak, as silicon is an indirect band-gap semiconductor, and is often neglected. Auger recombination only depends on the doping level of the material.

The most important recombination process in solar grade silicon is recombination through localized states in the band gap. These are caused by defects or impurities that possess energy states in the band gap region that can act as traps for carriers. This means that this recombination mechanism is dependent on material quality, and is as such possible to modify through process optimization. Figure 2-4 is showing energy levels within the forbidden gap for a range of impurity atoms in silicon. Also groups of atoms may behave as traps, such as the possible boron-oxygen related defect complex responsible for light induced degradation, which will be treated in detail in this thesis.

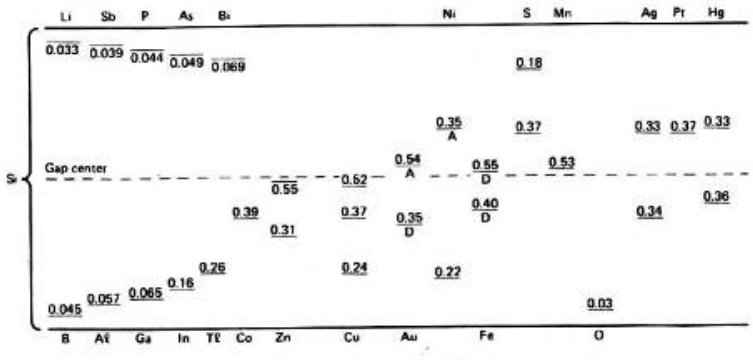

Figure 2-4 Energy levels within the forbidden gap for a range of impurities in silicon. All levels below the gap center are considered acceptor states (mainly traps for holes) and all levels above are considered donor states (mainly traps for electrons) except where they are indicated with A (acceptors) or D (donors). The figure is taken from [19].

Traps are commonly divided into two categories, shallow traps and deep level traps. The shallow trap states are localized near the band edges and are mainly occupied by one type of charge carriers. The carrier can subsequently be released back to the band it resided originally by thermal activation. Alternatively, if the trap is localized in the middle of the band gap (deep level traps) it is very likely that the state/trap captures a carrier of the opposite polarity before the first carrier is released. Thus, the two carriers have in effect recombined [16]. This process is called Shockley Read Hall (SRH) recombination and is visualized in Figure 2-5.

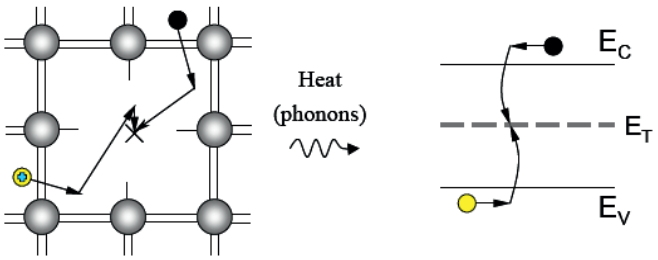

Figure 2-5 Recombination through deep level traps/SRH-recombination. Traps capture carriers of both polarities where they will recombine and be annihilated. The picture to the left shows that the trap can be represented by a crystal defect. The figure is taken from [17].

According to Shockley Read Hall theory the defect concentration can be directly related to the lifetime, provided that the generated defects are the dominating recombination path.

$$\tau_{SRH} = \frac{1}{\upsilon_n \sigma_n N_t} \qquad 2.10$$

Here τ_{SRH} is the lifetime of the electron, υ_n is the mean thermal velocity of the electron, σ_n is the capture cross-section of the defect and N_t is the concentration of the defect.

When the crystal lattice of the silicon is terminated at the surface of the sample, a special case of crystal defects occur. The large amount of partially bonded Si atoms at the surface (dangling bonds) induces a nearly continuous band of defect levels within the energy band gap. The SRH recombination analysis is still valid, although the problem is more commonly treated referring to surface recombination velocities (SRV).

Recombination of carriers is thus a big challenge in solar cell silicon and it is not only the lifetime of the carriers that is reduced but both the voltage and current output from the cell. This will be discussed in more detail in chapter 3.2.

2.2 INTRODUCTION TO LIGHT INDUCED DEGRADATION

The function of a solar cell is to generate power when exposed to sunlight. It therefore seems as a paradox that the solar cell can degrade under the same sunlight. This is caused by defects in the semiconductor material that are activated through illumination. As a result of this, recombination in the material will increase with illumination, reducing the lifetime of the material. This effect is known as light induced degradation (LID). In boron-doped silicon there are three different defects known to degrade silicon under illumination. These are the iron-boron pairs, the copper-copper pairs and the boron-oxygen complexes. The iron-boron pairs are different from the other two defects in the sense that they have positive or negative

effect on the minority carrier lifetime depending of the injection level. Also, this defect will go back to its initial state when the cell is stored in the dark for a couple of hours/days. It is relatively straightforward to differentiate between the effect of iron-boron pairs and the two other defects [6].

The fact that copper-pairs form a light sensitive defect has been known for quite some time [22] but it has not been until recently that some real light has been shed upon this defect [23]. It appears that the degradation kinetics of the copper-pair defect is remarkably similar to the kinetics of the boron-oxygen related defect and the authors of [23] claim that since undetectable amounts of copper is sufficient to degrade the material significantly copper may perfectly well be the reason for the observed degradation. The boron-oxygen related defect is, however, only occurring in silicon containing boron and oxygen (see list below). If copper was responsible for the degradation, the degradation should be observable in gallium doped and n-type materials as well if the production of these materials introduce comparable amounts of metal impurities to the production of CZ-material. Nevertheless, copper is shown to degrade silicon in a very similar manner as the B-O related defect even though experimental data is still limited. The materials used for the investigations in this thesis are high quality Cz-Si materials and the probability that these high lifetime wafers are polluted with copper and iron are very low but cannot be conclusively excluded. It is thus not forthright to exclude copper related defects as the source of light induced degradation. In the present work I will, however, refer to the defect responsible for LID as the B-O related defect but the conclusions drawn from this work are nevertheless autonomous and valid regardless of what the origin of the defect is.

An introduction to the B-O related defect is given in the next chapter.

2.2.1 BORON-OXYGEN RELATED RECOMBINATION CENTERS - A REVIEW

B-O related degradation reducing the solar cell efficiency through the generation of metastable defects is an inherent problem in boron-doped Czochralski silicon (Cz-Si). The phenomenon is found to be related to the simultaneous presence of boron and oxygen in the Si material, through a possible boron-oxygen defect (B-O defect). Neither the chemical composition nor the energy level of the defect has, however, so far been determined experimentally. LID has been known since the 1970s when Fischer and Pschunder [24] observed that LID in Cz-Si was present independently of particle irradiation (in space applications), and from a loss in the red response during light exposure it was concluded that a reduction of the minority carrier lifetime in the solar cell base was responsible for the observed degradation.

For years the apparent degradation was thought to be induced by light until Knobloch *et al*. in 1996 found that a similar degradation could be observed by applying a forward bias voltage to the cell [25]. Hence, it was concluded that the degradation in boron-doped silicon is caused by the presence of excess minority carriers, and that photons are not directly involved. Later, in 2003, Bothe *et al.* [26] showed that the metastable defect is also formed under equilibrium conditions (at elevated temperatures), indicating that it is not the excess carrier density that determines the degradation but the total number of minority carriers. The commonly used nomination for the degradation, namely light induced degradation (LID) is thus not very accurate, both in the sense that light is not really required and

also that other defects may induce efficiency degradation by light. In the continuation of this thesis I will therefore refer to the degradation as *B-O related degradation*.

In 2001, Glunz *et al.* [15] proposed a mechanism involving a recombination-enhanced defect reaction as a possible explanation for the formation of the boron-oxygen related recombination center due to the quadratic increase of defect generation rate with doping level. This mechanism assumes that it is the energy released from the recombination that triggers the generation of the active recombination center. On the basis of this mechanism Schmidt *et al.* [4] introduced a model where fast diffusing oxygen dimers capture substitutional boron atoms to form B_s-O_{2i} recombination centers. This model was prevailing for many years but was invalidated in 2009 when Macdonald *et al.* [27] discovered that both the concentration of defects and the rate is controlled by the concentration of holes (p_0) and not the concentration of boron [B]. The fact that the degradation effect has not been observed in gallium-doped but only boron-doped Cz silicon still ensures that the Cz-specific defect depends on boron and not just the position of the Fermi level [28].

In 2010/2011 Voronkov and Falster [11],[29], proposed a new degradation model. In this model latent recombination centers are already incorporated in the crystal before carrier injection and the centers responsible for the rapid and slow lifetime decays are B_sO_{2i} and B_iO_{2i} respectively. The reaction model is similar for the two decays, but with some differences: In p-type silicon the activation of B_sO_{2i}, the defect center responsible for the rapid lifetime decay, is explained through a series of steps where the quadratic proportionality observed between p_0 and lifetime is accounted for by the capture of two holes by a negative latent center (LC^-_{fast}) resulting in the formation of a positive latent center

$$LC^-_{fast} + 2h^+ \rightarrow LC^+_{fast}. \qquad 2.11$$

The positive latent center is then reconstructed into a transient center (TC_{fast}) by overcoming an energy barrier

$$LC^+_{fast} \xrightarrow{E_{A,1}} TC^+_{fast}, \qquad 2.12$$

which due to recharging by injection of electrons forms a neutral transient center TC^0_{fast}

$$TC^+_{fast} + e^- \rightarrow TC^0_{fast}, \qquad 2.13$$

and finally the recombination active center RC_{fast}

$$TC^0_{fast} \xrightarrow{E_{A,2}} RC_{fast}. \qquad 2.14$$

The defect center responsible for the slow lifetime decay also starts from a latent complex, but this time the substitutional boron is replaced by interstitial boron, B_iO_2. The latent center is now denoted LC_{slow}. In the reaction sequence for

the slow decay the first step is a recharge of the latent center into a neutral state by the assistance of injected minority carriers

$$LC_{slow}^{+} + e^{-} \rightarrow LC_{slow}^{0}. \quad 2.15$$

The second step is a temporary recharging to a double positive state by two holes, resulting in a transient center TC_{slow}

$$LC_{slow}^{0} + 2h^{+} \xrightarrow{E_{A,3}} TC_{slow}. \quad 2.16$$

The final step is controlled by overcoming a free energy barrier between TC_{slow} and a slow recombination active center $RC_{\mathrm{slow}}$and is thus governed by the attempt frequency and the Boltzmann energy

$$TC_{slow} \xrightarrow{E_{A,4}} RC_{slow}. \quad 2.17$$

This model is the first to explain the rapid degradation and the proportionality between the defect concentration and the hole concentration [p_0] in compensated silicon co-doped with boron and phosphorus [27]. In a recent work [30] where silicon co-doped with boron and gallium was investigated, it was, however, found that the defect concentration was proportional to [B] instead of p_0 (the rate was still found to be dependent on p_0). This implies a defect complex containing a substitutional boron atom [B_s] like in the model by Schmidt *et al.* [4]. The model by Schmidt *et al.* [4] involves, however, another debated issue: the diffusion of the oxygen dimer. Recent work by Murin *et al.* [31] states that the charge-state driven motion of an oxygen dimer is a highly unlikely mechanism in solar grade silicon. Presently no model is thus able to fully explain all experimentally observed characteristics associated with the defect responsible for light induced degradation. The LID community has, however, attained a large amount of empiric knowledge that can aid to solve this mystery. The main conclusions on the behavior of the defect found so far are given below:

1. Boron-doped *p*-type FZ silicon free of interstitial oxygen and other contaminations shows no lifetime degradation [15].
2. Boron-doped *p*-type FZ-Si (N_A = 2.2 × 10^{15} cm^{-3}) intentionally contaminated with oxygen, (O_i = 5.4 × 10^{17} cm^{-3}) shows a degradation behavior very similar to the one observed in boron-doped *p*-type Cz-Si, although no other contaminations are present in these FZ wafers [32].
3. Phosphorus-doped *n*-type Cz silicon shows no degradation [33].
4. Phosphorus-doped *n*-type FZ silicon intentionally contaminated with oxygen (O_i = 4.2 × 10^{17} cm^{-3}) shows no lifetime degradation [32].
5. Oxygen-free boron-doped *p*-type magnetic Cz-Si shows no degradation [34].
6. Gallium-doped oxygen-contaminated Cz-Si shows no degradation [33], [34].

7. Due to the fact that no trace of the defect has been found by Deep Level Transient Spectroscopy the concentration of the defects is believed to be very low (about 10^{11} cm^{-3}) [11]. Consequently a high defect capture cross-section and a low density of excess minority carriers to initiate the defect are expected.
8. The saturated value of the defect concentration (not an actual defect concentration but a normalized concentration deduced from lifetime and V_{OC} decay measurements, see Eq. 3.8) for both the fast stage and for the slow stage is found to be proportional to the product of the boron concentration [B] and the squared oxygen concentration, $[O]^2$ and both defect concentrations seem to be independent of temperature [3].
9. The kinetics of defect generation are found to be proportional to the inverse of [B] and independent of [O] and the temperature dependence of the rate constants for the fast and the slow decay is characterized by the activation energy E_f = 0.23 eV and E_s = 0.475 eV respectively [3].
10. By annealing in the dark, the lifetime is recovered to its initially high value. The recovery occurs in a range from 110°C to 200°C and also proceeds via a two step decay process [11].
11. A permanent deactivation of these centers can be achieved by illumination at temperatures in the range of 70 – 220°C [35], [36]. The stability of such deactivation is debated and there seem to be a link to the concentration of thermal donors in the sample and the instability [37].

REFERENCES

[3] K. Bothe and J. Schmidt, "Electronically activated boron-oxygen-related recombination centers in crystalline silicon," *Journal of Applied Physics,* vol. 99, pp. 013701-11, 2006.

[4] J. Schmidt and K. Bothe, "Structure and transformation of the metastable boron- and oxygen-related defect center in crystalline silicon," *Physical Review B,* vol. 69, p. 024107, 2004.

[6] J. Schmidt, K. Bothe, D. Macdonald, J. Adey, R. Jones, and D. W. Palmer, "Mechanisms of Light-Induced Degradation in Mono- and Multicrystalline silicon solar cells," in *20th European Photovoltaic Solar Energy Conference*, Barcelona, 2005.

[11] V. V. Voronkov and R. Falster, "Latent complexes of interstitial boron and oxygen dimers as a reason for degradation of silicon-based solar cells," *Journal of Applied Physics,* vol. 107, pp. 053509-8, 2010.

[15] S. W. Glunz, S. Rein, J. Y. Lee, and W. Warta, "Minority carrier lifetime degradation in boron-doped Czochralski silicon," *Journal of Applied Physics,* vol. 90, pp. 2397-2404, 2001.

[16] J. Nelson, *The physics of solar cells*. London: Imperial College Press, 2003.

[17] M. Zeman, "Solar Cells," Compendium to the course "Solar Cells", Delft University of Technology, Delft, 2006.

[18] M. A. Green, *Silicon Solar Cells: Advanced Principles & Practice*: Centre for Photovoltaic Devices and Systems, 1995.

[19] M. A. Green, *Solar cells operating principles, technology and system applications*. Kensington: University of New South Wales, 1998.

[20] K. A. Emery, "Solar simulators and I-V measurement methods," *Solar Cells,* vol. 18, pp. 251-260, 1986.

[21] A. Cuevas and D. Macdonald, "Measuring and interpreting the lifetime of silicon wafers," *Solar Energy,* vol. 76, pp. 255-262, 2004.

[22] J. Lagowski, P. Edelman, and A. Morawski, "Non-contact deep level transient spectroscopy (DLTS) based on surface photovoltage," *Semiconductor Science and Technology,* vol. 7, p. A211, 1992.

[23] H. Savin, M. Yli-Koski, and A. Haarahiltunen, "Role of copper in light induced minority-carrier lifetime degradation of silicon," *Applied Physics Letters,* vol. 95, p. 152111, 2009.

[24] H. Fischer and W. Pschunder, "Investigation of photon and thermal induced changes in silicon solar cells," in *the 10th IEEE Photovoltaic Specialists Conference*, Palo Alto, CA, 1973, pp. 404-411.

[25] J. Knobloch, S. W. Glunz, D. Biro, W. Warta, E. Schäffer, and W. Wettling, "Solar cells with efficiencies above 21% processed from Chochralski grown silicon," in *the 25th IEEE Photovoltaic Specialists Conference*, 1996, pp. 405-408.

[26] K. Bothe, R. Hezel, and J. Schmidt, "Recombination-enhanced formation of the metastable boron--oxygen complex in crystalline silicon," *Applied Physics Letters,* vol. 83, pp. 1125-1127, 2003.

[27] D. Macdonald, F. Rougieux, A. Cuevas, B. Lim, J. Schmidt, M. Di Sabatino, and L. J. Geerligs, "Light-induced boron-oxygen defect generation in compensated p-type Czochralski silicon," *Journal of Applied Physics,* vol. 105, pp. 093704-7, 2009.

[28] S. Rein, "Lifetime spectroscopy: a method of defect characterization in silicon for photovoltaic applications," ed: Springer-Verlag, Berlin, 2005, p. 422.

[29] V. V. Voronkov, R. Falster, K. Bothe, B. Lim, and J. Schmidt, "Lifetime-degrading boron-oxygen centres in p-type and n-type compensated silicon," *Journal of Applied Physics,* vol. 110, pp. 063515-7, 2011.

[30] M. Forster, E. Fourmond, F. E. Rougieux, A. Cuevas, R. Gotoh, K. Fujiwara, S. Uda, and M. Lemiti, "Boron-oxygen defect in Czochralski-silicon co-doped with gallium and boron," *Applied Physics Letters,* vol. 100, pp. 042110-4, 2012.

[31] L. I. Murin, E. A. Tolkacheva, V. P. Markevich, A. R. Peaker, B. Hamilton, E. Monakhov, B. G. Svensson, J. L. Lindstrøm, P. Santos, J. Coutinho, and A. Carvalho, "The oxygen dimer in Si: Its relationship to the light-induced degradation of Si solar cells?," *Applied Physics Letters,* vol. 98, p. 182101, 2011.

[32] S. W. Glunz, S. Rein, W. Warta, J. Knobloch, and W. Wettling, "On the degradation of Cz-silicon solar cells," presented at the 2nd World Conference on Photovoltaic Energy Conversion, Vienna, Austria, 1998.

[33] J. Schmidt, A. G. Aberle, and R. Hezel, "Investigation of carrier lifetime instabilities in Cz-grown silicon," in *the 26th IEEE Photovoltaic Specialists Conference*, 1997, pp. 13-18.

[34] S. W. Glunz, S. Rein, J. Knobloch, W. Wettling, and T. Abe, "Comparison of boron- and gallium-doped p-type Czochralski silicon for photovoltaic application," *Progress in Photovoltaics: Research and Applications,* vol. 7, pp. 463-469, 1999.

[35] Bianca Lim, Karsten Bothe, and Jan Schmidt, "Deactivation of the boron-oxygen recombination center in silicon by illumination at elevated temperature," *Physica Status Solidi - Rapid Research Letters,* vol. 2, pp. 93-95, 2008.

[36] A. Herguth, G. Schubert, M. Kaes, and G. Hahn, "Investigations on the long time behavior of the metastable boron–oxygen complex in crystalline silicon," *Progress in Photovoltaics: Research and Applications,* vol. 16, pp. 135-140, 2008.

[37] B. Lim, K. Bothe, and J. Schmidt, "Impact of oxygen on the permanent deactivation of boron--oxygen-related recombination centers in crystalline silicon," *Journal of Applied Physics,* vol. 107, pp. 123707-4, 2010.

CHAPTER 3

B-O RELATED DEGRADATION DECAY ANALYSIS

Under typical illumination conditions the B-O related degradation reaches saturation within a few days, and the exact saturation time is dependent on the hole concentration of the material. In paper IV an exponential relationship between the saturation time and the hole concentration is shown indicating that only Cz-Si with a hole concentration above 9×10^{15} cm^{-3} will saturate during the first 24 hours. Cz-Si with a hole concentration below this limit will require days, even weeks, to reach a saturated level of B-O related defects. This should be taken into account in future work.

The degradation occurs via two characteristic decays independent of the saturation time: one fast and one slowly occurring decay. The fast initial decay is taking place already during the first few minutes of the carrier injection (in paper II we show that Δn levels down to 1.7×10^{9} cm^{-3} is enough to observe degradation) and therefore highly time-resolved and accurate measurement techniques are required in order to assess the level and rate of degradation.

In the present work, three different techniques have been employed to measure the degradation. Before we discuss the actual techniques it is beneficial to note what parameters are actually measured. There are in principle three different ways of studying the B-O decay, these are: (i) decay in minority carrier lifetime as a function of illumination time, (ii) decay in open circuit voltage (V_{OC}) as a function of illumination time and (iii) decay in V_{OC} as a function of applied voltage over time often called current induced degradation (CID). Notice that (i) and (ii) are based on measurements performed during light exposure of the sample whereas method (iii) is performed in the dark. Furthermore, method (ii) and (iii) differ from method (i) in that these methods are based on the change in V_{OC} in contrast to change in carrier lifetime. The following chapter will deal with all the three mentioned principles

utilizing three different techniques. The main results from the work are given in paper I and IV but a more thorough discussion on the techniques employed will be given here in addition to some unpublished analyses. We start with the work on B-O related minority carrier lifetime decay as a function of illumination time, measured by time-resolved QSSPC.

3.1 LIFETIME DECAY ANALYSIS BY TIME-RESOLVED QSSPC

Lifetime decay as a function of time of light exposure can in principle be studied by any lifetime gauging technique (Microwave Photoconductance Decay (μW-PCD), Carrier Density Imaging (CDI), QSSPC, etc.). Finding a suitable technique requires the consideration of two main issues. The first issue is related to the injection level when comparing measured lifetimes for samples with different doping concentrations. There is a pronounced injection level dependence when carrier lifetimes are measured. This can be seen in Figure 3-1 where simulations of typical lifetime curves as a function of injection are given for four differently doped samples. It is obvious that comparisons of the lifetime of samples with different doping concentrations measured at a fixed injection level of i.e. 1×10^{15} cm^{-3} may lead to systematic errors. Hence, measurements at a given injection level relative to the doping concentration have to be specified for quantitative investigations of the B-O related defect concentration. This issue is especially of concern when it comes to the μW-PCD technique. In μW-PCD the exact injection level is in general not known and therefore quantitative investigations are not possible. With QSSPC measurements, on the other hand, the injection level is known explicitly, reducing uncertainties related to the injection level dependence of the carrier lifetime.

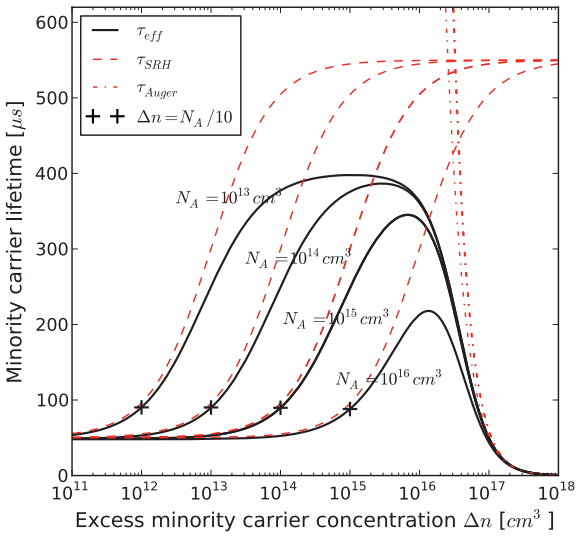

Figure 3-1 Impact of the doping concentration on the lifetime as a function of carrier injection level. In the present work we report the lifetime quantified at the injection level corresponding to one tenth of the doping concentration for the investigated sample indicated by the crosses. In the simulations of the minority carrier lifetime a initial electron and hole lifetime of $\tau_{n,0}$ = 50 µs and $\tau_{p,0}$ = 500 µs are used.

The second issue regarding finding suitable techniques for measuring lifetime decays over time is the actual time resolution. The rapid lifetime decay is occurring during the first hundred seconds of illumination, and if the sample has to be moved back and forth between the illumination stage and the measurement stage, an extremely fast and cautious handling will be required if a good time-resolution of the decay is to be obtained. Additionally it is essentially unrealistic not to expose the sample to any light during this kind of handling.

In this work we have solved the "handling issue" by illuminating the samples in-situ on a QSSPC sample stage while a computer records the lifetime sequentially in addition to turning off and on the illumination. A large set of decay data have been assembled this way and the main outcome has been the identification of a rate equation capable of describing the degradation decays in a better way than has been done before. We found that both the rapid and the slow lifetime decay can be described far better by a second order- than a first order rate equation as proposed in literature [4, 15],[3]. Information on the defect reaction kinetics extracted from the second order rate equation fit are used to discuss the rate determining steps of the rapid and slow defect reactions. This work is described in Paper IV and will not be repeated here. A result that, however, will be presented below, is the relation between the assessed lifetime decays and the concentration of holes, boron and oxygen. We will start by describing the employed technique, i.e. the custom built,

automated QSSPC experiment, but firstly we will have a closer look at the conventional QSSPC technique.

3.1.1 QUASI STEADY STATE PHOTOCONDUCTANCE (QSSPC)

The technique of QSSPC is primarily used for lifetime measurements but can also be used for resistivity and saturation current measurements. The most essential parts of the equipment are the flash lamp, the radio frequency bridge, the oscilloscope, the reference cell and an IR-filter as visualized in Figure 3-2. The lifetime measurement can be done in two different modes; carrier lifetime based on the measurement of the photoconductance under (i) quasi-steady-state or (ii) quasi-transient illumination but there is also the possibility of using a generalized mode where both (i) and (ii) are taken into account.

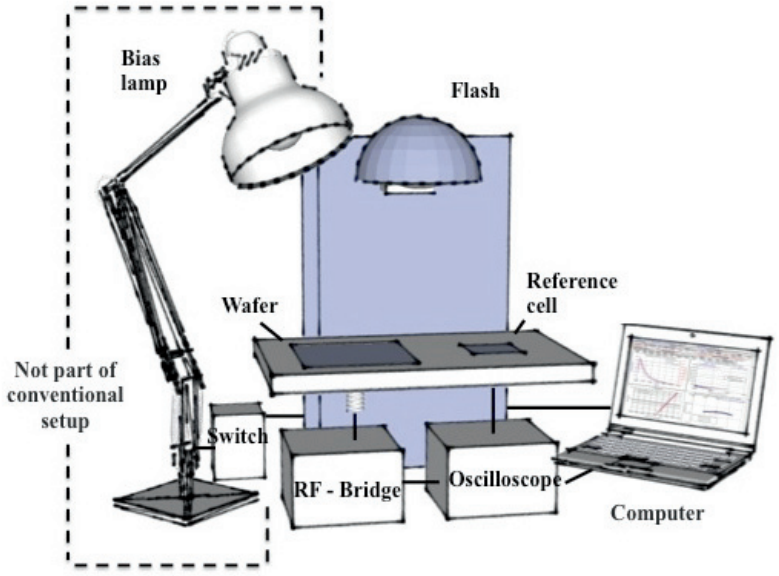

Figure 3-2 Principle drawing of the QSSPC instrument. The flash lamp illuminates the sample and generates electron hole pairs, the solar reference cell measures the light intensity and the coil connected to the radio frequency bridge records the increase of the conductance in the sample.

For both modes there are basically two quantities that are measured by the setup, the photoconductance $\Delta\sigma_{ph}$ and the generation rate, G. G is calculated from a measurement of the incoming photon flux, Φ_{ph}, with a reference photocell with known properties, and is determined by the following equation:

$$G = \frac{\Phi_{ph} f_{abs}}{W} \quad 3.1$$

where f_{abs} is the share of photons that are absorbed (determined by the optical properties of the sample) and W is the sample thickness.

$\Delta\sigma_{ph}$ is the difference between the dark conductance and the elevated conductance due to photogenerated carriers. The $\Delta\sigma_{ph}$ of the silicon wafer is measured inductively by a coil where the voltage output is converted to conductivity in Siemens using the equation

$$\Delta\sigma_{ph} = A(\Delta V - C)^2 + B(\Delta V - C) \quad 3.2$$

In this equation A, B and C are coefficients from a quadratic fit to a calibration curve originating from four point probe sheet resistance values by the manufacturer. If the calibration of the instrument is performed properly, the output conductivity can be used for calculating resistivity data.

The relation between $\Delta\sigma_{ph}$ and the photogenerated carrier concentration Δn is proportional and given by [38]

$$\Delta\sigma_{ph} = qW(\mu_n + \mu_p)\Delta n \quad 3.3$$

where μ_n and μ_p are the electron and hole mobilities, respectively. The mobility is a function of both the doping, temperature and the injection level and can be found in the literature. However, the equation can be iterated to find both Δn and $(\mu_n + \mu_p)$ consistent with the measured conductance.

In quasi steady state mode the decay time constant of the light pulse is typically a few milliseconds, thus samples with lifetimes in the microsecond regime are essentially measured in steady state[39]. Under such conditions Eq. 2.7 reduces to

$$\tau_{n,eff} = \frac{\Delta n}{G} \quad 3.4$$

where $\tau_{n,eff}$ is the measured and accordingly effective lifetime of the carriers. Inserting for Δn in Eq. 3.1 by rearranging Eq. 3.3 the effective lifetime τ_{eff} in the wafer can be expressed as

$$\tau_{eff} = \frac{\Delta\sigma_{ph}}{q f_{abs} \Phi_{ph}(\mu_n + \mu_p)} \quad 3.5$$

For samples with sufficiently high recombination lifetime, the contribution to the recombination rate from steady state generation becomes negligible. This is the situation where we use the transient mode and Eq. 2.7 reduces to

$$\tau_{n,eff} = \frac{\Delta n}{\frac{d\Delta n}{dt}} \tag{3.6}$$

The excess minority carrier density is still calculated from the measured $\Delta\sigma_{ph}$ through the use of Eq. 3.3, thus the effective lifetime under transient mode can be expressed as

$$\tau_{eff} = \frac{\Delta\sigma_{ph}}{q\mathrm{W}(\mu_n + \mu_p)\frac{d\Delta n}{dt}} \tag{3.7}$$

Both the steady state- and the transient mode have been used in the present work since the minority carrier lifetimes of the samples investigated have typically ranged between 100 and 2000 μs. The time duration of the flash is then adjusted so that it is long when the steady state mode is employed and short when the transient mode is employed. In order to assess frequent lifetime measurements during a full B-O related lifetime decay we automated the standard QSSPC setup. This is described in the following chapter.

3.1.2 AUTOMATED QSSPC SETUP

The lifetime degradation curves assessed in this thesis were measured by a custom-built, automated QSSPC experiment where the sample was illuminated by a bias light in situ on the QSSPC stage (See Figure 3-2.) The bias light is a halogen lamp, with an intensity of approximately 50 mW/cm^2 that is automatically turned off when the lifetime is measured. A computer program ensures that the external lamp is turned off during the lifetime measurement and records all measured lifetimes and the time they were measured. As discussed in Paper I the illumination will cause a temperature increase of the sample and stage and this may affect the measured lifetime. The temperature of the sample, was in this case, controlled by a resistance temperature detector coupled to the sample stage, and it turned out that the temperature change of the stage and sample due to illumination was not large enough to significantly influence the measured lifetime.

3.1.3 SURFACE PASSIVATION

Prior to the lifetime decay measurement all wafers were RCA-cleaned according to [40] and thereafter received a double side passivation by plasma-enhanced chemical-vapor deposited hydrogenated amorphous silicon (a-Si:H). Since we intend to study the decay in the bulk we need to ensure that it is not an increase in the SRV (that light degrades the surface passivation layer) that is observed. As float zone silicon (FZ-Si) contains no oxygen, LID is not occurring in such samples, and since light does not degrade them, they are useful as reference samples in order to rule out other possible degradation mechanisms. In these experiments, the effective lifetime was measured on both FZ p-type wafers and n-type wafers in order to ensure that no degradation of the passivation layer was occurring. Figure 3-3 shows a comparison between lifetime as a function of light exposure for a boron-

doped Cz-Si sample and a boron doped FZ-Si sample. The Cz-Si degrades significantly but the FZ-Si stays unaffected by the illumination implying that no degradation of the passivation layer is occurring. The surface recombination velocity (SRV) for the a-Si:H passivation layer of the investigated samples were estimated to be below 20cm/s.

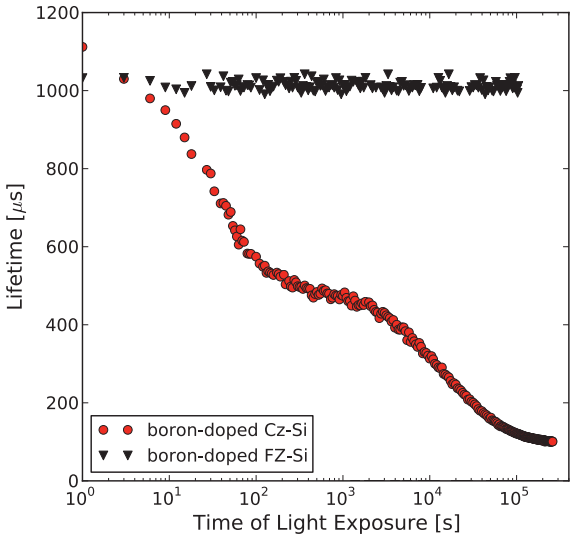

Figure 3-3 Lifetime as a function of light exposure for a-Si:H passivated boron doped Cz-Si and FZ-Si. FZ-Si shows no tendency of degradation indicating that the passivation layer is uninfluenced by the light exposure.

3.1.4 LIFETIME DECAY ANALYSIS

According to Shockley Read Hall theory [41] the B-O related defect concentration can be directly related to the lifetime, provided that the generated defects are the dominating recombination path (Eq. 2.10). The normalized defect concentration, N_t^*, for the B-O related defect is then related to the measured lifetime by the following equation

$$N_t^*(t) = \frac{1}{\tau(t)} - \frac{1}{\tau_0} \qquad 3.8$$

where τ_0 is the initial carrier lifetime before LID and $\tau(t)$ is the carrier lifetime after a certain exposure time. Upon prolonged illumination at a sufficiently high light intensity, N_t^* approaches a saturated value $N_{t,sat}^*$ where the lifetime is not decreasing anymore (see Figure 3-4b). A typical lifetime decay curve for a typical boron doped Cz-Si sample is given in Figure 3-4a. The figure shows an initial fast decay occurring during the first few minutes and a second slower decay proceeding

for hours. This is typical for light induced degradation caused by the B-O related defect [42],[43]. Figure 3-4b shows the calculated $N_t^*(t)$ from the lifetime decay in Figure 3-4a. Figure 3-4b reveals that it is mainly the slow lifetime decay that determines the final value of $N_{t,sat}^*$. This shows that $N_{t,sat}^*$ is not very sensitive to the initial lifetime of the sample, but is mainly determined by the degradation in lifetime in the low lifetime regime.

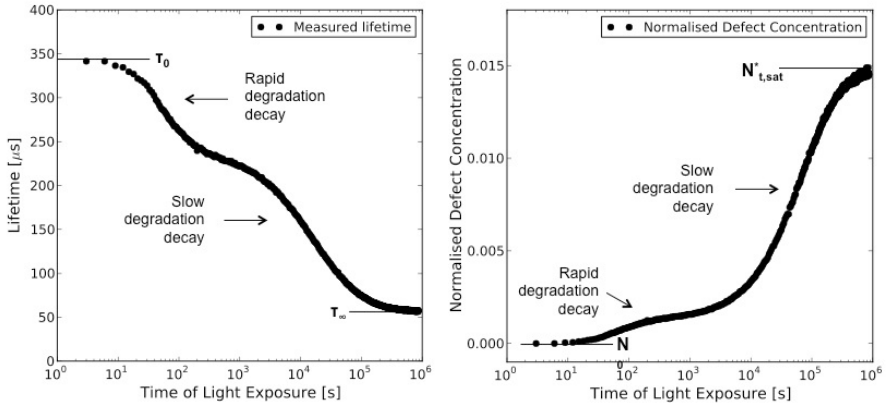

(a) (b)

Figure 3-4 Lifetime (a) and N_t^* (b) as a function of time of light exposure for a typical boron doped Cz-Si sample (N_A = 5.1 × 10^{15}). The N_t^* values are calculated according to Eq. 3.8 where $\tau(t)$ and τ_0 is taken from plot (a). Note that the time is plotted on a logarithmic scale and that the initial fast decay is occurring during the first few minutes and that the second slower decay is proceeding for days until it saturates.

In this thesis the lifetime degradation of a range of samples has been measured by the technique described above. The samples have been mainly boron doped Cz-Si but also some FZ-Si and some compensated material (boron doped Cz-Si co-doped with phosphorous). The samples have been surface passivated according to the procedure described in 3.1.3. The main findings from the work are a fit of the decay curves to a solution of a second order rate equation and a clear correlation between the hole concentration and the saturation time. This work is reported in paper IV. Earlier work where the same kinds of measurements have been performed is reported by [3]. In this work the authors compare the calculated $N_{t,sat}^*$ to the concentration of boron and oxygen and found that $N_{t,sat}^*$ is proportional to the boron concentration and the oxygen concentration squared ($N_{t,sat}^* \propto [B][O]^2$). The rate constant ($k$) extracted from a single exponential fit to the decay curves was also compared to the concentrations of boron and oxygen and here the authors found a correlation between k and the boron concentration squared, but no correlation to the oxygen concentration. We have performed the same analysis but with a slightly different outcome. This is not reported in any of the appended papers but will be

discussed below. Subsequently an analysis of whether the rate of the light induced degradation decay is related to the boron concentration or the hole concentration is given.

3.1.5 DEFECT CONCENTRATION DEPENDENCE ON DOPING CONCENTRATION

In previous work [3] lifetime decay measurements similar to those described in the present work have been performed and a proportional relationship between the normalized defect concentration $N^*_{t,sat}$ and the boron concentration [B] has been found. In our work, a range of boron-doped Cz-Si samples have been investigated for the same relationship and the results are summarized in Figure 3-5.

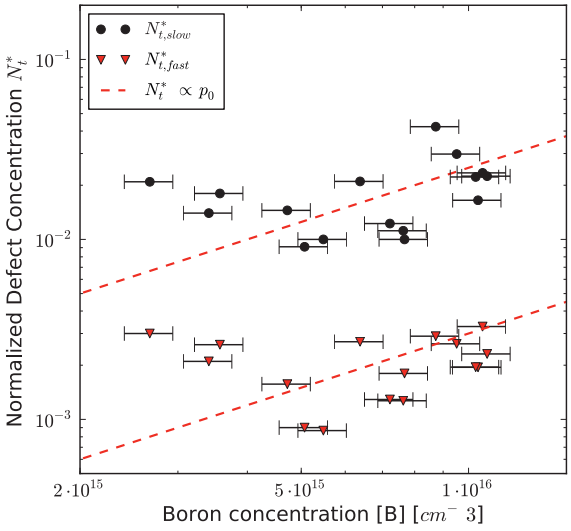

Figure 3-5 $N^*_{t,sat}$ as a function of [B] for the slow and the rapid degradation decay. Note that for the rapid decay $N^*_{t,sat}$ is calculated with $\tau(t)$ corresponding to where the lifetime decay goes from being rapid to slow (see Figure 3-4). The boron concentration [B] has been calculated from the resistivity determined by the QSSPC as described in chapter 3.1.1. The uncertainty (±10%) is an estimate given by the QSSPC manufacturer for the particular setup. A proportional relationship between $N^*_{t,sat}$ and [B] as found in [3] is indicated by the dashed line.

According to Figure 3-5 there is no clear correlation between $N^*_{t,sat}$ and [B] and the relationship that has been found in [3] can not be observed in these data. There are potentially two likely explanations for this; (i) the oxygen concentration of the samples is diverging to a large extent and (ii) the thermal donors are not annihilated. In the present work we have measured the oxygen concentration for a range of the samples, but not for all. The span in the oxygen concentration of the

samples measured was 8×10^{17} cm^{-3} - 1×10^{18} cm^{-3} and there is reason to believe that the rest of the samples that was not measured also have an oxygen concentration in this range. For comparison the span in the oxygen concentration for the same analysis performed by Bothe *et al*. was 7.5×10^{17} cm^{-3}. As such, we have a somewhat larger variation in the oxygen concentration, but not large enough to explain the large scatter in our results. Regarding thermal donors, we did a thermal anneal for 1 hour at 650 °C to annihilate thermal donors according to [44]. The resistivity was measured before and after this treatment and a slight difference could be seen for the samples with a low doping level. The reported [B] in Figure 3-5 is accordingly due to boron and not thermal donors. We can then exclude a large scatter in the oxygen concentration and occurrence of thermal donors in the samples as an explanation for the lack of proportionality between $N_{t,sat}^*$ and [B]. Hence, these results points toward a more complex relationship between $N_{t,sat}^*$ and [B] than earlier reported. The fact that the degradation effect has not been observed in gallium-doped but only boron-doped Cz silicon still indicates that the Cz-specific defect depends on boron, but boron does not necessarily need to be part of the defect complex.

3.1.6 DEFECT CONCENTRATION DEPENDENCE ON OXYGEN CONCENTRATION

The oxygen concentrations have been measured by Fourier Transform Infrared Spectroscopy (FTIR). The method is built upon an analysis of a sample's infrared absorption spectrum where the strength of the absorption is assumed proportional to the concentration of the molecular bonds. The technique is a single-beam technique in which the background- and sample spectra are consecutively measured at different times and are subsequently subtracted from each other. A more elaborate discussion on the technique can be found elsewhere [45]. The measurements have been performed partly at the Systems Engineering, Inc. in Tokyo and at MiNa lab at the University of Oslo.

In the work by Bothe et al. [3] a correspondence between the oxygen concentration [O] to the square of the $N_{t,sat}^*$ was found. In this work the N_t^* is divided by [B] since the authors found a proportionality between the two. In chapter 3.1.5 we showed that we, in the present work, do not find any proportionality between N_t^* and [B] and accordingly we are not obligated to do this normalization of N_t^* even though we plot [O] for samples with a large span in [B]. N_t^* is thus plotted directly against the oxygen concentration, and the results show that no clear correlation between N_t^* and [O] can be found neither for the rapid nor the slow decay (see Figure 3-6).

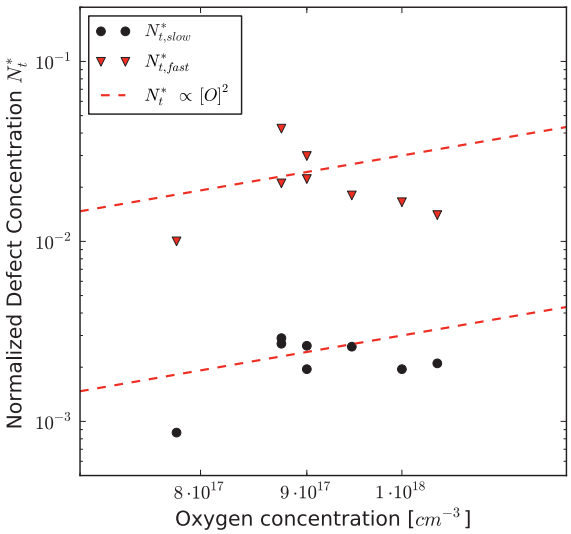

Figure 3-6 $N^*_{t,sat}$ as a function of [O] for the slow and the rapid degradation decay. The dashed lines indicate $N^*_{t,sat} \propto [O]^2$, as found in [3].

3.1.7 DEPENDENCE OF B-O RELATED DEFECT KINETICS DETERMINED ON [B] AND HOLES

As discussed in chapter 2.2.1 a model by Schmidt *et.al* [4] where the boron concentration determines both the defect concentration and the generation rate was prevailing from 2003 to 2009. In 2009 Macdonald *et al.* [27] discovered that the concentration of defects and the rate is controlled by the concentration of holes p_0 and not the concentration of boron [B]. They discovered this by investigating boron-doped silicon co-doped with phosphorous where p_0 is less than [B] because of the compensation. Referring to chapter 3.1.5 we did not find a strong correlation between either [B] or p_0 (the concentration of p_0 and [B] is equal for uncompensated samples) and the defect concentration. However, in Figure 3-7 we show a strong correlation between p_0 and the rate of the defect reaction. The rate of the reaction is in this case expressed through the half width, w_{slow}, of the slow decay. w_{slow} is plotted on the vertical axis and is the time where the latent defect concentration for the slow defect has been reduced to its half. The extraction of this parameter from the measured decay curves is thoroughly explained in Paper IV. The samples measured in this study is a range of boron doped Cz-Si in addition to a set of boron-doped Cz-Si co-doped with phosphorous.

From Figure 3-7 we see that when we plot w_{slow} as a function of [B] for the compensated samples these points fall outside the overall trend determined by the uncompensated samples plotted towards p_0 or [B]. When w_{slow} for the compensated samples are plotted versus p_0 they correspond well to the overall exponential trend.

We therefore conclude that the defect generation rate is controlled by p_0 and this correlation is also found by other groups [27], [30].

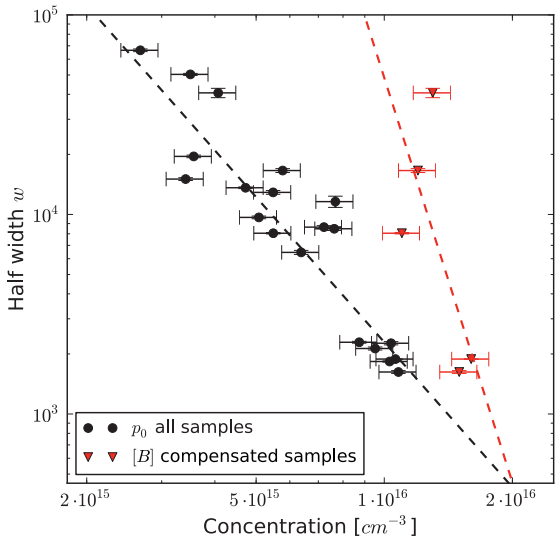

Figure 3-7 Half width w_{slow} plotted as a function of p_0 or [B]. The half width w_{slow} is the time where the latent defect concentration for the slow defect has been reduced to its half. For uncompensated samples the concentration of p_0 and [B] is equal, for compensated samples they are not. The red markers indicate w_{slow} when it is plotted against [B] for the compensated samples. We see that these points (red) are deviating from the trend (black curve) when all samples (both compensated and uncompensated samples) are plotted towards p_0. The dashed lines are fitted exponential curves.

3.2 LIGHT INDUCED DEGRADATION STUDIED BY LIGHT SOAKING OF SOLAR CELLS

In this chapter investigations of light induced degradation of solar cells is presented. There are several papers that have predicted the cell performance losses as a result of minority carrier lifetime reduction [46], [13] and simulations of the cell performance degradation clearly show that the degradation can be explained by the reduction in carrier diffusion length. In addition Bothe *et al.* [3] have found equal time decay constants for degradation profiles acquired by V_{OC} measurements and lifetime measurements.

The work reported herein has mainly been performed at IFE but measurements have also been performed at the University of Konstanz. The main work has been done using commercial current-voltage (I-V)-characterization

instruments, but some investigations on the decay in V_{oc} as a function of applied voltage over time has also been performed. The main results from this work is presented in paper I which addresses the challenges on studying light induced degradation (LID) using a high intensity light source. There are, however, some unpublished issues on the V_{OC} dependence on temperature that will be covered later in this chapter. First of all the I-V measurement setup will be presented together with the principle on how the electrical parameters are collected and a discussion on how the lifetime, which was the topic of the previous chapter, is related to J_{SC}, V_{OC} and η. Finally the technique where LID decay in V_{OC} is measured as a function of applied voltage over time is presented with some results.

3.2.1 CURRENT-VOLTAGE MEASUREMENTS

When V and I are measured an electronic load is swept from a reverse-bias to forward-bias while the cell is exposed to illumination equivalent to 1 sun. During the sweeping of this electronic load V and I data are recorded. An example of a typical measurement result was presented in Figure 2-3.

There are two types of solar simulators that are commonly used for I-V measurements of solar cells. The first type utilizes a continuous light source, while the other type uses a flash lamp to simulate the sun. If the solar simulator utilizes a continuous light source it is also possible to conduct light soaking experiments. The I-V measurement setup makes it possible to do very accurate measurements of a range of parameters with a time resolution down to 0.5 seconds.

In this work light soaking of solar cells was performed with a Wacom Solar Simulator Model WXS-150-10 AM 1.5. The cells were placed on a sample stage (Model STG-200VPXYZ) with temperature control by a liquid cooling system from Julabo. In order to ensure uniform temperature conditions for the cell, a thin copper plate was placed on top of the cooling chuck with a vacuum system in between. See Figure 3-8

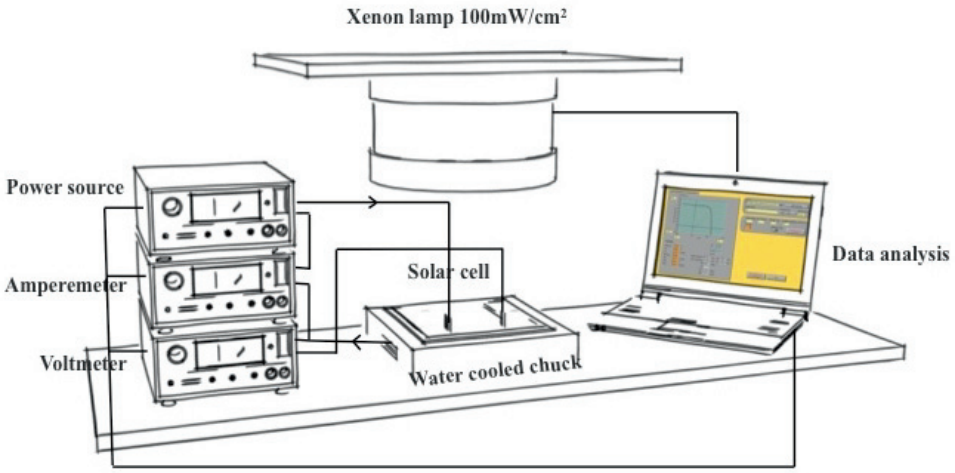

Figure 3-8 Sketch showing the I-V setup. The illumination source is calibrated to give 1 sun intensity AM 1.5 and the water cooled chuck ensures that the solar cell is kept at a temperature of 25°C.

The cells were illuminated with a xenon lamp with intensity equivalent to one sun (100 mW/cm², AM 1.5). A Fluke 8846A voltmeter was used to measure the V_{OC} with a maximum time resolution of 0.5 s and thermocouples (0.5 mm) measured the temperature on the cell front- and backside. The thermocouples are so thin that the shadowing on the cell is negligible. The ambient temperature was controlled by an air conditioning system and monitored by another thermocouple.

3.2.2 THE IMPACT OF LIGHT INDUCED DEGRADATION ON SOLAR CELLS

Recombination through defects, as discussed in chapter 2.1.3, reduces both the voltage (V) and current (I) output from the cell. The reduction in carrier lifetime due to light induced degradation is a consequence of an increase in recombination centers [13]. Recombination reduces both the short circuit current, through the probability of carrier collection, and the voltage, by increasing the dark current [16].

Several researchers have predicted the cell performance losses as a result of minority carrier lifetime reduction [46], [13]. Light induced defects in boron-doped mono-crystalline silicon solar cells can potentially degrade up to 1 % absolute i.e. resulting in an absolute change in efficiency from e.g. 20 to 19 %. The loss in efficiency is caused by loss in both current and voltage. The relative contribution depends on the cell processing. Simulations of the cell performance degradation clearly show that the degradation can be explained by the reduction in carrier diffusion length being a consequence of an increased number of recombination centers [6].

Recombination reduces the generated current by reducing the probability of carrier collection, i.e. the probability that the electron-hole pair reaches the contacts. Accordingly, B-O related defects reduce the current generated by the solar cell. Recombination will also reduce V_{OC}, by increasing the dark current [16].

In Figure 3-9 shows an example of a measurement done on a boron doped Czochralski silicon cell. The investigated solar cells are boron doped Cz-Si cells, 125 × 125 mm^2 semi squared and 210 µm thick with resistivities from 1 – 3 Ωcm. The cells were prepared using an industrial type solar cell process including CP5 saw damage etch, RCA cleaning, a 50 Ω/sq. phosphorous emitter from a $POCl_3$ diffusion, a SiN_x:H antireflection coating by plasma enhanced chemical vapor deposition and a screen printed silver front and aluminum back contact. Before all long-term measurements (24 h) the cells were annealed at 200°C for 10 min in order to reverse the slow degradation mechanism.

The cell was illuminated for 24 hours and the V_{OC} and the I_{SC} are displayed as a function of time on a logarithmic scale. V_{OC} and the I_{SC} behave very differently during the first 100 seconds. The reason for this is the effect of heating which influences V_{OC} more than I_{SC}. The temperature profile of a cell is shown in Figure 3-9 b together with the uncorrected V_{OC} , the intensity corrected V_{OC} and the temperature corrected V_{OC}. From this figure we can see that almost all of the apparent fast degradation is in fact only a matter of heating. The fast degradation in Figure 3-9 a is thus not an effect of a fast B-O related defect center, but is due to an increase in temperature in this case. This will be discussed in more detail in chapter 3.2.3.

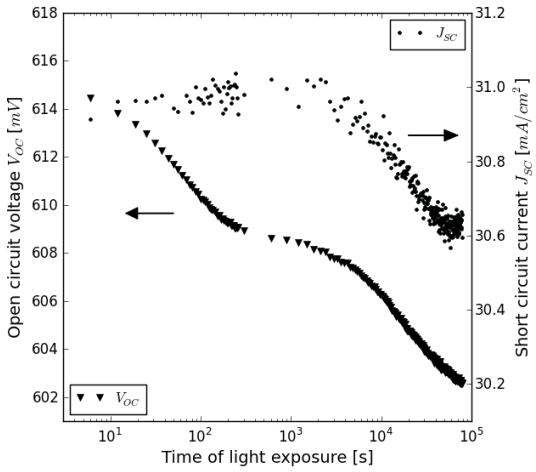

(a)

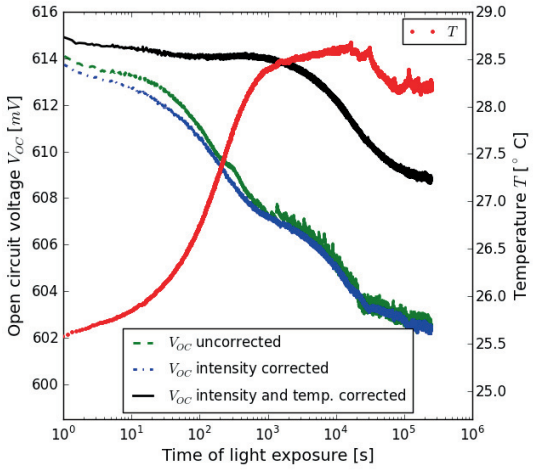

(b)

Figure 3-9 (a) (Triangles) Long-term V_{OC} decay transient of boron doped Cz-Si solar cell. After illumination is turned on (0 sec) the V_{OC} drops rapidly during the first hundreds of seconds before a slower decay proceeds for the next 24 hours. (Dots) Long-term I_{SC} decay transient showing a slow degradation but no rapid initial degradation. (b) Uncorrected and corrected V_{OC} decays and corresponding cell temperature

profile for the same time interval showing a significant temperature increase during the first hundreds of seconds after the illumination is turned on.

Ignoring the initial V_{OC} decay the relative loss of efficiency for the measured cells was in the order of 3 % being reduced from approximately 15 to 14.6 %. The drop in V_{OC} accounts for about 40% while the drop in I_{SC} accounts for about 50% of the loss. A small percentage (0-10 %) is also lost as a consequence of reduction in the fill factor. Similar findings are reported by other groups. [47],[13],[48]

3.2.3 THE V_{OC} DEPENDENCE ON TEMPERATURE

It is well known that the V_{OC} is highly dependent on the temperature of the solar cell. The effect is caused by the temperature dependence of the dark current, J_0, and the effect is reported to give a reduction in V_{OC} in the order of -2.0 to -2.3 mV/K [19]. A 100mW/cm^2 illumination source is introducing a significant amount of heat into the cell. Depending on the cooling system applied in the experiment the heating will occur during the first seconds to minutes of the illumination before it stabilizes. Accordingly, for boron-doped Cz-Si cells, where an initial B-O related defect decay is also occurring during the first minutes, special attention must be given to the temperature rise in the beginning of the measurement in order to differentiate between the heating and the B-O defect related effect.

In Figure 3-10 experimentally measured V_{OC} is plotted as a function of the corresponding cell temperature for the time interval equivalent to the initial rapid decay. The figure shows a linear decrease of V_{OC} versus T. This clearly indicates that the V_{OC} decay observed in this time interval for this particular sample is due to a temperature change. The reason why we do not observe any rapid B-O related defect for this sample is because J_0 is dependent on the *effective* minority carrier lifetime through the diffusion length L_n:

$$J_0 = q\frac{D_n n_i^2}{L_n N_A} \tag{3.9}$$

where

$$L_n = \sqrt{D_n \times \tau_{eff}} \tag{3.10}$$

and q is the electronic charge, D_n is the diffusivity of the minority carriers, N_A is the doping concentration and n_i is the intrinsic carrier concentration. The inverse of τ_{eff} is the sum of the inverse of all the individual contributions to lifetime as exemplified in Eq. 2.9. This means that if we have an area, e.g. the backside surface, which compared to the bulk, has a very low lifetime, small changes in the bulk lifetime will not be apparent in the effective lifetime because the contribution from the backside surface will be dominating. Consequently this will also be the case for the effective diffusion length. Accordingly, we believe that in this study the rapid lifetime decay is not detectible in V_{OC} because of high backside recombination velocity. Anyway, it is very important to be aware of the fact that a high intensity illumination source will induce heating of the cell until the whole system, table, chuck and cell have

stabilized. A proper temperature controlled sample stage can transfer heat equivalent to 10-100 mW/cm² absorbed by the cell and obtain steady state, but will not be able to compensate for the instantaneous heating of the cell. As already discussed, even the slightest cell heating will result in a decrease in the V_{OC}.

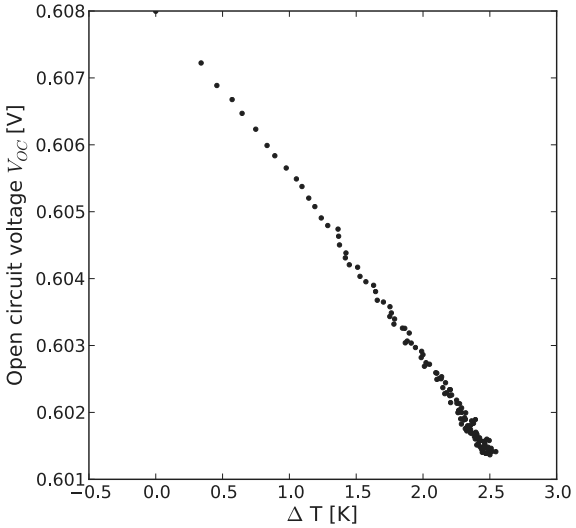

Figure 3-10 V_{OC} versus ΔT for the time interval corresponding to the initial rapid V_{OC} decay. The curve is approximately linear, indicating that changes in the temperature is the only mechanism affecting the V_{OC}. dV_{OC}/dT = -2.6 mV/°C.

3.2.4 CURRENT INDUCED DEGRADATION OF V_{OC} IN THE DARK

As the degradation not only occurs under illumination but also when minority carriers are injected in the dark, degradation of boron-doped silicon can also be induced by a forward bias to the cell in the dark. Some work in this area was performed at the University of Konstanz in Germany and has not been reported elsewhere. The motivation for reporting it here is to complete the review on methods to measure degradation decays and compare the various techniques for measuring B-O related degradation.

Before the current induced degradation (CID) the solar cells were annealed in the dark at 200°C for 10 min to recover the initially high lifetime value before placing on a preheated vacuum chuck in the dark. The temperature of the CID setup was measured using a PT-100 thermocouple and the temperature was stable within ±1 K. V_{OC} of the cell was measured by using a halogen lamp giving an intensity of 50 mW/cm² and the time resolution of the CID measurement is about 10 sec with this setup. The measurement data were corrected for temperature and intensity fluctuations the same way as for I-V measurements described in paper I. An example

of a CID measurement performed on a cell from a neighboring cell of the cell measured in Figure 2-3 is given in Figure 3-11. The voltage decrease has not yet reached saturation but it is clear that the curve approaches a saturation value. As in Figure 2-3 the rapid decay is not very evident in this measurement and a high backside recombination velocity will overshadow changes in the bulk lifetime at high values and thus the measured V_{OC}.

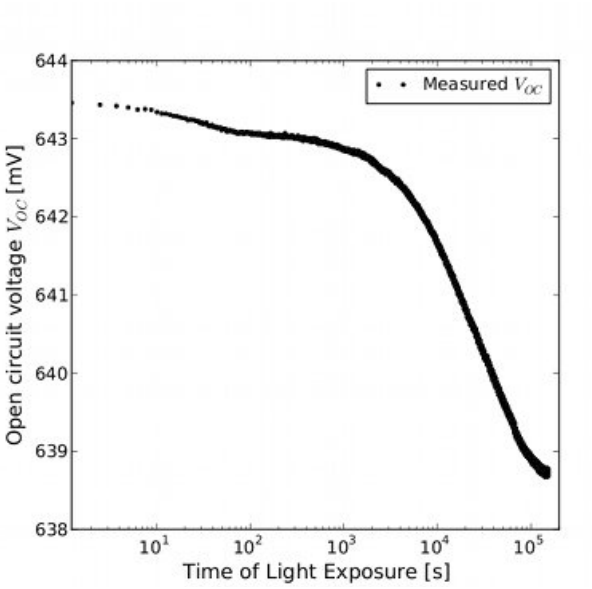

Figure 3-11 Current induced degradation curve. 225 mA for two days. The V_{OC} is measured at an intensity corresponding 0.5 sun. The rapid decay is detectable but is not as significant as expected.

The CID technique is in many ways a more robust way of measuring changes in V_{OC} due to B-O related degradation than LID. One advantage is the ability to precisely adjust the carrier density in the conduction and valence bands by applying a defined voltage in the dark. This opens for measuring recombination properties under very low carrier densities corresponding to light intensities well below 1/100 of a sun. Such low light intensities are difficult to control by adjusting a xenon or halogen lamp. In the next chapter we describe yet another technique to obtain low carrier densities, this is a fundamentally different technique where we can monitor the carrier concentration until it ceases by letting the carriers in a light-exposed area diffuse into an unexposed area.

Another advantage of the CID technique compared to LID with the I-V setup is that the temperature of the cell and setup are more easily controlled. A disadvantage is, however, that even though the degradation is caused by an applied bias in the dark the V_{OC} is still measured by illuminating the cell for a very short period of time. If a very low applied bias is employed such an illumination of the cell

can contribute significantly to the degradation and hence the measurements from the first minutes are vulnerable.

3.3 SUMMARY

In this chapter three different methods of measuring light and current induced degradation of p-type Cz-material have been described. Strengths and weaknesses of the three methods have been addressed. When B-O related defects are affecting the material, either as LID or CID, the number of recombination centers increases. This we can measure either by measuring the decay in the lifetime as the time of light exposure proceeds, or we can study the effect the degradation has on the electrical parameters (J_{SC} and V_{OC}) on a finished solar cell. In the present work we have custom-made an experiment for measuring light induced lifetime decay from a standard QSSPC instrument and an IV-measurement experiment with a continuous light source programmed to repeatedly do measurements throughout the light exposure. Since the degradation is caused by the presence of excess minority carriers and photons are not directly involved, the defects can also be generated simply by applying a forward bias to the cell. This principle is employed in an experiment for current induced degradation (CID).

Previously certain relations between [B], [O] have been reported together with the kinetics and concentration of the B-O related degradation. The saturated defect concentration for both the fast and the slow decay are reported to be proportional to [B] and $[O]^2$. Furthermore, the saturation times, related to the kinetics of the defect generation, was reported to be proportional to $1/[B]^2$, i.e. an exponential relationship, and independent of [O]. In the present work we did not find a correlating trend between the defect concentration and either [O] or [B]. We found, however, that the kinetics of defect degradation is closely related to p_0. Our conclusion is therefore that boron and oxygen do not necessarily act as constituents of the defect complex although both have to be present in the material in order for the defect to be generated (see chapter 2.2.1.) Accordingly, the present work opens for other possibilities concerning the elements constituting the defect complex. Further work is still needed in order to determine the composition of the defect complex.

B-O related defect centers reduce both the current and the voltage output from a solar cell. This is because recombination of carriers decreases the carrier collection and increases the dark current. The measured degradation in J_{SC} and V_{OC} can be fully explained by the reduction in charge carrier diffusion length as a result of the increasing concentration of B-O recombination centers, but J_{SC} and V_{OC} are sensitive to cell processing and the full picture of the degradation might be lost due to other process-induced recombination sites. When a 1 sun illumination source is applied it is impossible to avoid a slight increase in the temperature of the cell during the beginning of the illumination, which means that temperature control is crucial when V_{OC} is measured. In order to study the fundamentals of B-O related degradation we therefore recommend to study the decay in lifetime rather than studying the electrical parameters. By studying the change in lifetime both the fast and the slow lifetime decay can be accurately assessed allowing a better

understanding of the physical explanation behind this defect. Still, one should never forget that it is the conversion efficiency from the finished solar cell that in the end matters, so measuring the effect of B-O related degradation on the actual product will always be of relevance.

REFERENCES

[3] K. Bothe and J. Schmidt, "Electronically activated boron-oxygen-related recombination centers in crystalline silicon," *Journal of Applied Physics,* vol. 99, pp. 013701-11, 2006.

[4] J. Schmidt and K. Bothe, "Structure and transformation of the metastable boron- and oxygen-related defect center in crystalline silicon," *Physical Review B,* vol. 69, p. 024107, 2004.

[13] H. Hashigami, Y. Itakura, and T. Saitoh, "Effect of illumination conditions on Czochralski-grown silicon solar cell degradation," *Journal of Applied Physics,* vol. 93, pp. 4240-4245, 2003.

[15] S. W. Glunz, S. Rein, J. Y. Lee, and W. Warta, "Minority carrier lifetime degradation in boron-doped Czochralski silicon," *Journal of Applied Physics,* vol. 90, pp. 2397-2404, 2001.

[16] J. Nelson, *The physics of solar cells*. London: Imperial College Press, 2003.

[19] M. A. Green, *Solar cells operating principles, technology and system applications*. Kensington: University of New South Wales, 1998.

[27] D. Macdonald, F. Rougieux, A. Cuevas, B. Lim, J. Schmidt, M. Di Sabatino, and L. J. Geerligs, "Light-induced boron-oxygen defect generation in compensated p-type Czochralski silicon," *Journal of Applied Physics,* vol. 105, pp. 093704-7, 2009.

[30] M. Forster, E. Fourmond, F. E. Rougieux, A. Cuevas, R. Gotoh, K. Fujiwara, S. Uda, and M. Lemiti, "Boron-oxygen defect in Czochralski-silicon co-doped with gallium and boron," *Applied Physics Letters,* vol. 100, pp. 042110-4, 2012.

[38] R. A. Sinton, A. Cuevas, and M. Stuckings, "Quasi-steady-state photoconductance, a new method for solar cell material and device characterization," in *Photovoltaic Specialists Conference, 1996., Conference Record of the Twenty Fifth IEEE*, 1996, pp. 457-460.

[39] A. Cuevas, M. Stocks, D. McDonald, M. Kerr, and C. Samundsett, "Recombination and trapping in multicrystalline silicon," *Electron Devices, IEEE Transactions on,* vol. 46, pp. 2026-2034, 1999.

[40] W. Kern, "The Evolution of Silicon Wafer Cleaning Technology," *Journal of The Electrochemical Society,* vol. 137, pp. 1887-1892, June 1, 1990 1990.

[41] W. Shockley and W. T. Read, "Statistics of the recombination of holes and electrons," *Physical Review,* vol. 87, pp. 835-842, 1952.

[42] K. Bothe and J. Schmidt, "Fast-forming boron-oxygen-related recombination center in crystalline silicon," *Applied Physics Letters,* vol. 87, pp. 262108-3, 2005.

[43] J. S. H. Nagal, A. G. Aberle and R. Hezel, "Exceptionally high bulk minority-carrier lifetimes in block-cast multicrystalline silico," in *the 14Ih European Photovoltaic Solar Energy Conference*, 1997, pp. 762-765.

[44] L. I. Murin, J. L. Lindstrøm, V. P. Markevich, A. Misiuk, and C. A. Londos, "Thermal double donor annihilation and oxygen precipitation at around 650 C in Czochralski-grown Si: local vibrational mode studies," *Journal of Physics: Condensed Matter,* vol. 17, p. S2237, 2005.

[45] P. W. Atkins, *Physical chemistry*. Oxford: Oxford University Press, 1978.

[46] S. Rein, W. Warta, and S. W. Glunz, "Investigation of carrier lifetime in p-type Cz-silicon: specific limitations and realistic prediction of cell performance," in *the Conference Record of the Twenty-Eighth IEEE Photovoltaic Specialists Conference*, 2000, pp. 57-60.

[47] A. Herguth, G. Schubert, M. Kaes, and G. Hahn, "Avoiding Boron-Oxygen Related Degradation in Highly Boron Doped CZ Silicon," in *the 21st EU-PVSEC*, Dresden, 2006.

[48] M. Sheoran, A. Upadhyaya, and A. Rohatgi, "A Comparison of Bulk Lifetime, Efficiency, and Light-Induced Degradation in Boron- and Gallium-Doped Cast mc-Si Solar Cells," *IEEE Transactions on Electron Devices,* vol. 53, pp. 2764-2772, 2006.

CHAPTER 4

SPOT-LID

Spot-LID is a technique that we have developed to study the spatial variations of light induced degradation (LID) resulting from localized carrier excitation by a fine-tuned light source. The work is based on the idea that when the injected minority carriers are allowed to diffuse into an unexposed part of a boron-doped silicon wafer, B-O related recombination centers will form and by comparing the concentration of the excess minority carriers (Δn) to the reduced lifetime resulting from the B-O related centers, valuable information on the nature of the B-O related defects can be obtained. PL imaging is commonly used to study the concentration of minority carriers under homogenous illumination. The novel feature about our method is that we study the concentration of the diffusing minority carriers in a non-illuminated area. In this area the minority carriers form a decreasing concentration profile where the minority carrier concentration is high close to the light exposed area and reduced with the distance to the exposed area. This means that we have the opportunity to study a whole range of minority carrier concentrations simultaneously. The work has resulted in two papers, Paper II and Paper III. The results will not be repeated here, but a description of the technique and some supplemental analysis will be reviewed.

4.1 PHOTOLUMINESCENCE IMAGING

All the spot-LID measurements have been performed in a LIS-R1 photoluminescence (PL) imaging system from BTimaging. The two custom built setups for localized illumination of samples (Spot-LID setup 1 and Spot-LID setup 2) are both located within the PL imaging chamber and are described in Chapter 4.2 and Chapter 4.3 respectively. In the present chapter a description of the PL imaging technique in general will be presented.

PL imaging is a characterization technique based on the mapping of PL intensity across large sample areas. The method is a non-contact, non-destructive technique where light from a laser is directed onto a sample and photo-excitation will occur. The photo-excitation causes the electrons of the investigated material to be excited to a higher electronic state, and the material will release energy as photons as the electrons relax back to a lower energy level. These photons are collected by a detector that gives a PL signal in respect to the counted number of photons. The quantity of PL emitted from a material is directly related to the concentration of the excess minority carriers, which in turn can be directly related to the rate of the recombination of the carriers.

PL imaging in the LIS-R1 setup is accomplished by using a laser with a wavelength of 808 nm that exposes the entire wafer by the use of a beam expander (See Figure 4-1). The penetration depth for this wavelength is about 11.5 μm but due to immediate diffusion of carriers the excited minority carriers will almost instantly spread uniformly over the thickness of the sample. This is valid as long as the diffusion length of the minority carriers in the sample is significantly longer than the thickness of the samples. This is more thoroughly described under chapter 4.3.5 *Carrier diffusion profile over the sample thickness.* The resulting variation in PL-emission is measured with a CCD-camera.

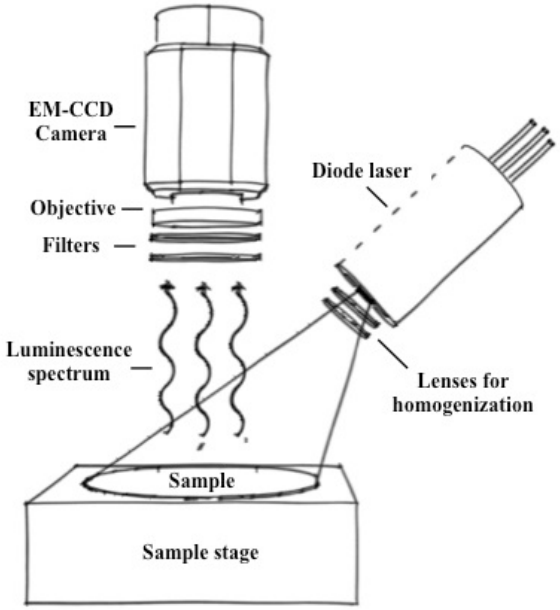

Figure 4-1 Illustration of the PL imaging equipment. A diode laser is used to inject carriers homogenously over the full sample and the generated photoluminescence from when the

carriers thermalize is detected by a charge coupled device camera, which has a resolution down to 0.023 mm.

The band-to-band luminescence of an illuminated silicon sample is determined by the radiative band to band recombination rate R_{rad} (given for p-type silicon):

$$R_{rad} = B_{rad} np \approx B\Delta n(\Delta n + N_A) \quad 4.1$$

Δn is effectively the integrated excess minority carrier density throughout the sample thickness and it is assumed that Δn is much larger than the intrinsic concentrations. N_A is the dopant density and B_{rad} is the radiative recombination coefficient of silicon at room temperature.

The fraction of the total luminescence that is detected in the CCD camera of the PL imaging setup is determined by the optical surface properties of the samples, the geometry of the setup (e.g. distance to sample, reflectance from stage), and the optics of the CCD camera. This is included in the calibration factor C that relates the sample luminescence to the detected PL intensity I_{PL} in the PL image:

$$I_{PL} = CB\Delta n(\Delta n + N_A) \quad 4.2$$

where I_{PL} is the camera signal and the calibration constant, C, can be determined by an independent lifetime measurement by QSSPC. There is a built-in QSSPC in the PL imaging setup where the measurement principles described in 3.1.1 are applied. As already mentioned in chapter 2.1.3 the relation between the effective lifetime τ_{eff} and the injection level Δn (at steady state) is known:

$$\tau_{eff} = \frac{\Delta n}{G} \quad 4.3$$

τ_{eff} can thus be determined when the generation rate, G is known. G is the effective generation rate, determined from the photon flux ϕ_e of the excitation laser, the thickness of the wafer W, and the reflectance R_e of the sample at the excitation wavelength (808 nm for the LIS-R1 setup). With these parameters, G becomes:

$$G = \frac{\phi_e(1 - R_e)}{W} \quad 4.4$$

It is assumed that all the photons (with 808 nm wavelength) absorbed generate an electron-hole pair in the sample. (When determining Δn, in Paper II and III, G is calculated by the same principal as given above taking also the depth of the sample into consideration. The flux ϕ_e is determined as given in 4.3.4.)

The PL imaging technique is a true steady-state technique because of the constant laser intensity. The imaging is very fast (seconds) and the resolution is good (down to 23 μm). An example where a PL image is taken before and after spot-LID through a slit is given in Figure 4-2. The image contains high and low luminescence intensity areas, which can be related to carrier lifetime through Eq. 4.1. However, low intensity regions can also be due to lower doping concentrations

or local defects as elemental impurities, physical defects or grain boundaries in multi-crystalline silicon. Optical effects such as scratches must be separated from material effects.

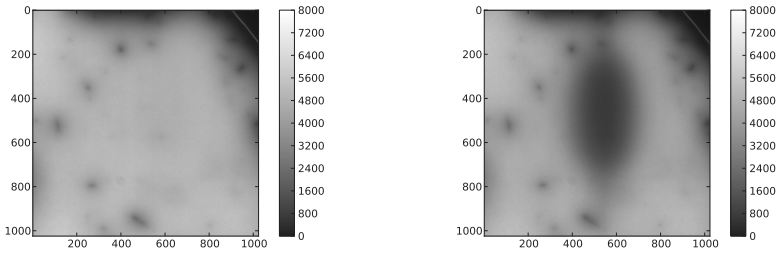

(a) (b)

Figure 4-2 An example of PL images. Black regions are regions of low PL signal and accordingly low lifetime. Lighter regions are regions of enhanced lifetime. a) and b) are images of a sample before and after spot-LID (with setup 1) for 25 h. The scales are PL intensity, which is relative to the acquisition time. The images are taken with a high magnification lens and are measuring 23 × 23 mm (1024 × 1024 pixels).

4.2 SETUP FOR LOCALIZED CARRIER EXCITATION (SPOT-LID EXPERIMENT 1)

Exciting carriers locally generates a B-O defect profile as the excited minority carriers diffuse into the unexposed neighboring area. With the Spot-LID experiment 1 we studied the effect of this defect profile by lifetime measurements/PL imaging. In Figure 4-3 the setup for localized carrier excitation (spot-LID experiment 1) used to obtain the results in Paper II is shown. Here the wafer is locally illuminated in a small area on the rear side through a mask with a slit measuring 0.29 mm in width, e.g. a large part of the mask is illuminated but only a small area of the wafer is exposed. The width of the slit is not critical but for practical reasons, i.e. being able to observe degradation on both sides of the slit within the boarders of the magnified lens image (23 × 23 mm), it is convenient to use a narrow slit. A too narrow slit can, however, result in problems with light diffraction at the edges of the slit mask and should be avoided. The illumination source is a broad band halogen spectrum lamp from Ocean Optics (HL-2000-HP) with a connected optical fiber and a 900 nm short pass filter resulting in a photon flux of $1.41 \pm 0.1 \times 10^{16}$ cm^{-2} s^{-1}. A halogen spectrum cut off at 900 nm has a penetration depth of approximately 15 μm in silicon. Notice that for this experiment the spot-illumination is turned off when the PL image is taken. This is different from the SpotLID experiment 2 where the spot-illumination was left on during the image acquisition in order to monitor Δn directly. This was not possible with the Spot-LID 1 setup due to the light source we had available at that time. The profile of Δn was,

however, successfully simulated in the Spot-LID 1 work and from the simulation of the Δn profile and the measured extension of B-O related defects we could investigate the relation between the two. The results are given in Paper II.

Simulations of the minority carrier distribution over the thickness of the sample showed that due to immediate diffusion of carriers there was, as for the excitation of minority carriers by the 808 nm laser, virtually no minority carrier concentration difference in this direction. This is more thoroughly described in chapter 4.3.5.

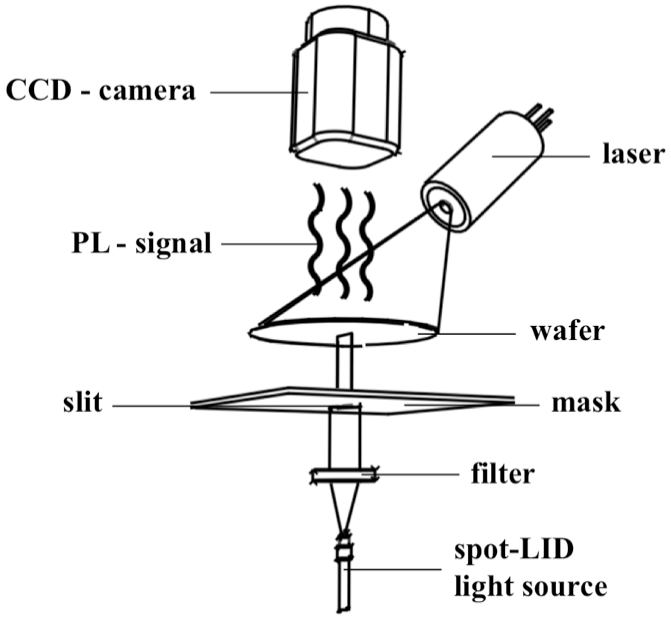

Figure 4-3 The localized carrier excitation (Spot-LID) setup for Paper II. The wafer is exposed to light through a confined slit on the rear side of the wafer while photoluminescence from the entire wafer, generated by the LIS-R1 PL-imaging system laser, is collected from the other side.

4.3 SETUP FOR DIRECT MONITORING OF MINORITY CARRIER DENSITY (SPOT-LID EXPERIMENT 2)

In this experiment (basis for Paper III) a 4.5 mW diode laser with a wavelength of 780 nm was employed to illuminate a specific area of the wafer (See Figure 4-4). The major difference in this setup compared to the Spot-LID setup 1 is that in this setup no mask is used to limit the illuminated area but a laser beam is shaped and focused into a narrow line with a Gaussian half width of 50 ± 5 µm. The incidence angle was set to 10 degrees to avoid detection of the specular reflection from the laser beam by the charge-coupled device (CCD) camera. When the laser is turned on, the generated excess minority carriers (Δn) will diffuse from the illuminated area into the adjacent area following the continuity equation and the PL can be measured directly as the electrons falls back to the valence band (see Figure 4-5). Using the Spot-LID setup 2 we are able to measure the Δn profile directly as opposed to in Spot-LID setup 1 where we had to simulate this profile. An example of such a measurement is shown in Figure 4-6.

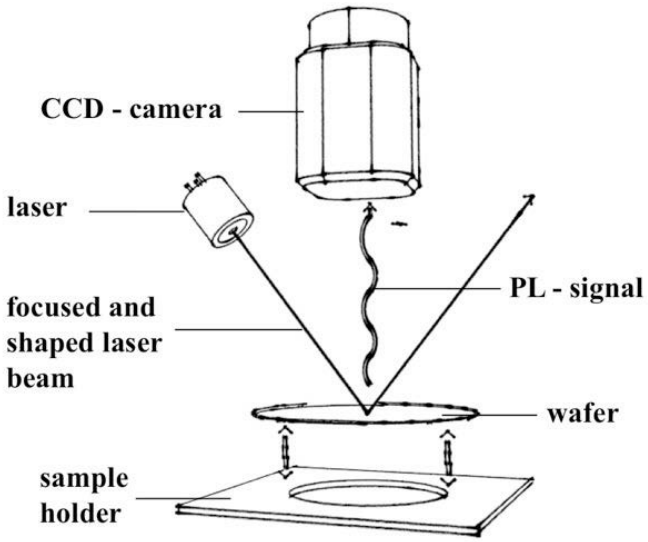

Figure 4-4 Sketch showing the Spot-LID 2 setup for direct monitoring of excess carrier density during light induced degradation. The wafer is exposed to a focused and shaped laser beam while the PL signal is collected by the CCD camera.

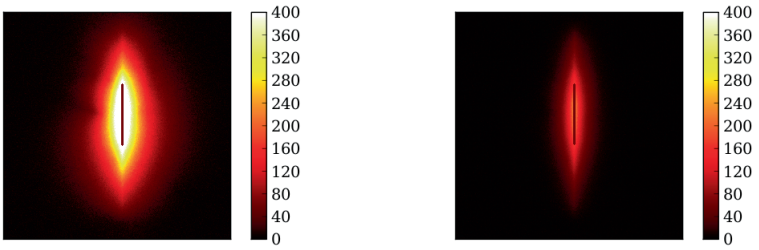

(a) (b)

Figure 4-5 PL intensity data (normalized to exposure time) taken a) immediately when the light soaking is started, t = 0 and b) after light soaking for t = 3 min. The position and width of the exposed area is superimposed on the image, as indicated by the vertical grey line. Data acquisition time is 0.5 s. By comparing the images it is obvious that the carrier density decreases with increased time of light exposure. This is due to the shorter minority carrier lifetime caused by the generation of B-O related defects. The images are taken with a high magnification lens and are measuring 23 × 23 mm (1024 × 1024 pixels).

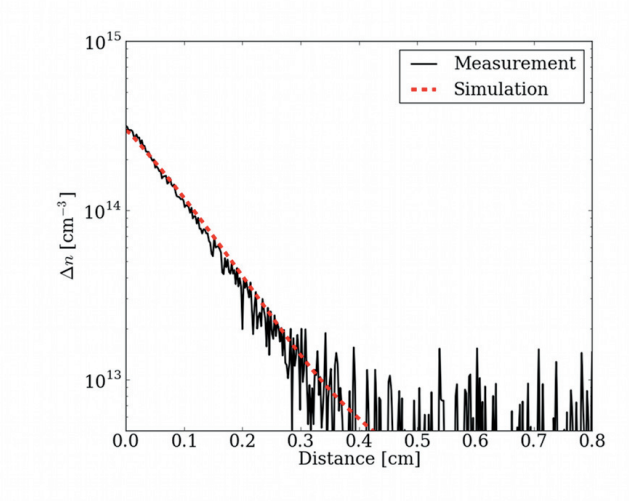

Figure 4-6 The measured and calibrated Δn profile (black curve) The dashed curve corresponds to a simulation of the profile described in Paper III.

In order to quantify the Δn profile in the Spot-LID 2 experiment, from the detected PL signal, a calibration is necessary. Such a procedure is described in chapter 4.3.1. When this calibration is performed the diffused minority carrier density distribution (during light exposure) can be compared to the observed defect generation in the same area. The method is not limited to materials that degrade

with light but can be employed on any material where a Δn profile is of interest. The results from this analysis are reported in Paper III.

4.3.1 CALIBRATION PROCEDURE

Accurate calibration of LID-samples requires some adaptation of the standard calibration procedure described in chapter 4.1. Since the sample degrades rapidly directly after annealing (see chapter 3.1), even the short exposure to light during a standard QSSPC measurement will introduce significant errors. When the sample is annealed, the state of the sample will already be different during the PL image acquisition and the QSSPC measurement used for the calibration. Furthermore, for inhomogeneous samples (scratches etc.) it is necessary to take into account the sensitivity function of the QSSPC coil.

In order to carry out a correct calibration, taking into account the above-mentioned effects, some adjustments to the standard QSSPC calibrations were made. The following procedure was used for this work:

1. The sample is light soaked (a normal desktop lamp is sufficient) for 5 hours before carrying out the calibration, in order to have a more stable sample during the calibration.

2. The time profile of the light pulse used for the QSSPC measurement is adapted to a box-shaped pulse, with maximum amplitude corresponding the excitation intensity used during the PL imaging (typically 1 sun). The length of the pulse is also minimized in order to minimize heating and LID during the calibration. The result of the QSSPC measurement should give a constant level of carrier density corresponding to the maximum amplitude of the excitation pulse.

3. Three sets of calibration measurements are carried out, while light soaking for 30 minutes between each measurement to ensure that the stability of the sample is sufficient. The calibration factor should be independent of the further light soaking.

SUPPLEMENTING ANALYSIS

In order to do the work described in this chapter some supplementing analysis was needed. All of the analyses listed below are relevant for both the Spot-LID setup 1 and 2, reported in Paper II and Paper III, respectively.

4.3.2 SURFACE PASSIVATION

As discussed in chapter 3.1.3 surface passivation is essential when measuring bulk minority carrier lifetime. When measuring light induced lifetime decay, introducing a film of a-Si:H on the sample opens up for the possibility that it is the film that is degrading and not the bulk. If the a-Si:H passivation layer is degrading with light the measured effective lifetime τ_{eff} would be reduced and could have led to the misinterpretation that the bulk lifetime had been degraded. Thorough testing with both of the described spot-LID setups was therefore performed with both float zone wafers and n-type wafers (not subject to LID) deposited with the identical a-Si:H passivation as the reported samples. In Figure 4-7 images of a FZ-Si sample before (a) and after (b) spot-LID is shown. In (b) the sample is moved away from the mask and no sign of degradation can be seen. The surface recombination velocity (SRV) for the a-Si:H passivation layer of the investigated samples were estimated to be below 20cm/s.

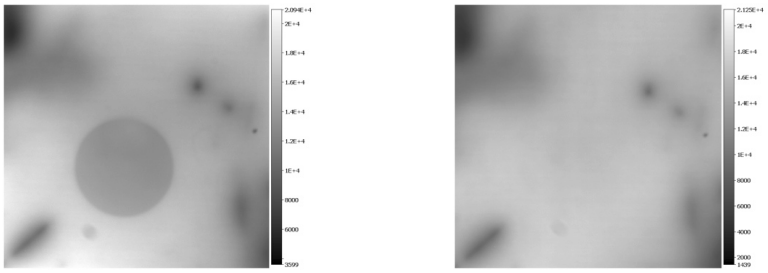

(a) (b)

Figure 4-7 PL images of FZ Si before and after spot-LID. In (a) the sample is not exposed to any light yet but one can clearly see the circle/hole of which the sample is going to be illuminated through. The hole in the mask is visible in (a) because no PL is reflected here. (In (b) the sample is moved away from the hole.) In (b) the sample has been exposed to a light source through the hole in the mask for 17 h but no sign of degradation can be seen. This proves that the a-Si:H passivation is not degraded by this treatment.

4.3.3 REFLECTANCE MEASUREMENTS

Reflectance measurements were performed with a Solar Cell Analysis System from pv-tools. The reflectance data is used as input in the PL imaging measurements. Reflectance values were measured for all sample types for the different light sources (integrated PL imaging laser (λ = 808 nm), halogen lamp for Spot-LID I setup and laser (λ = 780 nm) for Spot-LID II setup). The basics for the measurements are a halogen/xenon lamp (λ > 300 nm) where the beam is sent via a monochromator into an integrated sphere positioned directly over the sample of interest. The reflectance from the sample is compared to a known reflectance standard. A typical reflectance as a function of wavelength measurement is shown in Figure 4-8.

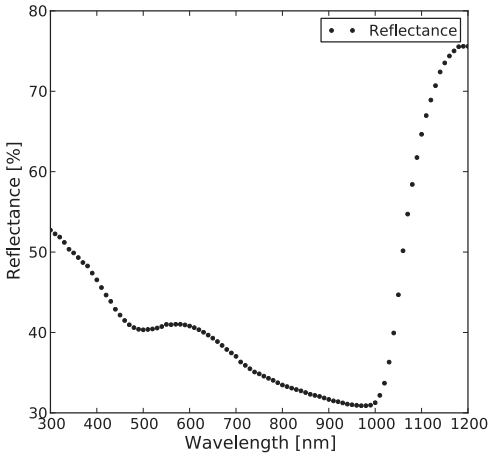

Figure 4-8 Reflectance in % as a function of wavelength for a typical sample used for Spot-LID measurements.

4.3.4 PHOTON FLUX MEASUREMENTS

In Paper II the photon flux ϕ of the Spot-LID light source is used to tune the laser intensity of the integrated PL-imaging laser so that the calibrated lifetime measured at this laser intensity can be used as estimate for the spot-illumination source. In Paper III the photon flux ϕ is used to calculate the generation rate G necessary to simulate the spatial carrier concentration profile. The photon flux was measured by a calibrated photon spectrometer from Avantes (AvaSpec - 2048) with a cosine corrector connected to the calibrated fiber.

To determine the peak photon flux ϕ and the Gaussian beam half width, σ, of the laser used for spot illumination in the spot-LID experiment 2, a beam profile

measurement was performed by a Camera Beam Profiler (BC106-VIS) from ThorLabs.

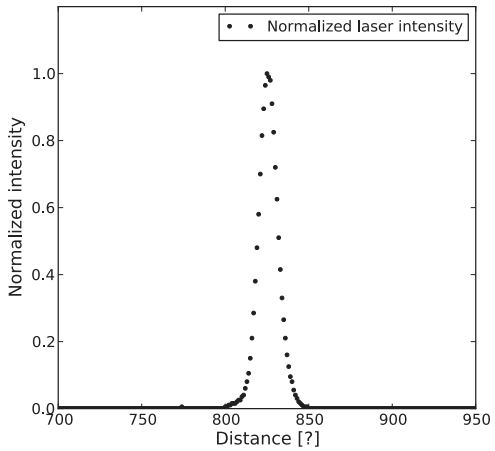

Figure 4-9 Beam profile measurement of the laser used in the Spot-LID 2 experiment. The Gaussian beam half width, σ, was determined to 50 ± 5 µm.

4.3.5 CARRIER DIFFUSION PROFILE OVER THE SAMPLE THICKNESS

In order to measure and simulate the lateral Δn profile generated by a localized illuminated area we need to know how Δn is distributed over the thickness of the wafer. In this work mainly high lifetime wafers are used where the diffusion length is several millimeters. If the diffusion length is in the same order as the thickness of the sample, this would lead to non-uniformity. A second requirement for uniform distribution of carriers is that there is a high quality passivation layer on both sides of the wafer. If there was a high recombination velocity on the surfaces this would lead to a decline of carriers in the vicinity of the surfaces. Simulations of the minority carrier distribution showed that due to immediate diffusion of carriers there is, as for the excitation of minority carriers by the 808 nm laser, virtually no minority carrier concentration difference over the thicknesses of the different samples studied. This is also confirmed by other groups [49],[12].

4.4 SUMMARY

In this chapter we have explained and discussed the two experiments developed for the work on spot-LID. Spot-LID is simply explained a technique where the concentration of the B-O related defect concentration is directly related to the concentration of excess minority carriers in the material. Spot-LID is a new way of studying the B-O related defect process, in which the excess minority carrier concentration is quantified during the light exposure. Local excess carrier generation, where the wafer is exposed to light in a confined area, causes the excess electrons to diffuse out into the wafer, allowing us to study the degradation effect of a continuously varying electron concentration. This concentration can be monitored by means of photoluminescence (PL) imaging. Both the conventional PL imaging technique and the two custom-made Spot-LID experiments are explained. In order to do Spot-LID analysis on a material a reflectance measurement of the sample must be performed. It is also crucial to have full control of the time and illumination stability of the passivation layer.

The excess minority carrier concentration (Δn) profile is determined from the PL signal from the wafer. The PL signal is directly related to Δn through a relation involving a calibration factor. In order to quantify Δn it is thus crucial to properly determine this calibration factor and a procedure on how to do this is given.

The main differences in the two spot-LID experiments presented is that in the Spot-LID 1 setup a mask is used to limit the illuminated area whereas in the 2 setup a laser beam is shaped and focused into a narrow line circumventing the need of a physical mask. Also the Spot-LID 2 setup enables us to measure the Δn profile directly as opposed to the Spot-LID setup 1 where this profile was simulated. The Spot-LID 2 setup can in many ways be regarded as a refinement of the Spot-LID 1 setup, but the results and outcome from the work with the Spot-LID 1 setup is still unique and valuable as a proof of concept for the Spot-LID principle.

REFERENCES

[12] V. V. Voronkov, R. Falster, J. Schmidt, K. Bothe, and A. V. Batuninac, "Lifetime Degradation in Boron Doped Czochralski Silicon," *Electrochemical Society Transactions,* vol. 33, pp. 103-112, 2010.

[49] T. Trupke, "Influence of photon reabsorption on quasi-steady-state photoluminescence measurements on crystalline silicon," *Journal of Applied Physics,* vol. 100, p. 063531, 2006.

CHAPTER 5

CONCLUDING REMARKS

The main motivation for this thesis has been to gain more fundamental insight into the topic of B-O related degradation of boron doped Czochralski silicon and a new approach to study the B-O related defect has been developed: a method that enables us to observe the generation of the defect as a function of the concentration of excess minority carriers (Δn).

With the Spot-LID 1 experiment particular attention was paid to the determination of the minimum Δn being responsible for the *observable* lifetime degradation by the B-O related defect generation. Our measurements showed a measurable B-O related lifetime degradation for Δn down to $1.7 \pm 0.2 \times 10^9$ cm^{-3} (for the slow mechanism) but we believe that even the smallest minority carrier concentration will generate B-O related defects and that there is really no lower Δn limit for the generation of these defects.

With the Spot-LID 2 experiment we showed that above a certain minority carrier concentration limit (Δn_{lim}) the rate of the boron oxygen (B-O) defect generation is fully independent of the Δn. Δn_{lim} was determined for six different materials with six different normalized defect concentrations ($N^*_{t,sat}$) but no correlation between the obtained Δn_{lim} value and $N^*_{t,sat}$ was found. Our findings are in agreement with a model where the role of the minority carriers in the rapid degradation is to shift the quasi-Fermi energy causing a charge state change of a possible latent defect center, which must be in place for a further process to occur. The arithmetic average Δn_{lim} concentration from the measurement series yielded $1.84 \pm 0.9 \times 10^{11}$ cm^{-3} and the energy level of the latent defect center in its passive state was determined to be $E_{lat} = E_V + (635 \pm 18)$ meV.

Regarding the work on B-O related degradation kinetics we found that both the fast and the slow decay curves, for all the investigated samples, can be fitted very well to the solution of a simple second order rate equation. This indicates that the defect generation process can be described by second order reaction kinetics. The

rate equation describing our system thus shows that the rate of the reaction is changing with the square of a latent defect concentration. This shows that a reaction between two individual reactant molecules of different species cannot be the case, as the solution of a second order rate equation with two different reactants cannot fit the measured data. Previous work has suggested both substitutional and interstitial boron as possible constituents in the defect complex, however, in this work we have not seen any indication that $N_{t,sat}^{*}$ correlates to the boron concentration. The fact that the degradation effect has not been observed in gallium-doped but only boron-doped Cz silicon still ensures that the defect depends on boron, but not necessarily through directly being a constituent in the defect complex.

Referring to the list of B-O related degradation characteristics in chapter 2.2.1, these are the contributions to the understanding of B-O related defect from this thesis:

1. We show experimentally that above a certain minority carrier concentration limit, Δn_{lim}, the boron oxygen (B-O) defect generation rate is fully independent of the injected carrier concentration and we have determined the Δn value where the rate of the degradation becomes independent of Δn ($\Delta n_{\mathrm{lim}} = 1.84 \pm 0.9 \times 10^{11}$ cm^{-3}).
2. We have shown that B-O related degradation is occurring for Δn values at least as low as $1.7 \pm 0.2 \times 10^{9}$ cm^{-3}.
3. We have found that both the rapid and the slow B-O related lifetime decay fit well to a solution of a second order rate equation meaning that the concentration of the final defect center is changing with the square of a latent defect center. Further on, the reaction between two individual reactant molecules of different species can be ruled out, as the solution of a second order rate equation with two different reactants cannot fit the measured data.
4. We have verified that the kinetics of the light induced lifetime decay scales with the concentration of holes and not with the concentration of boron.
5. We have not found any clear correlation between the [B] and [O] and the B-O related defect concentration, indicating that these two do not necessarily need to be constituents in the defect complex.

CHAPTER 6

FURTHER WORK

With the Spot-LID 2 experiment, described in the Chapter 4.3, we monitor a minority carrier profile from an exposed to an unexposed area of the wafer directly by photoluminescence imaging. This is done by exciting a large concentration of carriers with a focused laser and detecting the generated photoluminescence by a photoluminescence imaging device. As noted in Paper III this can in principle be performed on any type of silicon material and the two topics that we will discuss in this chapter are both examples of this.

6.1 SPOT-LID ANALYSIS OF GRAIN BOUNDARIES IN MULTICRYSTALLINE SILICON

The Spot-LID principle applied on multicrystalline silicon (mc-Si) could possibly give interesting insight into recombination and transport across grain boundaries. A work on this was performed with the Spot-LID I setup (presented as a poster at the Crystalline Silicon Solar Cell Conference (CSSC-5) in Boston, November 2011) but could have been significantly improved by using the Spot-LID 2 setup. The mc-Si work with the Spot-LID I setup was based on the idea that when the injected minority carriers are allowed to diffuse into an unexposed part of a boron-doped silicon wafer, a footprint of activated B-O related recombination centers would delineate the extension of the minority carrier spreading and from this, information about the recombination activity of the grain boundaries could be obtained. With the Spot-LID 2 setup there is no requirement that the material must degrade from B-O related defects, the spreading of the excess carriers can be monitored directly. In **Figure 6-1** a summary of the mc-Si work performed with the Spot-LID 1 setup is

shown. 3 different types of grain boundaries and one grain with numerous dislocations were investigated. These were identified by electron backscattered diffraction (EBSD) and dislocation etching. Minority carriers were then allowed to diffuse from an illuminated spot in a small distance from the grain boundary and over the boundary. The continuity of the B-O related degradation over the boundary was subsequently analyzed. The extent of degradation on the other side of the boundary thus gave information about the recombination of minority carriers at the actual grain boundary. The results from this project showed that grain boundaries are not straightforward to categorize. There are a vast number of variations and if the objective is to draw general conclusions about the recombination activity of grain boundaries a large dataset with numerous of different grain boundaries should be collected. Our suggestion to further work is thus to use the Spot-LID 2 principle combined with scanning of large samples and theoretical analysis that can be used to model the recombination activity of each grain boundary in the sample. The novel feature about this method is that in conventional lifetime mapping techniques the recombination activity of the point of interest is a result of carrier diffusion from all sides. What is measured with Spot-LID 2 is how the point of interest is influenced by carrier diffusion in one particular direction. Combining data on carrier diffusion from different directions in the same point would give new insight into recombination activity of grain boundaries.

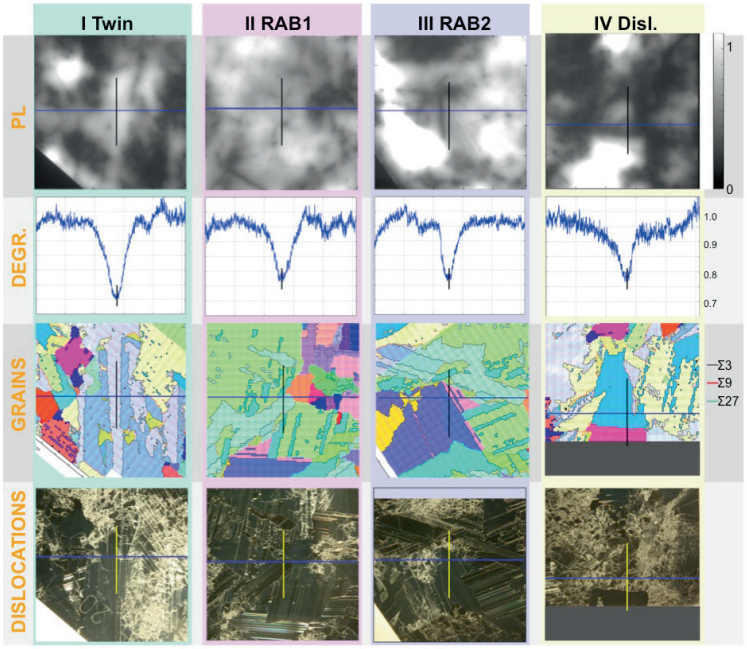

Figure 6-1 PL-maps, degradation profile, EBSD grain maps and dislocation maps for I) a twin boundary, II) a clean random angle boundary (RAB1), III) a decorated random angle boundary

(RAB2) and IV) a grain with numerous dislocations. The vertical black/yellow line demonstrates the position of the illuminated slit. The blue line shows the position of the normalized line scan (degradation). All maps are 23 x 23 mm.

6.2 USING SPOT-LID TO DETERMINE MINORITY CARRIER MOBILITY

This is a suggestion for an application of the described Spot-LID 2 experiment. The idea is to use the direct carrier concentration profiles to determine minority carrier mobility in for example compensated silicon material as a complement to other techniques like Hall effect measurements. Additionally, what the Hall effect measurement determines is the majority carrier mobility, whereas spot-LID quantifies the minority carrier mobility.

With Spot-LID 2 the minority carriers diffuse laterally into an unexposed area and logarithmic plots of the slope of the curves gives the diffusion length L_n directly. It is not even necessary to convert the PL signal into carrier concentration. The idea is then to determine the mobility μ_n from

$$\mu_n = \frac{L_n q}{\tau_n kT} \tag{6.1}$$

where q is the electronic charge, k is the Boltzmann constant, T is the temperature and τ_n is the lifetime of the electrons, which needs to be determined in a way that is independent of μ_n. The lifetime mapping technique *Carrier density imaging* (CDI) can provide this and by combining minority carrier diffusion length measurements by Spot-LID 2 with minority carrier lifetime measurements from CDI a method where the minority carrier mobility can be determined is available.

BIBLIOGRAPHY

[1] European Photovoltaic Industry Association, "Global market outlook for photovoltaics 2013-2017," 2013.

[2] International Energy Agency, "Technology Roadmap, Solar photovoltaic energy," 2010.

[3] K. Bothe and J. Schmidt, "Electronically activated boron-oxygen-related recombination centers in crystalline silicon," *Journal of Applied Physics,* vol. 99, pp. 013701-11, 2006.

[4] J. Schmidt and K. Bothe, "Structure and transformation of the metastable boron- and oxygen-related defect center in crystalline silicon," *Physical Review B,* vol. 69, p. 024107, 2004.

[5] E. Napolitani, D. De Salvador, R. Storti, A. Carnera, S. Mirabella, and F. Priolo, "Room Temperature Migration of Boron in Crystalline Silicon," *Physical Review Letters,* vol. 93, p. 055901, 2004.

[6] J. Schmidt, K. Bothe, D. Macdonald, J. Adey, R. Jones, and D. W. Palmer, "Mechanisms of Light-Induced Degradation in Mono- and Multicrystalline silicon solar cells," in *20th European Photovoltaic Solar Energy Conference*, Barcelona, 2005.

[7] M. Sanati and S. K. Estreicher, "Boron-oxygen complexes in Si," *Physica B: Condensed Matter,* vol. 376-377, pp. 133-136, 2006.

[8] A. Carvalho, R. Jones, M. Sanati, S. K. Estreicher, J. Coutinho, and P. R. Briddon, "First-principles investigation of a bistable boron-oxygen interstitial pair in Si," *Physical Review B,* vol. 73, p. 245210, 2006.

[9] M.-H. Du, H. M. Branz, R. S. Crandall, and S. B. Zhang, "Bistability-Mediated Carrier Recombination at Light-Induced Boron-Oxygen Complexes in Silicon," *Physical Review Letters,* vol. 97, p. 256602, 2006.

[10] D. W. Palmer, K. Bothe, and J. Schmidt, "Kinetics of the electronically stimulated formation of a boron-oxygen complex in crystalline silicon," *Physical Review B (Condensed Matter and Materials Physics),* vol. 76, pp. 035210-6, 2007.

[11] V. V. Voronkov and R. Falster, "Latent complexes of interstitial boron and oxygen dimers as a reason for degradation of silicon-based solar cells," *Journal of Applied Physics,* vol. 107, pp. 053509-8, 2010.

[12] V. V. Voronkov, R. Falster, J. Schmidt, K. Bothe, and A. V. Batuninac, "Lifetime Degradation in Boron Doped Czochralski Silicon," *Electrochemical Society Transactions,* vol. 33, pp. 103-112, 2010.

[13] H. Hashigami, Y. Itakura, and T. Saitoh, "Effect of illumination conditions on Czochralski-grown silicon solar cell degradation," *Journal of Applied Physics,* vol. 93, pp. 4240-4245, 2003.

[14] J. Schmidt and K. Bothe, "Structure and transformation of the metastable boron- and oxygen-related defect center in crystalline silicon," *Physical Review B (Condensed Matter and Materials Physics),* vol. 69, pp. 024107-8, 2004.

[15] S. W. Glunz, S. Rein, J. Y. Lee, and W. Warta, "Minority carrier lifetime degradation in boron-doped Czochralski silicon," *Journal of Applied Physics,* vol. 90, pp. 2397-2404, 2001.

[16] J. Nelson, *The physics of solar cells*. London: Imperial College Press, 2003.

[17] M. Zeman, "Solar Cells," Compendium to the course "Solar Cells", Delft University of Technology, Delft, 2006.

[18] M. A. Green, *Silicon Solar Cells: Advanced Principles & Practice*: Centre for Photovoltaic Devices and Systems, 1995.

[19] M. A. Green, *Solar cells operating principles, technology and system applications*. Kensington: University of New South Wales, 1998.

[20] K. A. Emery, "Solar simulators and I-V measurement methods," *Solar Cells,* vol. 18, pp. 251-260, 1986.

[21] A. Cuevas and D. Macdonald, "Measuring and interpreting the lifetime of silicon wafers," *Solar Energy,* vol. 76, pp. 255-262, 2004.

[22] J. Lagowski, P. Edelman, and A. Morawski, "Non-contact deep level transient spectroscopy (DLTS) based on surface photovoltage," *Semiconductor Science and Technology,* vol. 7, p. A211, 1992.

[23] H. Savin, M. Yli-Koski, and A. Haarahiltunen, "Role of copper in light induced minority-carrier lifetime degradation of silicon," *Applied Physics Letters,* vol. 95, p. 152111, 2009.

[24] H. Fischer and W. Pschunder, "Investigation of photon and thermal induced changes in silicon solar cells," in *the 10th IEEE Photovoltaic Specialists Conference*, Palo Alto, CA, 1973, pp. 404-411.

[25] J. Knobloch, S. W. Glunz, D. Biro, W. Warta, E. Schäffer, and W. Wettling, "Solar cells with efficiencies above 21% processed from Chochralski grown silicon," in *the 25th IEEE Photovoltaic Specialists Conference*, 1996, pp. 405-408.

[26] K. Bothe, R. Hezel, and J. Schmidt, "Recombination-enhanced formation of the metastable boron--oxygen complex in crystalline silicon," *Applied Physics Letters,* vol. 83, pp. 1125-1127, 2003.

[27] D. Macdonald, F. Rougieux, A. Cuevas, B. Lim, J. Schmidt, M. Di Sabatino, and L. J. Geerligs, "Light-induced boron-oxygen defect generation in compensated p-type Czochralski silicon," *Journal of Applied Physics,* vol. 105, pp. 093704-7, 2009.

[28] S. Rein, "Lifetime spectroscopy: a method of defect characterization in silicon for photovoltaic applications," ed: Springer-Verlag, Berlin, 2005, p. 422.

[29] V. V. Voronkov, R. Falster, K. Bothe, B. Lim, and J. Schmidt, "Lifetime-degrading boron-oxygen centres in p-type and n-type compensated silicon," *Journal of Applied Physics,* vol. 110, pp. 063515-7, 2011.

[30] M. Forster, E. Fourmond, F. E. Rougieux, A. Cuevas, R. Gotoh, K. Fujiwara, S. Uda, and M. Lemiti, "Boron-oxygen defect in Czochralski-silicon co-doped with gallium and boron," *Applied Physics Letters,* vol. 100, pp. 042110-4, 2012.

[31] L. I. Murin, E. A. Tolkacheva, V. P. Markevich, A. R. Peaker, B. Hamilton, E. Monakhov, B. G. Svensson, J. L. Lindstrøm, P. Santos, J. Coutinho, and A. Carvalho, "The oxygen dimer in Si: Its relationship to the light-induced degradation of Si solar cells?," *Applied Physics Letters,* vol. 98, p. 182101, 2011.

[32] S. W. Glunz, S. Rein, W. Warta, J. Knobloch, and W. Wettling, "On the degradation of Cz-silicon solar cells," presented at the 2nd World Conference on Photovoltaic Energy Conversion, Vienna, Austria, 1998.

[33] J. Schmidt, A. G. Aberle, and R. Hezel, "Investigation of carrier lifetime instabilities in Cz-grown silicon," in *the 26th IEEE Photovoltaic Specialists Conference*, 1997, pp. 13-18.

[34] S. W. Glunz, S. Rein, J. Knobloch, W. Wettling, and T. Abe, "Comparison of boron- and gallium-doped p-type Czochralski silicon for photovoltaic application," *Progress in Photovoltaics: Research and Applications,* vol. 7, pp. 463-469, 1999.

[35] Bianca Lim, Karsten Bothe, and Jan Schmidt, "Deactivation of the boron-oxygen recombination center in silicon by illumination at elevated temperature," *Physica Status Solidi - Rapid Research Letters,* vol. 2, pp. 93-95, 2008.

[36] A. Herguth, G. Schubert, M. Kaes, and G. Hahn, "Investigations on the long time behavior of the metastable boron–oxygen complex in crystalline silicon," *Progress in Photovoltaics: Research and Applications,* vol. 16, pp. 135-140, 2008.

[37] B. Lim, K. Bothe, and J. Schmidt, "Impact of oxygen on the permanent deactivation of boron--oxygen-related recombination centers in crystalline silicon," *Journal of Applied Physics,* vol. 107, pp. 123707-4, 2010.

[38] R. A. Sinton, A. Cuevas, and M. Stuckings, "Quasi-steady-state photoconductance, a new method for solar cell material and device characterization," in *Photovoltaic Specialists Conference, 1996., Conference Record of the Twenty Fifth IEEE*, 1996, pp. 457-460.

[39] A. Cuevas, M. Stocks, D. McDonald, M. Kerr, and C. Samundsett, "Recombination and trapping in multicrystalline silicon," *Electron Devices, IEEE Transactions on,* vol. 46, pp. 2026-2034, 1999.

[40] W. Kern, "The Evolution of Silicon Wafer Cleaning Technology," *Journal of The Electrochemical Society,* vol. 137, pp. 1887-1892, June 1, 1990 1990.

[41] W. Shockley and W. T. Read, "Statistics of the recombination of holes and electrons," *Physical Review,* vol. 87, pp. 835-842, 1952.

[42] K. Bothe and J. Schmidt, "Fast-forming boron-oxygen-related recombination center in crystalline silicon," *Applied Physics Letters,* vol. 87, pp. 262108-3, 2005.

[43] J. S. H. Nagal, A. G. Aberle and R. Hezel, "Exceptionally high bulk minority-carrier lifetimes in block-cast multicrystalline silico," in *the 14Ih European Photovoltaic Solar Energy Conference*, 1997, pp. 762-765.

[44] L. I. Murin, J. L. Lindstrøm, V. P. Markevich, A. Misiuk, and C. A. Londos, "Thermal double donor annihilation and oxygen precipitation at around 650 C in Czochralski-grown Si: local vibrational mode studies," *Journal of Physics: Condensed Matter,* vol. 17, p. S2237, 2005.

[45] P. W. Atkins, *Physical chemistry*. Oxford: Oxford University Press, 1978.

[46] S. Rein, W. Warta, and S. W. Glunz, "Investigation of carrier lifetime in p-type Cz-silicon: specific limitations and realistic prediction of cell performance," in *the Conference Record of the Twenty-Eighth IEEE Photovoltaic Specialists Conference*, 2000, pp. 57-60.

[47] A. Herguth, G. Schubert, M. Kaes, and G. Hahn, "Avoiding Boron-Oxygen Related Degradation in Highly Boron Doped CZ Silicon," in *the 21st EU-PVSEC*, Dresden, 2006.

[48] M. Sheoran, A. Upadhyaya, and A. Rohatgi, "A Comparison of Bulk Lifetime, Efficiency, and Light-Induced Degradation in Boron- and Gallium-Doped Cast mc-Si Solar Cells," *IEEE Transactions on Electron Devices,* vol. 53, pp. 2764-2772, 2006.

[49] T. Trupke, "Influence of photon reabsorption on quasi-steady-state photoluminescence measurements on crystalline silicon," *Journal of Applied Physics,* vol. 100, p. 063531, 2006.

Section 2

PAPERS

The work presented in this thesis has mainly been performed by the candidate but on all publications I received indispensable help from colleagues. Below, I will describe my own involvement in the publications presented in this thesis.

The work in Paper I was primarily carried out by the candidate. The atomatization of the I-V setup at IFE was done in collaboration with Birger Retterstøl Olaisen, who also was a large help with the analysis of the degradation curves. At the University of Konstanz I received a lot of help with the I-V setup and the CID-setup by Axel Herguth and Svenja Wilking. The paper was written by the candidate.

Paper II was written in collaboration with Post. Doc. Hallvard Angelskår. I brought knowledge and experience on B-O related defects while Hallvard Angelskår is skilled and experienced on the photoluminescence setup. As the work required both of these contributions, the majority of the work was done in close collaboration, with the exception of the implementation of the simulation programs, for which Hallvard Angelskår was responsible. After succeeding to establish the technique, the measurements and simulations were performed by the candidate, while analysis was performed in collaboration with Hallvard Angelskår. The paper was written by the candidate except from chapter A and B in III *Data analysis and simulations* which were written by Hallvard Angelskår. Several important remarks were given by all co-authors.

Paper III is essentially a refinement of the technique from Paper II and the work was divided as in Paper II where I performed the majority of the lab work and Hallvard Angelskår performed the majority of the simulations. The paper was written by the candidate except for chapter III *Data analysis and simulations,* which was written by Hallvard Angelskår. Several important remarks were given by Erik Stensrud Marstein.

Paper IV was primarily carried out by the candidate alone. The atomatization of the QSSPC setup was done by Birger Retterstøl Olaisen and assistance with the data analysis and discussion and derivation of the kinetic equations was given by Halvard Haug. The paper was written by the candidate but with several important remarks from all co-authors.

PAPER I

Studying light soaking of solar cells by the use of solar simulator

T. U. Nærland, B. R. Olaisen, and L. Arnberg,

Solid State Phenomena, vol. 178-179, pp. 435-440, 2011.

Is not included due to copyright

PAPER II

The role of excess minority carriers in light induced degradation examined by photoluminescence imaging

T. U. Naerland, H. Angelskar, M. Kirkengen, R. Sondena, and E. S. Marstein,

Journal of Applied Physics, vol. 112, pp. 033703-8, 2012.

JOURNAL OF APPLIED PHYSICS **112**, 033703 (2012)

The role of excess minority carriers in light induced degradation examined by photoluminescence imaging

Tine Uberg Nærland,[1,a)] Hallvard Angelskår,[1] Martin Kirkengen,[2] Rune Søndenå,[1] and Erik Stensrud Marstein[1]
[1]*Institute for Energy Technology, Instituttveien 18, 2007 Kjeller, Norway*
[2]*Renewable Energy Corporation ASA, Sandvika, Norway*

(Received 25 January 2012; accepted 9 June 2012; published online 2 August 2012)

A new approach to investigate light induced degradation (LID) effects in boron-doped silicon has been developed. By studying spatial variations in LID resulting from localized carrier excitation (spot-LID), it is verified that the generation of the boron-oxygen complexes responsible for the degradation is directly related to the presence of excess minority carriers. Through the examination of the diffused minority carrier density distribution (during light exposure), from an exposed into an unexposed wafer area compared to the observed defect generation, we are able to monitor the generation of excess carrier induced defects over a range of carrier concentrations. The results show that very low concentrations of minority excess carrier densities are sufficient to generate the defects. For the investigated material carrier concentrations down to $1.7 \pm 0.2 \times 10^9\,\mathrm{cm}^{-3}$ are observed to cause lifetime degradation. © *2012 American Institute of Physics*. [http://dx.doi.org/10.1063/1.4735992]

I. INTRODUCTION

Light induced degradation (LID) reducing the solar cell efficiency through the generation of metastable defects is an inherent problem in boron-doped Czochralski silicon (Cz-Si). This phenomenon is found to be related to the simultaneous presence of boron and oxygen in the Si material, through a possible boron-oxygen defect (BO-defect), but neither the chemical composition nor the energy level of the defect has so far been determined experimentally. LID has been known since the 1970s when Fischer and Pschunder[1] observed that LID in Cz-Si was present independently of particle irradiation (in space applications), and from a loss in the red response during light exposure it was concluded that a reduction of the minority carrier lifetime in the solar cell base was responsible for the observed degradation.

For years, the apparent degradation was thought to be induced by light until Knobloch *et al.* in 1996 found that a similar degradation could be observed by applying a forward bias voltage to the cell.[2] Hence, it was concluded that the degradation in boron-doped silicon is caused by the presence of excess minority carriers, and that photons are not directly involved. Later, in 2003, Bothe *et al.*[3] showed that the metastable defect is also formed under equilibrium conditions (at elevated temperatures), indicating that it is not the excess carrier density that determines the degradation but the total number of minority carriers.

In 2001, Glunz *et al.*[4] proposed a mechanism involving a recombination-enhanced defect reaction as a possible explanation for the formation of the boron-oxygen related recombination center due to the quadratic increase of defect generation rate with doping level. This mechanism assumes that it is the energy released from the recombination that triggers the generation of the active recombination center. On the basis of this mechanism, Schmidt and Bothe[5] introduced a model where fast diffusing oxygen dimers capture substitutional boron atoms to form B_s-O_{2i} recombination centers. This model was prevailing for many years but was invalidated in 2009 when Macdonald *et al.*[6] discovered that the degradation is controlled by the concentration of holes [p_0] and not the concentration of boron [B]. The fact that the degradation effect has not been observed in gallium-doped but only boron-doped Cz silicon still ensures that the Cz-specific defect depends on boron and not on the position of the Fermi level.[7]

In 2010, Voronkov and Falster[8] proposed a new degradation model. In this model the degradation starts from a latent complex, B_iO_2, of an interstitial boron atom and an oxygen dimer by a minority excess carrier assisted recharge from a doubly positively charged into a neutral state. The model is the first to explain the proportionality between the defect concentration and the hole concentration [p_0] in compensated silicon co-doped with boron and phosphorus.[6] In a recent work,[9] however, where silicon co-doped with boron and gallium was investigated, it was found that the defect concentration was proportional to [B] instead of p_0. This implies a defect complex containing a substitutional boron atom [B_s] like in the model by Schmidt and Bothe.[5] However, the model by Schmidt and Bothe[5] involves another debated issue: the diffusion of the oxygen dimer. Recent work by Murin[10] states that the charge-state driven motion of an oxygen dimer is a highly unlikely mechanism in solar grade silicon. Presently, no model is able to fully explain all experimentally observed characteristics associated with the defect responsible for light induced degradation. Some conclusions on the nature of the defect can still be drawn. Due to the fact that no trace of the defect has been found by Deep Level Transient Spectroscopy the concentration of the

[a)]Author to whom correspondence should be addressed. Electronic mail: tine.narland@material.ntnu.no. Telephone: +47 99 04 05 08. Fax: +47 63 89 99 64.

defects is believed to be very low (about $10^{11}\,\mathrm{cm}^{-3}$).[8] Consequently, a high defect capture cross-section and a low density of excess minority carriers are to initiate the expected defect.

In this work, we investigate the role of the excess minority carriers in the defect generation. Imaging of the steady state band-to-band photoluminescence (PL) from a sample allows determination of the spatial variations in excess minority carrier concentration (Δn) due to recombination. The sensitivity of PL is high even at very low injection levels, $\Delta n < 1 \times 10^{9}\,\mathrm{cm}^{-3}$.[11] In light induced degradation experiments, a light source is used to generate excess minority carriers (Δn_{LID}) which in turn activate the defects responsible for minority carrier lifetime degradation. PL imaging before and after such injection of minority carriers (Δn_{LID}) therefore allows for an accurate image of the effect of the introduced recombination centres across the wafer. This is utilized in a newly developed method of local light induced defect monitoring (spot-LID), where the wafer is exposed to light through a confined aperture/slit from one side of the wafer while a PL image from the entire wafer is collected from the other (see Fig. 1). The laser excitation time for the PL image is short compared to the duration of the illumination through the slit. As the excess minority carriers, generated by the light source from below, diffuse from the illuminated area into the adjacent area, the PL images will show a depreciation of the unexposed area close to the slit with time. The extension of the darkened area depends on the minority carrier diffusion length, while the reduction in PL intensity is determined mainly by the increase of recombination active defects over time, which again is a function of the local electron injection history. From these data, conclusions on the nature of the minority carrier-induced centers can be made.

In this paper, we present the procedures and models applied to extract true recombination activity and minority carrier densities from measured data. The findings and succeeding analysis are discussed with regard to related work. Particular attention is paid to the determination of the minimum minority carrier concentration being responsible for observable lifetime degradation by BO-defect generation. Such information has not been experimentally verified before.

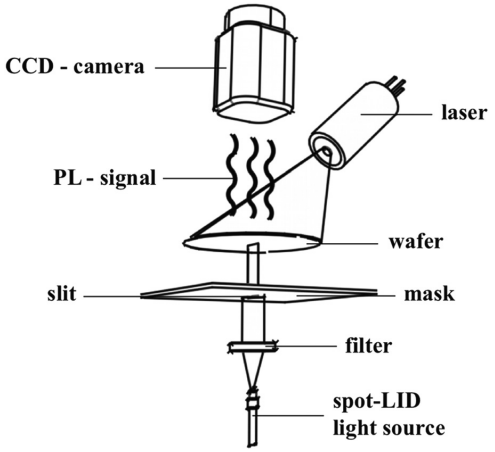

FIG. 1. The spot-LID setup. The wafer is exposed to light through a confined slit on the rear side of the wafer while photoluminescence from the entire wafer, generated by an expanded diode laser, is collected from the other side.

II. EXPERIMENTAL METHODS

A 320 μm p-type Cz-Si wafer with a boron concentration of $3.6 \times 10^{15}\,\mathrm{cm}^{-3}$ (3.8 Ω cm) and an oxygen concentration of $8.9 \times 10^{19}\,\mathrm{cm}^{-3}$ was used for this investigation. Prior to the measurement, the wafer was cleaned with RCA and thereafter received a double side passivation by plasma-enhanced chemical-vapour deposited (PECVD) hydrogenated amorphous silicon. The surface recombination rate is estimated to be approximately 40 cm/s. In order to ensure that no defect centres are generated before the start of the measurement the sample was deactivated by an annealing at 200 °C for 10 min on a hotplate.[12]

The PL measurements were performed with a LIS-R1 system from BTimaging. A laser with a wavelength of 808 nm is used to expose the entire wafer and the resulting band-to-band PL signal is measured with a (focused) one-megapixel silicon charge-coupled device camera. The penetration depth for this wavelength is about 11.5 μm but due to immediate diffusion of carriers the excited minority carriers will almost instantly spread uniformly over the thickness of the sample. This is valid as long as the diffusion length of the minority carriers in the sample is significantly longer than the thickness of the sample, which is true for the samples in this work. The intensity of the band-to-band PL signal scales with the number of (photo-) excited minority charge carriers. A separate quasi steady state photo conductance (QSSPC) calibration measurement is carried out to convert the PL intensity into absolute charge carrier density. For the images, we used an incident photon flux of $2.97 \times 10^{17}\,\mathrm{cm}^{-2}\,\mathrm{s}^{-1}$, corresponding approximately to 1 sun illumination intensity. The PL acquisition time was 0.5 s per image.

A system for illuminating a small area on the rear side of the cell was installed *in situ* in the PL chamber as illustrated in Fig. 1. The wafer is positioned on a stage with a mask with a slit measuring 0.29 mm in width immediately below the wafer. The illumination source is a broad band halogen spectrum illumination source from Ocean Optics with a connected optical fibre and a 900 nm short pass filter resulting in a photon flux of $1.41 \pm 0.1 \times 10^{16}\,\mathrm{cm}^{-2}\,\mathrm{s}^{-1}$. A halogen spectrum cut off at 900 nm will be absorbed within the first 15 μm of the silicon. Simulations of the minority carrier distribution over the thickness of the sample show that due to immediate diffusion of carriers there is, as for the excitation of minority carriers by the 808 nm laser, virtually no minority carrier concentration difference in this direction. Both float zone wafers and n-type wafers were tested in order to ensure that no degradation of the passivation layer was occurring.

The lifetime at the injection levels in the wafer during spot-LID is estimated by QSSPC calibrated PL imaging, by tuning the excitation laser to the same photon flux as that of

the fiber-connected light source. This procedure is further discussed in Sec. III B. As the sensitivity to PL is very high even at low injection levels, this technique enables us to measure lifetime at much lower injection levels than with a conventional QSSPC setup.

III. DATA ANALYSIS AND SIMULATIONS

The presence of minority carriers is presumed to be a requirement in the generation of LID-related recombination centres in boron-doped silicon.[2] The recombination centres will thus be formed within a distance from where the minority carriers are injected, determined by the minority carrier diffusion length. If the injected minority carriers are allowed to diffuse into an unexposed part of a boron-doped silicon wafer, a footprint of subsequent recombination centres will delineate the extension of the minority carrier spreading. If the degraded sample is kept in the dark at room temperature, the distribution of generated recombination centres, and thus the footprint of minority carrier spreading, will be stable over time.

In Fig. 2 principle sketches of a silicon wafer before and after light exposure through a slit and the corresponding line scans are shown. The slit is assumed uniformly exposed to light and is situated in the middle of the wafer. The variations in PL intensity correspond to variations in Δn generated by the laser diode. For simplicity, we study the lifetime in a line section perpendicular to- and through the middle of the slit (marked by the horizontal line).

The PL images are acquired in steady state, i.e., with a constant laser excitation intensity. The Δn determined by the PL image is translated to lifetime by applying the steady state equation,[13]

$$\tau_{eff} = \frac{\Delta n}{G}. \tag{1}$$

Here the generation rate G, determined by optical properties of the sample and the excitation laser during the PL measurement,

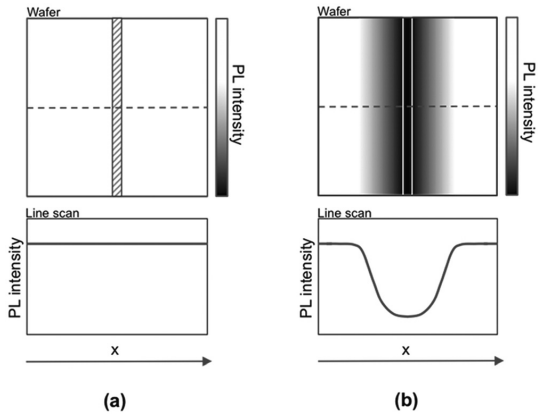

FIG. 2. Principle sketch of the PL intensity on a passivated silicon wafer before (a) and after (b) light exposure through a slit. The position and width of the slit are indicated by the shaded area in (a) and the white lines in (b). The horizontal line indicates the principle line scans.

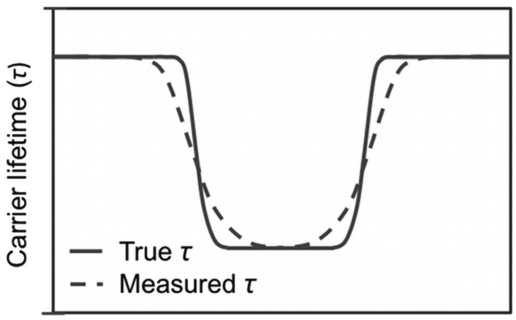

FIG. 3. Principle sketch showing the effect of diffusing carriers from areas of high lifetime to areas with low lifetime (contrast smearing) during PL imaging on the lifetime line scan after spot-LID.

is assumed to be constant and homogeneous over the wafer. In typical cases, this analysis gives a good approximation to the variations in lifetime in a silicon wafer. However, the resulting lifetime map also includes the effects of diffusion from areas of high charge carrier density (high lifetime) to areas of lower charge carrier density. This results in a smearing effect in areas where the lifetime varies significantly. In the case of spot-LID measurements, we generate a localized area of very low lifetime and the problem with diffusing charge carriers becomes prominent. In Fig. 3 a principle sketch of how this blurring will affect a PL line scan after spot-LID treatment is given.

In Sec. III A, a procedure to decouple the effect of smearing from the true lifetime is given.

A. Determining recombination activity from the PL data

In an attempt to study the variations in recombination activity more precisely, we decouple the effects of recombination variations and smearing described above by fitting the measured PL data to a theoretical model. During the PL measurement, the illumination is homogeneous over the whole sample, so the generation rate (G) is constant. Furthermore, the slit shape allows us to simplify the problem to 1D. The continuity equation, see for instance,[14] in steady state for p-type material yields

$$G + D_n \frac{\partial^2 \Delta n(x)}{\partial x^2} - R(\Delta n(x), x) = 0 \tag{2}$$

Here D_n is the diffusion coefficient for electrons, G is the constant generation rate, x is the lateral distance from the slit edge, and $R(\Delta n,x)$ is the recombination rate. $\Delta n(x)$ is the excess minority carrier concentration, averaged over the thickness of the wafer. During spot-LID, the recombination rate $R(\Delta n,x)$ goes from being an approximately constant function of x (at $t=0$) to being strongly dependent on x at $t \neq 0$. The reason for the large variation at $t \neq 0$ is that recombination centres have been activated, due to diffused electrons from the slit edge. We can write the recombination rate as

$$R(\Delta n(x), x) = \frac{\Delta n(x)}{\tau_{eff}(x)} = \Delta n(x) r(x), \tag{3}$$

with $r(x)$ as the reciprocal effective lifetime. Inserting this into Eq. (2) we get

$$G + D_n \frac{\partial^2 \Delta n(x)}{\partial x^2} - \Delta n(x) r(x) = 0. \tag{4}$$

The goal of the decoupling analysis is to determine $r(x)$ (and thus $\tau_{\mathrm{eff}}(x)$) from the PL data. This is done by solving Eq. (4) for different $r(x)$-profiles and fitting this to the PL data. Equation (4) was solved numerically by using a partial differential equation (PDE) solver.[15] In Secs. IV and V, we will refer to the recombination activity in terms of lifetime as these are directly related.

After spot-LID, we expect two regions where the lifetime is constant, as illustrated in Figure 3. Close to the slit there is a region where the injected carrier concentration is sufficiently large such that the defect generation (and hence lifetime) is not limited by the carrier concentration.[5] Far away from the slit the injected carrier concentration goes to zero, and the lifetime should be constant. Thus a sigmoidal shape of the reciprocal lifetime is assumed, which proved to fit well with experimental data.

From the PL measurement at $t > 0$, the lifetime for large x and in the slit can be directly obtained. The reason for this is that there are no large variations in lifetime near these extremes, and thus the contribution from smearing to the measured Δn is negligible. Thus we have that the reciprocal lifetime decreases from $r_{\mathrm{deg}} = 1/\tau_{\mathrm{deg}}$, at the slit edge, to $r_0 = 1/\tau_0$, in a distance from the slit, as

$$r(x) = r_0 + \frac{(r_{\mathrm{deg}} - r_0)}{1 + \exp((x - \Delta x)/l_{\mathrm{r}})}. \tag{5}$$

Here l_{r} and Δx are the parameters, which are varied to fit the reciprocal lifetime function to the measured PL data.

B. Determining Δn profiles during spot-illumination

In order to emphasize the difference between the excess charge carrier density during the PL measurement (Δn), and the charge carrier density during LID, we have in the following chosen to call the latter Δn_{spot}. To relate the degradation (reduction in lifetime) to Δn_{spot}, we determine Δn_{spot} from the 2D continuity equation where we also take into account the non-uniform carrier concentration in the z-direction (depth of the wafer),

$$G(x, z) + D_{\mathrm{n}} \nabla^2 \Delta n_{\mathrm{spot}}(\mathrm{x}, \mathrm{z}) - \frac{\Delta n_{\mathrm{spot}}(x, z)}{\tau_{\mathrm{spot}}(x)} = 0. \tag{6}$$

Here the generation rate $G(x,z)$ is a function of the lateral position x, and the distance z from the illuminated backside of the wafer. We assume that the generation rate drops sharply to zero on the slit edge. Due to symmetry we solve the continuity equation for one half-plane from the centre of the slit. The boundary conditions on the top and bottom surfaces of the wafer are set to

$$D_{\mathrm{n}} \frac{\partial \Delta n(x, z)}{\partial \mathrm{z}}\bigg|_{z=\mathrm{surf}} = -\mathrm{S}\ \Delta \mathrm{n}(\mathrm{x}, \mathrm{z})|_{z=\mathrm{surf}}, \tag{7}$$

where S is the surface recombination velocity, assumed to be approximately $S = 40$ cm/s.

The lifetime in Eq. (6) is written $\tau_{\mathrm{spot}}(x)$ to emphasize that this is the lifetime under spot illumination conditions, i.e., at low injection levels. It is evident that the carrier concentration profile due to diffusion from the slit decreases during the illumination, as the lifetime $\tau_{\mathrm{spot}}(x)$ decreases. $\tau_{\mathrm{spot}}(x)$ is estimated by QSSPC calibrated PL measurements at a similar excitation photon flux as from the spot-LID illumination. The real injection level (and thus the lifetime) will be slightly lower than in the PL measurement, due to diffusion away from the exposed area. But while the lifetime is dependent on injection history, it is only weakly dependent on the current injection level under low injection conditions. Hence, we assume that the injection dependence, related to the reduced concentration of diffused carriers away from the slit, to be negligible.

The continuity equation was then solved numerically for $\Delta n_{\mathrm{spot}}(x,z)$, with different $\tau_{\mathrm{spot}}(x)$ corresponding to the duration of the spot-illumination, by using a PDE solver.[15] The carrier concentration is then averaged over the thickness of the wafer (simulations show that this approximation is unambiguous) to find the averaged carrier concentration $\Delta n_{\mathrm{spot}}(x)$ a distance x away from the slit edge.

IV. RESULTS AND DISCUSSION

During spot-LID, electrons are excited in a localized region, defined by the illuminated area in the slit. From this localized region, the excess electrons diffuse out into the wafer, allowing us to study the degradation effect of a continuously varying electron concentration. The measurements to be analysed are calibrated band-to-band PL images[16] before and after spot-LID carried out for different times. The raw PL data before calibration to lifetime is plotted in Fig. 4 where PL images of the wafer before and after spot-LID of 25 h are shown. The line scans corresponding to the position of the horizontal line in the top figures in Fig. 4 are given in the bottom images where the depreciation in PL intensity in the slit-close areas is clearly seen. The black dots in the top images are imperfections in the material/passivation layer but have no implications on the data used for the analysis.

A set of PL line scans performed at different times is presented in Fig. 5. Both the raw data and the lifetime without contrast smearing, described in Sec. III A, are shown for all times. The plot shows a depreciation of slit-close areas with time until saturation (saturation is occurring at approximately 80 h for the given material with the current light source). For symmetry reasons only one side of the slit is shown. Note that the right-hand edge of the slit is in position $x = 0$ in the figure, (corresponding to $x = 13$ mm in Fig. 4) so that all degradation observable in the figure is degradation in the dark caused by diffused excess carriers from the slit.

As the lifetime of the degraded area ($\tau(x)$), both in the exposed and the unexposed part of wafer, decreases with time, the diffusion length of the carriers from the exposed area into

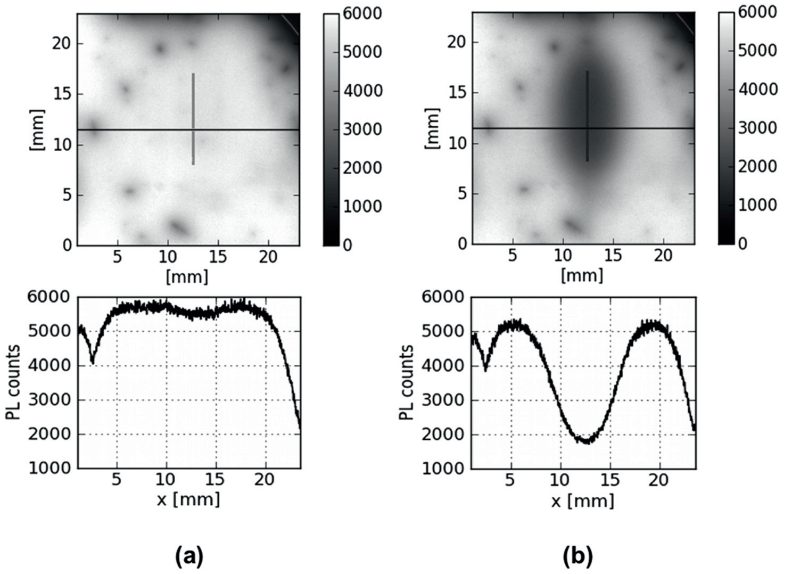

FIG. 4. PL intensity before (a) and after (b) spot-LID for 25 h. The position and width of the slit are superimposed on the image, as indicated by the vertical grey line. Data acquisition time is 0.5 s. The horizontal line indicates the position of the line scan in the bottom figures.

the unexposed area will decrease. This decrease will continue until defect saturation. A plot showing the simulated minority carrier profiles (Δn_{spot}), during localized carrier excitation (spot-LID), before spot-illumination ($t = 0$) and after saturation ($t = 125$ h) is given in Fig. 6. The simulated curves are obtained according to the method described in Sec. III B, *determining Δn profiles during spot-illumination*. Before spot-illumination the minority carrier lifetime ($\tau(x)$) obtained from calibration of the PL line scan is homogenous for all x, while after a given time of spot-illumination the lifetime (proportional to PL counts) is altered as shown in Fig. 4(b). This calibrated lifetime (obtained with PL laser intensity with a photon flux similar to the spot illumination) is utilized to simulate the Δn_{spot}, profiles in Fig. 6.

The $\Delta n_{spot,\ (t=0)}$ and $\Delta n_{spot,\ (t=125\ h)}$ profiles in Fig. 6 set the upper and lower limits for the diffusing minority carrier concentration during the generation of defect centres. From $t = 0$ to $t = 125$ h, the Δn_{spot} will never be higher nor lower than these limits for any distance from the slit but the profile will change gradually from the $\Delta n_{spot,\ t=0}$ curve to the $\Delta n_{spot,\ t=125\ h}$ curve. Accordingly, Fig. 6 shows the upper and lower limits of carrier density, for every distance from the slit edge, responsible for the activation of the defect during spot-LID for 125 h. Further on, it can be seen that both $\Delta n_{spot,\ t=0}$ and $\Delta n_{spot,\ t=125\ h}$ are gradually decreasing from the slit edge but the $\Delta n_{spot,\ t=125\ h}$ curve shows a more pronounced steepening of the profile in the slit-close regions. This is an effect of the screening behaviour of the already generated defects. Beyond the point of where the majority of

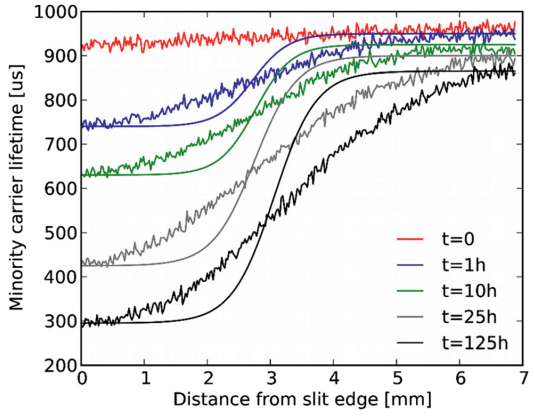

FIG. 5. PL line scans (raw-data and decoupled lifetime curves) performed after different times of spot-LID. The rough curve corresponds to the raw-data and the smooth curves to the decoupled lifetime. The top curve corresponds to $t = 0$, the second curve to $t = 1$ h, and so forth. The lifetime values are given at one sun illumination.

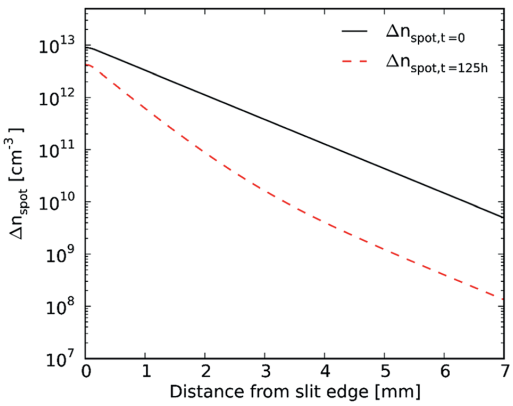

FIG. 6. Figure showing minority carrier profiles during spot-LID (Δn_{spot}) before spot-illumination ($t = 0$) and after saturation ($t = 125$ h). Notice that the Δn_{spot} profiles are plotted logarithmically. The simulations are performed according to the procedure described in Sec. III B.

the defect centres are generated (approx. at a distance of 3 mm from the slit edge) the diffusion continues parallel to the diffusion of carriers at $t = 0$.

A necessary condition for the spot-LID measurement to be correct is that only the material uncovered through the slit and no other parts of the wafer is exposed to light. This is accomplished for the backside of the cell (see Fig. 1). On the front side, however, the whole area of the wafer is exposed to light every time a PL measurement is performed. In the measurement series shown in Fig. 5 this involves a laser exposure with an intensity of 1 sun for 0.5 s for every measurement. Considering that LID occurs through two mechanisms where the first mechanism causes degradation during the first minutes of light exposure,[17] the laser exposure to the front side of the wafer due to PL measurements is sufficient to degrade the lifetime of the wafer. In Fig. 5 this can be seen as the slightly decreasing PL intensity level in the part of the wafer that is not influenced by degradation caused by spot-LID ($x > 6$ mm). These levels should ideally have had the same level as the curve equal to $t = 0$. However, in the slit-close region the rapid degradation has already been completed by spot-LID. Accordingly, in Fig. 5, the part of the lifetime curves that are influenced by spot-LID can be considered to be unaffected by the additional PL measurement laser exposure. In order to obtain the same $\tau_{spot,\ x=\infty}$ for the different times in the measurements forming the basis for following discussion, the sample has been deactivated between each spot-LID measurement.

A. Expected minority carrier diffusion length versus observed extension of LID defects

As discussed in earlier sections, the presence of minority carriers is required to produce the metastable BO defects. This has, amongst others, been shown by Hashigami *et al.*[18] who showed that blue light illumination absorbed near the surface in a solar cell resulted in degradation in the bulk. The BO defects are consequently not limited to be created in the point where the photon is absorbed, but at any point the light injected carrier diffuse to. According to the model proposed by Voronkov and Falster[8] in 2010, there is a direct correlation between the recombination centre and the minority carriers through the recharging of the defect from a doubly positively charged into a neutral state. In our case, this would imply that the recombination centres should be formed within a distance from where the minority carriers were injected, determined by the minority carrier diffusion length.

The diffusion length L_n is commonly determined through the expression $L_n = \sqrt{(D_n \times \tau_n)}$, where D_n is electron diffusivity and τ_n the minority carrier lifetime which is the average time needed for a decrease in the excess carrier density of 1/e. This understanding of the minority carrier diffusion length assumes a single exponential decay with time. In our case where the excess carriers diffuse out into an area of non-uniform recombination rate the term will not be applicable in its conventional form. The simulated Δn_{spot} profiles in Fig. 6, however, gives the upper and lower minority carrier concentration at all distances from the excitation point and thereby provides more information than the conventional 1/e diffusion length does.

Comparing Fig. 5 to Fig. 6 we see that at the distance where the lifetime ceases to be degraded, at about $x = 6$ mm for $t = 125$ h in Fig. 5, the minority carrier concentration in Fig. 6 is small but far from zero. This observation indicates that a certain concentration of minority carriers is required for a detectable degradation to occur but it cannot confirm nor disprove whether there is a direct relation between the minority carriers and the defect generation through recharging. Other models, like the recombination enhanced triggering of defect activation as proposed by Glunz *et al.*[4] could also be applicable.

B. Minimum minority carrier concentration required to cause LID

In Fig. 7(a), the decoupled lifetime profile for $t = 125$ h ($\tau_{t\,=\,125h}$) is plotted as a function of the simulated $\Delta n_{spot,\ t=0}$ and $\Delta n_{spot,\ t\,=\,125\ h}$, given in Fig. 6. In this plot, the low

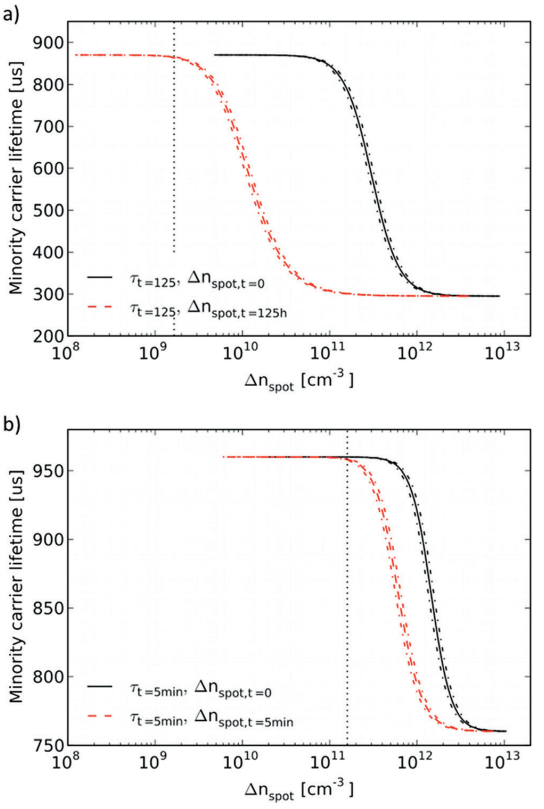

FIG. 7. Degradation profiles (lifetime) for (a) $t = 125$ h and (b) $t = 5$ min plotted as a function of minority carrier density during spot-illumination (Δn_{spot}) determined for $t = 0$, $t = 125$ h in (a) and $t = 0$, $t = 5$ min in (b). The uncertainty of Δn_{spot} is given by the dashed curves on both sides of the lifetime curves. Also note that Δn_{spot} is plotted logarithmically and that the range of the y-axes is different for (a) and (b). The dashed vertical line in (a) is the lower carrier concentration limit (1.7×10^9 cm^{-3}) of which the recombination-active BO defects are detectable with respect to lifetime changes (1% relative to the total lifetime reduction) after saturation. The dashed line in (b) is the lower carrier concentration limit (1.6×10^{11} cm^{-3}) of which is responsible for generation of BO-defects during 5 min of spot-LID.

Δn_{spot} values correspond to slit-distant regions and the high Δn_{spot} values to slit-close regions. The slit edge is accordingly on the right side of the plot, opposite to Fig. 5. The two curves in Fig. 7(a) give the upper and lower minority carrier density limits for the degradation to occur. Bear in mind that the degradation curve at $t = 125$ h is a result of the injection history through the whole time period of spot-LID, i.e., the carrier concentration profile at any time contributes to the defect generation. However, in Fig. 5 it is obvious that the extension of defects, with respect to the distance from the slit, increases with time. This implies that the total number of defects is a product of both carrier concentration and time. For example, a comparison between Figs. 7(a) and 7(b) is apposite. In Fig. 7(b) a corresponding plot to Fig. 7(a) is given, but in this plot with a time duration of 5 min instead of 125 h. If we look at the carrier concentration of $1 \times 10^{11}\,cm^{-3}$ in Fig. 7(b), we observe that this concentration has not generated any defects so far. However, if we go to the same carrier concentration for $t = 125$ h in Fig. 7(a) we observe a considerable loss in minority carrier lifetime. A carrier concentration of $1 \times 10^{11}\,cm^{-3}$ is thus not sufficient to produce detectable lifetime degradation for 5 min but is indeed so for 125 h.

Returning to Fig. 7(a) the "$\tau_{t\,=\,125\ h}$, $\Delta n_{spot,\ t\,=\,0}$" and the "$\tau_{t\,=\,125h}$, $\Delta n_{spot,\ t\,=\,125h}$" curves characterize the upper and lower limits for the carrier concentration responsible for the degradation at $t = 125$ h. The $\Delta n_{spot,\ t\,=\,0}$ profile defines the upper limit, though after 125 h of spot-LID we know from Fig. 6 that Δn_{spot} has decreased significantly. According to the increasing extension of degradation with time in Fig. 5 the last defects to be created are therefore most likely generated by a carrier concentration comparable to the $\Delta n_{spot,\ t\,=\,125\ h}$ profile. Hence, even though the $\tau_{t\,=\,125\ h}$, $\Delta n_{spot,\ t\,=\,0}$ profile characterizes the lower limit, this profile is not unrealistic regarding what is the minimum carrier concentration responsible for lifetime degradation.

According to Figs. 7(a) and 7(b), the lifetime or more precisely the level of degradation is independent of the excess carrier density at both high and low levels. The observation that degradation is independent of the excess carrier density at high levels is in accordance with previous work that reports that under an illumination intensity between 1 and 100 mW/cm^2 the generation rate of LID defects is independent of the illumination intensity.[5,18] The defect generation dependence on illumination intensity will, however, be highly influenced by material properties such as doping and carrier lifetime, optics of the surface and the wafer passivation. Hence, working with injected charge carrier concentrations instead of illumination intensities is essential when relating LID to light-exposure for different materials.

In order to determine the lowest value of Δn_{spot}, that produces a detectable change in lifetime as a consequence of BO-defect generation we determined the Δn_{spot} value that corresponds to a change in lifetime of 1% relative to the total reduction in lifetime (vertical dashed line in Fig. 7(a)). As discussed previously, it is shown that the lateral extension of the degradation is increasing over time even though the lateral carrier concentration decreases. This proves that very low concentrations of excess carrier densities are sufficient to generate the BO defect and the lowest carrier concentration being responsible for lifetime degradation ($\Delta\tau = 1\%$ of total loss) in this work was determined to $1.7 \pm 0.2 \times 10^9\,cm^{-3}$. We cannot rule out, however, that defects can be generated at lower concentrations, although the effect on lifetime is not detectable. Nevertheless, we expect the reported lower excess carrier concentration limit to be altered with latent defect complexes, i.e., boron and oxygen concentrations and a study, of the dependencies of this limit on the material quality, is in progress. The concentration limit determined in this work is, however, in agreement with several works[4,12,19] which has indicated that the BO defect has a large electron capture cross section implying that a very low concentration of Δn, less than $10^{11}\,cm^{-3}$, is sufficient to cause the reported degradation.

V. CONCLUSION

In the present work, we presented a way to investigate the LID effect for a broad range of excess carrier densities circumventing the operation at different illumination intensities. The range of excess carrier density studied is continuous and the defect generation dependency of Δn can be determined.

Through the examination of the diffused minority carrier density distribution, from an exposed area into an unexposed wafer area, and the observed defect generation by photoluminescence imaging a lower limit of minority carrier concentration being responsible for lifetime degradation by BO-defect generation is observed. For normal quality p-type Cz-Si material, degradation due to the BO defect centre was detected when the wafer was exposed to excess carrier densities down to $1.7 \times 10^9\,cm^{-3}$.

ACKNOWLEDGMENTS

This project has been funded by "The Norwegian Research Centre for Solar Cell Technology" and REC Wafer, REC Solar, Elkem Solar, and the Norwegian Research Council through the KMB project "Defect engineering for crystalline silicon solar cells."

Lars S. Løvlie is acknowledged for valuable discussions on carrier diffusion, Jo Gjessing for help with photon flux measurements, Halvard Haug for help with surface passivation and Kaori Watanabe at Systems Engineering, Inc. in Tokyo for FTIR measurements.

[1]H. Fischer and W. Pschunder, in *Proceedings of the 10th IEEE Photovoltaic Specialists Conference, Palo Alto, CA* (IEEE, New York, 1973), p. 404.
[2]J. Knobloch, S. W. Glunz, D. Biro, W. Warta, E. Schäffer, and W. Wettling, in *Proceedings of the 25th IEEE Photovoltaic Specialists Conference* (IEEE, New York, 1996), p. 405.
[3]K. Bothe, R. Hezel, and J. Schmidt, Appl. Phys. Lett. **83**, 1125 (2003).
[4]S. W. Glunz, S. Rein, J. Y. Lee, and W. Warta, J. Appl. Phys. **90**, 2397 (2001).
[5]J. Schmidt and K. Bothe, Phys. Rev. B **69**, 024107 (2004).
[6]D. Macdonald, F. Rougieux, A. Cuevas, B. Lim, J. Schmidt, M. Di Sabatino, and L. J. Geerligs, J. Appl. Phys. **105**, 093704 (2009).
[7]S. Rein, *Lifetime Spectroscopy: A Method of Defect Characterization in Silicon for Photovoltaic Applications* (Springer-Verlag, Berlin, 2005).
[8]V. V. Voronkov and R. Falster, J. Appl. Phys. **107**, 053509 (2010).

[9]M. Forster, E. Fourmond, F. E. Rougieux, A. Cuevas, R. Gotoh, K. Fujiwara, S. Uda, and M. Lemiti, Appl. Phys. Lett. **100**, 042110 (2012).
[10]L. I. Murin, Appl. Phys. Lett. **98**, 182101 (2011).
[11]T. Trupke and R. A. Bardos, in *Proceedings of the Photovoltaic Specialists Conference, 2005. Conference Record of the Thirty-first IEEE* (IEEE, 2005), p. 903.
[12]K. Bothe and J. Schmidt, J. Appl. Phys. **99**, 013701 (2006).
[13]H. Nagel, J. Appl. Phys. **86**, 6218 (1999).
[14]D. K. Schroder, *Semiconductor Material and Device Characterization* (Wiley, Hoboken, NJ, 2006).
[15]Flexpde 6 (PDE Solutions Inc.).
[16]T. Trupke, Appl. Phys. Lett. **89**, 044107 (2006).
[17]K. Bothe and J. Schmidt, Appl. Phys. Lett. **87**, 262108 (2005).
[18]H. Hashigami, Y. Itakura, and T. Saitoh, J. Appl. Phys. **93**, 4240 (2003).
[19]V. V. Voronkov, R. Falster, J. Schmidt, K. Bothe, and A. V. Batuninac, ECS Trans. **33**, 103 (2010).

PAPER III

Direct monitoring of minority carrier density during light induced degradation in Czochralski silicon by photoluminescence imaging

T. U. Naerland, H. Angelskar, and E. S. Marstein,

Journal of Applied Physics, vol. 113, pp. 193707-7, 2013.

JOURNAL OF APPLIED PHYSICS **113**, 193707 (2013)

Direct monitoring of minority carrier density during light induced degradation in Czochralski silicon by photoluminescence imaging

Tine Uberg Naerland,[1,2,a)] Hallvard Angelskår,[1] and Erik Stensrud Marstein[1]
[1]*Institute for Energy Technology, Instituttveien 18, 2007 Kjeller, Norway*
[2]*Department of Material Science and Engineering, NTNU, 7491 Trondheim, Norway*

(Received 12 February 2013; accepted 2 May 2013; published online 20 May 2013)

In this paper, we present a new method for studying the light induced degradation process, in which the minority carrier density is monitored directly during light soaking by photoluminescence imaging. We show experimentally that above a certain minority carrier concentration limit, Δn_{lim}, the boron oxygen (B-O) defect generation rate is fully independent of the injected carrier concentration. By simulation, we determine Δn_{lim} for a range of p-type Czochralski silicon samples with different boron concentrations. The normalized defect concentrations, N_t^*, are determined for the same samples by time-resolved Quasi Steady State Photoconductance measurements. After 10 min of light degradation, no correlation between Δn_{lim}, and N_t^* is observed. These results indicate that the role of the excess carriers during the rapid decay is to first change the charge state of the defects by shifting the electron quasi-Fermi level across the energy level of the defect centre in its passive state ($E_{\mathrm{lat}} = E_{\mathrm{V}} + (635 \pm 18)$ meV) and that, subsequently, another rate-determining step proceeds before the defect centre becomes recombination active. © *2013 AIP Publishing LLC*. [http://dx.doi.org/10.1063/1.4806999]

I. INTRODUCTION

Severe lifetime reduction with carrier injection is an unfortunate characteristic of p-type Czochralski silicon materials. During a time period of a day or less, the electron lifetime is typically reduced to about 10% of the initial lifetime. The lifetime reduction is attributed to a recombination centre that becomes activated by charge carriers.[1] Two exponential decay processes, one rapid and one slow, describe the degradation kinetics. Both decays are found to be related to the simultaneous presence of oxygen and boron in the Si material, through a possible boron-oxygen defect (B-O defect),[2] but neither the chemical composition nor the energy level of the defect has so far been determined experimentally. It has been shown that the rates of the rapid and slow degradation are proportional to the square of the boron concentration [B],[2] while they are independent of the oxygen concentration.[2] The role of the excess carriers has, however, not been studied in detail.

In the model of Schmidt *et al*., the role of the excess minority carriers in the defect generation were believed not to be directly involved in the defect reaction, but their presence was thought to trigger the reaction by (i) charging the state of the O_{2i}, which might lead to an increase in the O_{2i} diffusivity; or (ii) enhancing the O_{2i} diffusivity via a recombination-enhanced diffusion process.[3] Recent work published in 2011[4] stated, however, that this type of motion of an oxygen dimer is a highly unlikely mechanism in solar grade silicon. Accordingly, this hypothesis disputed the role of the excess carriers in the model.

In 2010/2011, Voronkov and Falster[5,6] proposed a new degradation model wherein a latent recombination centre is already incorporated in the crystal before carrier injection. According to this model, the centres responsible for the slow and rapid lifetime decays are B_iO_{2i} and B_sO_{2i}, respectively. In p-type silicon, the activation of B_sO_{2i} (defect centre responsible for the rapid lifetime decay) is explained through a series of steps where the quadratic proportionality between hole concentration and lifetime is accounted for by the capture of holes by a negative latent centre. The positive latent centre is then reconstructed into a transient centre. One of the final transitions leading to the formation of a recombination-active centre is a de-charging of the transient centre from positive to neutral by electron injection.

Commonly, the light induced degradation (LID) is monitored either by Microwave Photo Conductance Decay (μw-PCD) or Quasi Steady State Photo Conductance (QSSPC) lifetime measurements of a sample during light exposure or by measuring the change in open circuit voltage (V_{OC}) of a solar cell being subjected to an applied forward bias. However, none of these methods retain the information of the minority carrier density in the sample during the extended light exposure or applied forward bias treatments. It has been shown that very low carrier density levels are sufficient to activate the recombination centres,[7,8] but the degradation process is, nevertheless, completely reliant on increased carrier densities.[8] If the injection or heat source is removed, the degradation will cease immediately. Several groups have studied the influence of varying illumination intensity on the B-O defect generation rate. These studies[9,10] have shown that the generation rate of the defect saturates at a certain illumination intensity. For highly degradable material, i.e., material with high concentrations of boron and oxygen, the defect generation rate saturates at about 1 mW/cm^2. The intensity of the illumination source and the excess

a)Author to whom correspondence should be addressed. Electronic mail: tine.narland@material.ntnu.no. Tel.: +47 99 04 05 08. Fax: +47 63 89 99 64.

carrier density is linked through the optical properties of the sample and the carrier lifetime. A certain illumination intensity threshold value therefore corresponds to a certain excess carrier threshold value, Δn_{lim}, but the same illumination intensity gives widely different excess carrier densities for different materials.

In this work, we experimentally demonstrate that such an excess carrier threshold value, Δn_{lim}, exists and that above Δn_{lim} the generation rate is fully independent of carrier concentration. These findings are uncovered by a new way of studying the LID process, in which the excess carrier density is monitored directly during the light soaking. Local light induced defect generation, wherein the wafer is exposed to light in a confined area, causes the excess electrons to diffuse out into the wafer, allowing us to study the degradation effect of a continuously varying electron concentration. This concentration can be monitored by means of photoluminescence (PL) imaging. By applying simulations for the very low carrier concentrations, we are able to quantify Δn_{lim}. The procedure is performed on a series of samples and the results are used to investigate whether there is a correlation between Δn_{lim} and the B-O defect density. Finally, we discuss whether the role of the excess carriers is to simply shift the quasi-Fermi energy causing a charge state change.

II. EXPERIMENTAL METHODS

The samples used in this study are boron doped Cz-Si wafers with a boron concentration ranging from 3.5×10^{15} to $8.5 \times 10^{15}\,\text{cm}^{-3}$. Prior to the measurements, the wafers were cleaned with RCA and thereafter received a double side passivation by plasma-enhanced chemical-vapor deposited (PECVD) hydrogenated amorphous silicon (a-Si:H). a-Si:H passivation has the advantage compared to silicon nitride (a-SiN_x:H) passivation that no inversion channel is formed on p-type material. An inversion channel could possibly introduce a smearing effect on the PL signal detected by the camera.[11] The a-Si:H.-passivation still provides an excellent and stable level of surface passivation with a surface recombination velocity below 40 cm/s. In order to ensure that no defect centres are generated before the start of the measurements, the samples were deactivated by an annealing at 210 °C for 15 min on a hotplate.[2]

The B-O defect densities are determined by time resolved lifetime measurements. The lifetime degradation was monitored by a custom built, automated QSSPC setup using an externally controlled bias lamp for in-situ illumination between measurements. The bias light source was a halogen lamp with an intensity of approximately 50 mW/cm. The temperature of the sample was monitored by a thermistor coupled to the sample stage, but the temperature change of the stage and sample due to illumination was not significant for the measured lifetime. According to Shockley Read Hall theory,[12] the defect concentration can be directly related to the lifetime, provided that the generated defects are the dominating recombination mechanism. The normalized defect concentration, N_t^*, is related to the measured lifetime by the following equation $N_t^*(t) = 1/\tau(t) - 1/\tau(0)$ where $\tau(0)$ is the initial carrier lifetime before LID and $\tau(t)$ is the carrier lifetime after a certain exposure time.[13] The lifetimes were measured at a fixed injection level corresponding to one tenth of the doping level for each sample, respectively.[2]

The PL measurements were performed with a LIS-R1 system from BTimaging. In the chamber, a 4.5 mW diode laser with a wavelength of 780 nm was installed in order to illuminate a specific area of the wafer. A principle sketch of the setup is given in Fig. 1. The laser beam was shaped and focused into a narrow line with a Gaussian half width of $50 \pm 5\,\mu$m. The incidence angle was set to 10° to avoid detection of the specular reflection from the laser beam by the charge-coupled device (CCD) camera. When the laser is turned on, the generated carriers will diffuse from the illuminated area into the adjacent area following the continuity equation. In silicon containing boron and oxygen, the diffusing carriers generate B-O defects that reduce the lifetime far beyond the borders of the illuminated area. As the concentration of B-O defects increases with time, the diffusion length of the carriers decreases. This can easily be observed by imaging the PL generated from a localized area in a p-type Cz-Si sample at $t = 0$ and $t \neq 0$, see Fig. 2.

The laser shown in Fig. 1 has two functions. One is to provide enough excess carriers over time to create an area of reduced lifetime, visible as a groove-shaped feature in the lifetime maps. The other is to act as an excitation source during the PL measurements of direct monitoring of minority carrier density with local excitation, which in principle can be performed on any type of silicon material. As discussed in the introduction, the B-O defect *generation rate* is independent of carrier concentration above a certain value, Δn_{lim}. Therefore, a lifetime plateau in the bottom of the generated lifetime groove-shaped profile is formed. In Fig. 3, a principle sketch of approximately one half of the lifetime profile is shown. The four regions correspond to the degraded region, the exposed region, the transition region, and the unaffected region. Looking at the charge carrier concentration profile for an arbitrary time ($t \neq 0$), the carriers that are generated in the exposed region will be subject to a uniform diffusion length in the already degraded region. However, upon reaching the transition region, the lifetime will rapidly change to the better. This will appear as a change in the slope of the

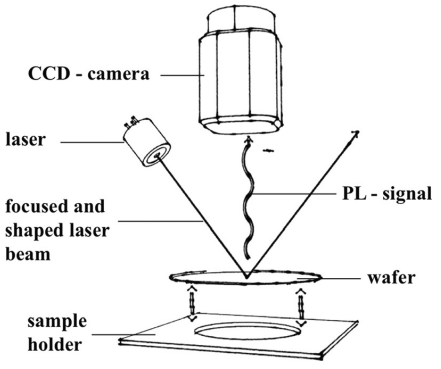

FIG. 1. Sketch showing the setup for direct monitoring of excess carrier density during light induced degradation. The wafer is exposed to a focused and shaped laser beam while the PL signal is collected by a CCD camera.

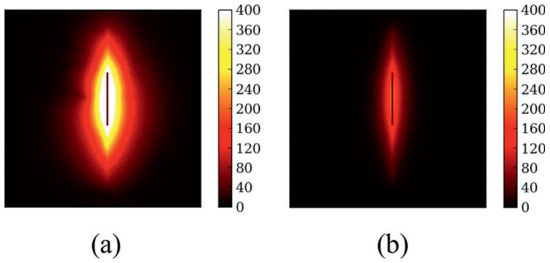

FIG. 2. PL intensity data (normalized to exposure time) taken (a) immediately when the light soaking is started, t = 0 and (b) after light soaking for t = 3 min. The position and width of the exposed area are superimposed on the image, as indicated by the vertical grey line. Data acquisition time is 0.5 s. By comparing the images, it is obvious that the carrier density decreases with increased time of light exposure. This is due to the shorter minority carrier lifetime caused by the generation of B-O defects.

spatial carrier concentration profile in the transition region. The carrier concentration that corresponds to this change in the slope is thus the carrier concentration limit value, Δn_{lim}, where the defect generation rate becomes saturated.

In the present work, we illuminated the material with a focused, low-flux laser for 10 min (peak photon flux, $\phi_{low} = 2.9 \times 10^{16}\,\text{s}^{-1}\,\text{cm}^{-2}$). After 10 min, a groove-shaped lifetime profile is formed and an image of the spatial carrier profile was taken. Unfortunately, the CCD camera cannot detect a PL signal low enough to directly observe the carrier concentrations in the transition region. With a larger carrier concentration (increased excitation), the effect can, however, be seen on the spatial carrier profile. A high photon flux will thus demonstrate the change in the slope on the carrier profile but will not represent the carrier concentration that was responsible for creating the defects. In order to determine the actual Δn_{lim} where the defect generation rate becomes saturated we have simulated the spatial carrier profile for these low carrier concentrations. The procedure will be described in Sec. III.

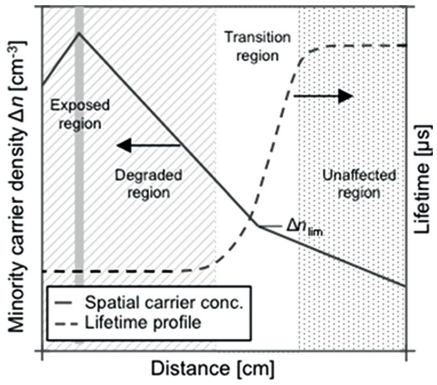

FIG. 3. Principle sketch showing the spatial carrier concentration in a sample exposed to a thin laser line. For simplicity only half of the lifetime groove is illustrated. The continuous line shows the spatial carrier concentration and the dashed line shows the spatial lifetime profile. The figure shows four regions; the shaded region corresponds to the degraded region, the grey to the exposed, the white to the transition region and the dotted to the unaffected region. The duration of the exposure determines the depth of the lifetime groove.

The basis for the simulations are; (i) a calibrated PL image of the lifetime groove measured by conventional PL imaging (5 s) where another (integrated) laser, with a wavelength of 808 nm, is used to expose the entire wafer and the resulting band-to-band PL signal is measured by a one-megapixel silicon CCD camera, and (ii) two QssPC measurements of the sample performed at $t = 0$ and $t = 10$ min illumination.

III. DATA ANALYSIS AND SIMULATIONS

The goal of the simulations and analysis presented here is to determine the value of Δn_{lim}. As explained in Sec. III, the minority carrier density in the transition region during the spot illumination is too low to be measured directly with the PL imaging setup. Therefore, we rely on simulations of the minority carrier profile, which is determined by measurements of the lifetime spatial profile and injection-level dependence before and after illumination.

The simulations of the spatial carrier concentration profile are based on the 2D continuity equation, describing a plane (x,z) normal to the focused laser line,

$$G(x,z) + D_n \nabla^2 \Delta n(x,z) - \frac{\Delta n(x,z)}{\tau(\Delta n, x)} = 0, \qquad (1)$$

where D_{n} is the electron diffusion length. The generation rate G(x,z) for the focused laser line is given by

$$G(x,z) = (1 - R_\lambda)\phi \exp\left(-\left(\frac{x}{\sigma}\right)^2\right)\alpha_\lambda \exp(-\alpha_\lambda z). \qquad (2)$$

Here α_λ is the attenuation coefficient for silicon, and R_λ is the reflectance at the laser wavelength ($\lambda = 780$ nm). The peak photon flux ϕ and Gaussian beam half width σ were measured by a beam profilometer and a calibrated photo spectrometer to be $\phi = 2.9 \times 10^{16}\,\text{s}^{-1}\,\text{cm}^{-2}$ and $\sigma = 50 \pm 5\,\mu$m for the spot used during the 10 min of light soaking. This illumination generates the defects and hence creates a spatial lifetime profile that reflects the carrier concentration profile during illumination. The carrier density in steady state is approximately homogeneous in the z-direction (depth of the sample), so the resulting carrier density values from the simulations are integrated throughout the thickness of the sample and reported only as function of x.

After the light soaking, the *spatial dependence of the lifetime* is determined by acquiring a standard PL lifetime image. The procedure to extract the true spatial lifetime profile from the diffusion-affected PL image is described in Ref. 7. This yields a sigmoidal curve that rises from a low lifetime plateau τ_{low} near the spot location to a high lifetime plateau τ_{high} far away from the spot, as sketched in Fig. 3.

The *injection level dependence* is determined by QSSPC measurements on the samples in their deactivated state, and after being light soaked for 10 min with a halogen lamp illuminating the whole sample. The light source is intense enough to reach the regime of constant defect generation, and the sample temperature change due to the illumination is negligible. The QSSPC data obtained before light soaking (deactivated sample) are then representative for the injection level

dependence of the lifetime in the unaffected region ($\tau_{high}(\Delta n)$), far away from the laser spot ($x \gg \sigma$). The QSSPC data obtained after light soaking are representative for the low-lifetime ($\tau_{low}(\Delta n)$) plateau near the spot. An example of such measurements is shown in Fig. 4. For the transition region, the lifetime is assumed to follow the sigmoidal shape determined from the standard PL lifetime image, but with $\tau_{low}(\Delta n)$ and $\tau_{high}(\Delta n)$ lifetimes adjusted by the injection dependence. The QSSPC data are fitted to a lifetime model to obtain values below the detection limit in the low-injection regime. The effective lifetime of the samples is typically not perfectly uniform, due to surface scratches and damage to the passivation layers caused by handling. Thus, the area-averaged QSSPC lifetime is lower than the lifetime in the spot-illuminated areas. The latter are measured in as homogeneous areas as possible to avoid discrepancies with the simulations. A factor is introduced to scale the averaged QSSPC lifetime to the PL-determined lifetime in the uniform region. The assumption is then that the injection level dependence measured by QSSPC is representative also for the small uniform area probed by the focused line laser.

With $\tau(\Delta n,x)$ and $G(x,z)$ determined from measurements, Eq. (1) is solved numerically using the partial differential equation solver FlexPDE.[14] The carrier concentration limit, Δn_{lim}, is extracted from the simulated carrier profile by fitting two exponentially decaying curves to the regions corresponding to the two lifetime plateaus. In this low-injection regime (of constant lifetime with injection level) the decay constant of each fitted curve corresponds to the diffusion length in the corresponding region. The limit, Δn_{lim}, is extracted from the carrier profile curve where the normal of the simulated curve crosses the intersection of the two fitted curves, see Fig. 5.

The simulations are verified by comparison to a measurement carried out with a laser line spot of higher intensity than the one used during the light soaking. A laser line spot with peak flux of $\phi_{high} = 1 \times 10^{18}\,s^{-1}\,cm^{-2}$ and $\sigma = 50 \pm 5\,\mu m$ Gaussian half width was used during acquisition of the spatial carrier concentration profiles. Fig. 6 shows an example where the simulation fits well to the measured carrier concentration profile. The noise floor around $\Delta n = 5 \times 10^{12}\,cm^{-3}$ is also visible.

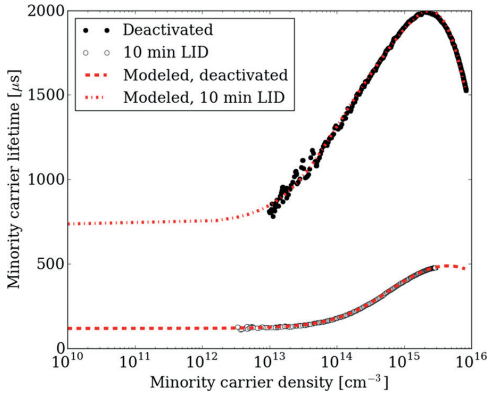

FIG. 4. Example of QSSPC measurements before and after light soaking for 10 min with a normal halogen lamp illuminating the whole sample.

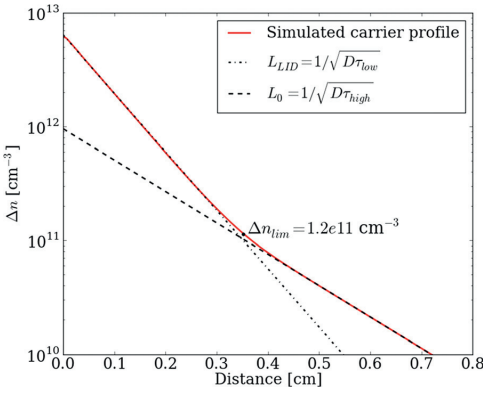

FIG. 5. Simulated carrier profile for the low-flux beam exposure at which the 10 min degradation was performed. The intersection of the two exponential curve fits (dashed lines) gives the *carrier concentration limit*, Δn_{lim}.

The simulation and analysis procedure are summarized below

1. The *spatial profile of the lifetime* is obtained from a calibrated PL image taken after 10 min spot illumination at low photon flux, ϕ_{low}.
2. The *injection level dependence* of the lifetime is determined by QSSPC measurements of the samples in their deactivated state and after 10 min light soaking.
3. The *continuity equation is solved numerically*, with the spatial and injection level dependent lifetime data from points 1 and 2.
4. The *carrier concentration limit, Δn_{lim}, is extracted* from the simulated carrier profile.

IV. RESULTS AND DISCUSSION

A. Direct monitoring of locally injected carriers

In this work, a region of light induced degraded lifetime is generated by locally exposing a sample to a low-flux laser beam. The regions of interest are the degraded, the

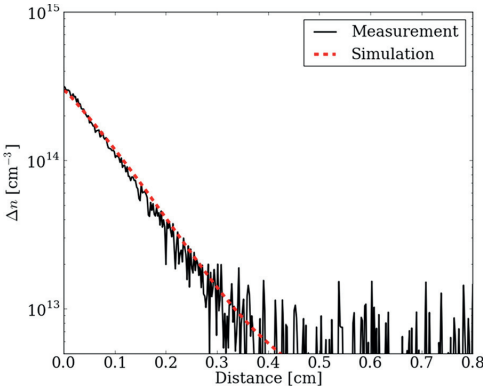

FIG. 6. Verification of the employed model. The black curve corresponds to a measurement of the spatial carrier profile carried out with the high-flux laser beam. The dashed curve corresponds to Eq. (2) with $\tau(\Delta n, x)$ and $G(x,z)$ determined from measurements.

unaffected and the transition region, where the lifetime changes (see Fig. 3). By a new method, described in the previous sections, we monitor the minority carrier density directly by photoluminescence imaging. By exciting a large enough concentration of carriers to detect the subsequent PL signal, we can observe what happens to the carrier concentration in the regions of interest. As already discussed, the actual values for Δn_{lim} are too low to be measured directly, but carrier profiles generated by a high-flux laser provide valuable information as well. The diffusion length of the material is given directly by the slope of the measured spatial carrier profile independently of the excited carrier concentration. By analyzing the slope of the spatial carrier concentrations generated by the high-flux laser, changes in the diffusion lengths can be identified. In Fig. 7, two spatial carrier profiles, generated by a high-flux laser beam, at two different positions x, are plotted. The grey carrier concentration profile is resulting from a high-flux laser line positioned in $x = 0$, but the carrier concentration is not high enough to reach the transition region before the PL detection limit is reached. The slope of the profile is, however, completely uniform demonstrating that the diffusion length in this region is uniform. This proves that above a certain Δn_{lim}, the B-O defect generation rate is fully independent of the carrier concentration and that the assumption of a lifetime plateau, inside the degraded region, used in Sec. III is correct.

The black carrier concentration profile in Fig. 7 is generated by moving the high-flux laser beam closer to the transition region. This time the carrier concentration is high enough to reach the transition region before the PL detection limit is reached. The detection of the direct PL signal in the transition region at high injection must be performed very quickly in order to not degrade the transition region, which is highly sensitive to degradation by excess carriers. Even though we use an exposure time of 15 s, we are still able to observe a change in the slope of the profile. The x-position

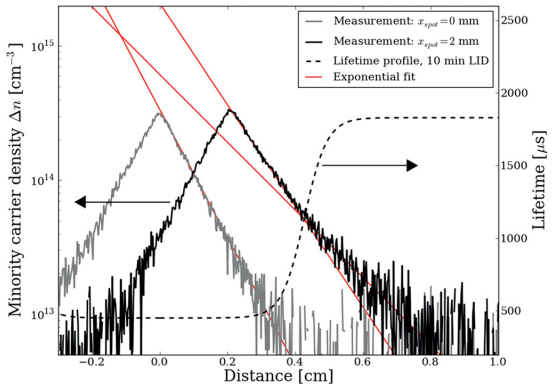

FIG. 7. Figure showing measured minority carrier density and lifetime after 10 min of low-flux laser beam exposure in $x = 0$ for a given sample. The grey curve corresponds to the carrier density profile when the high-flux laser beam is positioned in $x = 0$ and the black curve when the beam is positioned at $x = 0.2$ cm. Two individual exponential fits are shown on the $x = 0.2$ mm curve. The intersection of these fits gives the x position of where the diffusion length of the excess carriers changes. The dashed line is the measured lifetime profile.

of the change in the slope is determined by fitting two exponentially decaying curves to the right side of the decaying carrier profile. The intersection between these two curves corresponds well to the transition region of the measured lifetime profile, where the lifetime changes from being degraded to unaffected by the carrier concentration, given by the dashed curve. This finding shows that there exists a carrier threshold value at which the generation rate of B-O defects is no longer limited by carrier access.

B. Comparison of Δn_{lim} for different $N_{t\ rapid}^{*}$

The carrier concentration limit, Δn_{lim}, is extracted from the simulated carrier profiles, according to the method described in Sec. III, for a set of six samples with different doping and normalized defect concentration, N_t^*. In this study the Δn_{lim} values have been determined after exposing the samples for 10 min with a localized laser beam. This time is chosen for different reasons; (i) After 10 min, a lifetime groove with a well-defined shape is formed, suitable to test whether the slope of the spatial carrier profile will change in the transition from the degraded to the unaffected region. (ii) At 10 min small concentrations, $\Delta n < \Delta n_{\text{lim}}$, have not yet had time to cause significant degradation in the transition region, which would complicate the understanding of the spatial lifetime profile.[7] (iii) The lifetime profile after 10 min exposure is a result of the injection history during the whole 10 min exposure sequence. This means that at $t = 0$, when the lifetime of the sample is not yet degraded, the carrier concentration will be larger for all x-positions. A large difference in the diffusion length of the carriers is, however, only significant during the first few seconds of the exposure and according to previous work,[7] it was found that the extension of the degraded lifetime plateau does not change considerably over time. It is therefore realistic to employ the determined Δn_{lim} at 10 min as the actual threshold value for the Δn dependence of the B-O defect generation rate. (iv) To ease the interpretation of the results, it is convenient to look at one degradation mechanism at a time; At 10 min, the rapid degradation is complete, while the slow degradation is not yet evident. This is demonstrated in Fig. 8 where the normalized defect concentration N_t^* is plotted as a function of time for the samples of interest in this study. Accordingly, we can relate our measurement results to the rapid decay alone.

Individual Δn_{lim} values determined for each material together with their respective error bars are plotted in Fig. 9 as a function of the normalized defect concentration for the rapid decay, $N_{t\ rapid}^{*}$. The black error bars give the uncertainty of Δn_{lim} when the uncertainties of the calibration factor and the QSSPC measurements are taken into account. The red error bars indicate when the measurement with high-flux laser deviates from the simulation results. As can be seen from Fig. 9, the right-most point deviates quite substantially. This sample is the sample corresponding to $[B] = 8.4 \times 10^{11}\ \text{cm}^{-3}$ in Fig. 8. In Fig. 8, we see that at 10 min the slow degradation decay has already started for this specific sample. This might explain the deviation in simulation result to high-flux laser measurement. The deviations in the low-flux simulations are, however, expected to deviate much less from the experimental values,

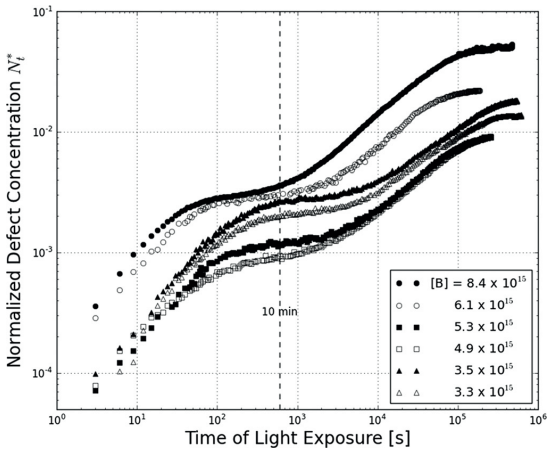

FIG. 8. Normalized defect concentration plotted as function of time for the six uncompensated boron-doped Cz-Si samples investigated in this study. The doping concentrations are given in the legend.

as the carrier lifetime is independent of the carrier injection level in this injection region.

C. Physical interpretation of Δn_{lim}

There is no indication of any obvious correlation between Δn_{lim} and $N_{t\ rapid}^{*}$ in the plot in Fig. 8. This signifies that the amount of carriers required to enable the degradation rate at full speed is independent of how many latent rapid B-O defect centres that occur in the sample. The finding is in agreement with a model where the activation is attributed to the change of the charge-state occurring when the electron quasi-Fermi level shifts across the energy level of the latent centre in its passive state. The determined Δn_{lim} concentration enables us to determine this energy level directly, since the Δn_{lim} concentration corresponds to the quasi-Fermi level at which a further

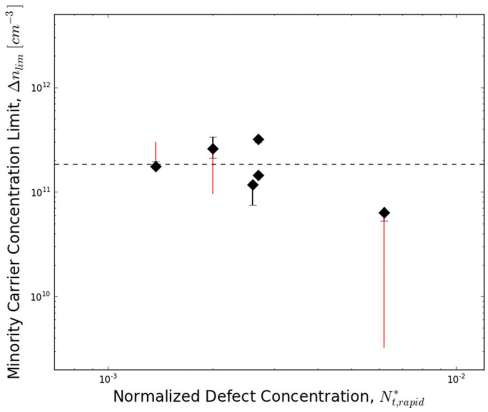

FIG. 9. Figure showing the minority carrier concentration limit, Δn_{lim}, as a function of N_{t}^{*}rapid. No correlation between Δn_{lim} and N_{t}^{*} can be observed. The black error bars give the uncertainty of Δn_{lim} when the uncertainties of the calibration factor and the QSSPC measurements are taken into account. The red error bars indicate when the measurement with high-flux laser deviates from the simulation results.

rise in the band gap will not cause any further increase in the defect generation rate. This is, however, only true if the equilibrium constant, k, of the charge state reaction $LC + e^{-} \leftrightarrow LC^{-}$ is sufficiently high (LC = Latent Centre). If k is $\ll 1$, it is possible that the defect energy level is positioned lower in the band gap and that an increase in the quasi-Fermi energy above this level simply causes an increase in k. This scenario cannot, however, be correct according to a measurement by Bothe,[15] where sub band gap illumination was used. In the first case, photons with energy above 0.50 eV were blocked. In this case, no defects were created. Subsequently, photons with energy above 0.73 eV were blocked and the experiment was repeated. In this case, defect generation was observed. Thus, the energy level must lie in between these limits. The determined Δn_{lim} concentration therefore enables us to determine the quasi-Fermi level responsible for the charge-state change of the latent defect centre directly.

The arithmetic average Δn_{lim} concentration from the measurement series shown in Fig. 9 is given by the dashed line and yields $\Delta n_{\text{lim}} = 1.84 \pm 0.9 \times 10^{11}\,\text{cm}^{-3}$. The quasi-Fermi energy from this concentration gives $E_{\text{lat}} = E_{\text{V}} + (635 \pm 18)$ meV determined by[16]

$$E_F{}^{n} - E_i = kT \times \ln\frac{n}{n_i}, \tag{3}$$

where E_{F}^{n} is the quasi-Fermi energy level for the electrons in this case equivalent to E_{lat}, E_{i} is the intrinsic Fermi energy (eV), k is the Boltzmann's constant, T is the temperature, n is the electron concentration in this case equivalent to Δn_{lim}, and n_{i} is the intrinsic concentration of electrons. Previously, Bothe *et al.*[2] have determined this level by a fundamentally different route, including temperature dependence on forward bias induced open circuit voltage degradation and PC1D simulations. They calculated the level to be $E_{\text{lat}} = E_{\text{V}} + (635 \pm 20)$ meV which is in good agreement with our result. The activation of the fast recombination centre is thus after all likelihood attributed to the change of the charge-state occurring when the electron quasi-Fermi level shifts across an energy level corresponding to the reported value. A simple recharge cannot, however, explain the complete transition from a latent to recombinative defect centre. The total supply of electrons over time under illumination is much larger than the concentration of B-O defects which is assumed to be in the order of $1 \times 10^{11}\,\text{cm}^{-3}$.[5] Accordingly, if a recharging effect was the final step in the generation of recombinative centres, the hypothetical reaction $LC + e^{-} \leftrightarrow RC$ (RC = Recombinative Centre) should be complete almost immediately. From Fig. 8, we see that this is not the case. The normalized rapid defect concentration does not saturate until approximately 200–300 s. Thus, the charging of the latent defects cannot be the last step before a final recombinative complex is in place. Another rate limiting event, when $\Delta n > \Delta n_{\text{lim}}$, must be occurring subsequently after the recharging. This is in correspondence to the model proposed by Voronkov *et al.*[8]

V. CONCLUSION

We have developed a new method based on photoluminescence imaging to directly monitor the excess carrier

density during light induced degradation. The laser used for light soaking is continuously exposing the sample to light, generating a spatially varying profile of activated B-O defects. By this method, we show experimentally that above a certain minority carrier concentration limit, Δn_{lim}, the B-O defect generation rate is fully independent of the minority carrier concentration. By simulation, we are able to determine the carrier concentration where the generation rate of the B-O defect saturates, $\Delta n_{\text{lim}} = 1.84 \pm 0.9 \times 10^{11}\,\text{cm}^{-3}$. Our results are consistent with a model where the role of the excess carriers during the rapid decay is to change the charge state of the defects by shifting the electron quasi-Fermi level across the energy level of the centre in its passive state. The energy level of the passive state of the latent defect centre is determined and yields $E_{\text{lat}} = E_{\text{V}} + (635 \pm 18)$ meV.

ACKNOWLEDGMENTS

This project has been funded by "The Norwegian Research Centre for Solar Cell Technology" and REC Wafer, REC Solar, Elkem Solar and the Norwegian Research Council through the KMB project "Defect engineering for crystalline silicon solar cells." H. Angelskår acknowledges funding from "The Norwegian Research Centre for Solar Cell Technology" (Project No. 193829).

Birger Retterstøl Olaisen is acknowledged for making the program performing the time-resolved LID with QSSPC measurements. Helge Malmbekk for valuable discussions on trap levels in the band-gap, Jo Gjessing for help with the photon flux measurements and Halvard Haug for help with surface passivation.

[1]H. Fischer and W. Pschunder, in *Proceedings of the 10th IEEE Photovoltaic Specialists Conference*, Palo Alto, CA (IEEE, New York, 1973), p. 404.
[2]K. Bothe and J. Schmidt, J. Appl. Phys. **99**, 013701 (2006).
[3]J. Schmidt and K. Bothe, Phys. Rev. B **69**, 024107 (2004).
[4]L. I. Murin, Appl. Phys. Lett. **98**, 182101 (2011).
[5]V. V. Voronkov and R. Falster, J. Appl. Phys. **107**, 053509 (2010).
[6]V. V. Voronkov, R. Falster, K. Bothe, B. Lim, and J. Schmidt, J. Appl. Phys. **110**, 063515 (2011).
[7]T. U. Naerland, H. Angelskar, M. Kirkengen, R. Sondena, and E. S. Marstein, J. Appl. Phys. **112**, 033703 (2012).
[8]K. Bothe, R. Hezel, and J. Schmidt, Appl. Phys. Lett. **83**, 1125 (2003).
[9]V. V. Voronkov, R. Falster, J. Schmidt, K. Bothe, and A. V. Batuninac, ECS Trans. **33**, 103 (2010).
[10]H. Hashigami, Y. Itakura, and T. Saitoh, J. Appl. Phys. **93**, 4240 (2003).
[11]M. Kessler, T. Ohrdes, P. P. Altermatt, and R. Brendel, J. Appl. Phys. **111**, 054508 (2012).
[12]W. Shockley and W. T. Read, Phys. Rev. **87**, 835 (1952).
[13]K. Bothe, J. Schmidt, and R. Hezel, in *Proceedings of the 3rd World Conference on Photovoltaic Energy Conversion*, Osaka, Japan, 2003, p. 1077.
[14]Flexpde 6, PDE Solutions Inc.
[15]K. Bothe, Ph.D. The University of Hannover, 2006.
[16]D. A. Neamen, *Semiconductor Physics and Devices: Basic Principles* (McGraw-Hill, New York, 2012).

PAPER IV

Studying light-induced degradation by lifetime decay analysis: Excellent fit to solution of simple second order rate equation

Tine Uberg Nærland, Halvard Haug, Hallvard Angelskår, Rune Søndenå, Erik Stensrud Marstein and Lars Arnberg,

IEEE Journal of Photovoltaics, vol. 3, pp. 1265-1270, 2013.

Is not included due to copyright